CERN/PSCC/86-2
PSCC/P94
16 January, 1986

A MEASUREMENT OF THE GRAVITATIONAL ACCELERATION OF THE ANTIPROTON

Universita di Pisa
Los Alamos National Laboratory
Rice University
Texas A&M University
Universita di Genova
Kent State University
Case Western Reserve University
CERN
NASA/Ames Research Center

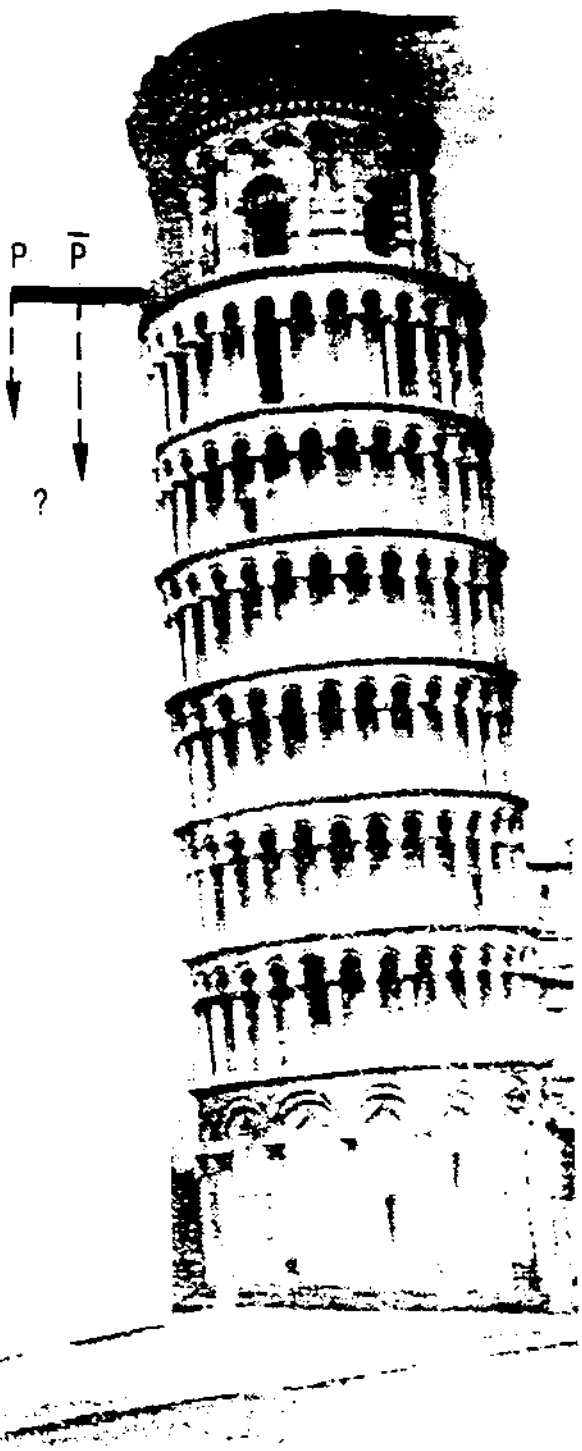

GALILEO, *Discorsi e Dimostrazioni Matematiche intorno à Due Nuove Scienze Attenenti alla Mecanica e i Movimenti Locali*. . . . Leyden, 1638. *Ed. Naz.* 8.108-9

SIMPLICIO. Ma chi possesse la maggior sopra la minore?

SALVIATI. Le accrescerebbe peso, quando il suo moto fusse più veloce: ma già si è concluso che quando la minore fusse più tarda, ritarderebbe in parte la velocità della maggiore, tal che il lor composto si moverebbe men veloce, essendo maggiore dell' altra; che è contro al vostro assunto. Concludiamo per ciò, che i mobili grandi e i piccoli ancora, essendo della medesima gravità in spezie, si muovono con pari velocità.

SIMP. Il vostro discorso procede benissimo veramente: tuttavia mi par duro a credere che una lagrima di piombo si abbia a muover così veloce come una palla d' artiglieria.

SALV. Voi dovevi dire, un grano di rena come una macina da guado. Io non verrei, Sig. Simplicio, che voi faceste come molt' altri fanno, che, divertendo il discorso dal principale intento, vi attaccaste a un mio detto che mancasse dal vero quant' è un capello, e che sotto questo capello voleste nasconder un difetto d'un altro, grande quant' una gomona da nave. Aristotele dice: 'Una palla di ferro di cento libbre, cadendo dall' altezza di cento braccia, arriva in terra prima che una di una libbra sia scesa un sol braccio'; io dico ch' ell' arrivano nell'istesso tempo; voi trovate, nel farne l'esperienza, che la maggiore anticipa due dita la minore, cioè che quando la grande percuote in terra, l'altra ne è lontana due dita: ora vorreste dopo queste due dita appiattare le novantanove braccia d'Aristotele.

Galileo, *Dialogues and Demonstrations concerning Two New Sciences; Appertaining to Mechanics and Locomotion.* Leyden, 1638. *Ed. Naz.* 8. 108-9

SIMPLICIO. But what if one placed the larger stone upon the smaller?

SALVIATI. The weight would increase if the larger moved more rapidly. But we have already concluded that if the smaller stone moved more slowly, it would in a measure retard the speed of the larger, so that the combination would move more slowly, though larger yet; and this is contrary to your assumption. We thus infer that large and small bodies alike, when they have the same specific gravity, move with the same speed.

SIMP. Your discussion is really admirable; yet I find it hard to believe that a bird-shot is going to move with the speed of a cannon-ball.

SALV. You ought to say a grain of sand and a millstone. But, Simplicio, I trust you will not follow the example of many others who divert the discussion from its main intent, nor fasten on some statement of mine which wants a hair's-breadth of the truth, and under this hair hide another man's fault as big as a hawser. Aristotle says: 'An iron ball of one hundred pounds, falling from a height of one hundred cubits, reaches the ground before a one-pound ball has fallen a single cubit.' I say that they arrive at the same time. You find, on making the experiment, that the larger precedes the smaller by two finger-breadths; that is, when the large one has struck the ground, the other is short of it by two fingers. Now you would not conceal behind these two fingers the ninety-nine cubits of Aristotle.

A MEASUREMENT OF THE GRAVITATIONAL ACCELERATION OF THE ANTIPROTON

N. Beverini,[1] J.H. Billen,[2] B. E. Bonner,[3] L. Bracci,[1] R. E. Brown,[2] L. J. Campbell,[2] D. A. Church,[4] K. R. Crandall,[2] D. J. Ernst,[4] A. L. Ford,[4] T. Goldman,[2] D. B. Holtkamp,[2] M. H. Holzscheiter,[2] S. D. Howe,[2] R. J. Hughes,[2] M. V. Hynes,[2] N. Jarmie,[2] R. A. Kenefick,[4] N. S. P. King,[2] V. Lagomarsino,[5] G. Manuzio,[5] M. M. Nieto,[2] A. Picklesimer,[2] J. Reading,[4] W. Saylor,[2] E. R. Siciliano,[2] J. E. Stovall,[2] P. C. Tandy,[6] R. M. Thaler,[7] G. Torelli,[1] T. P. Wangler,[2] M. Weiss,[8] F. C. Witteborn[9]

[1]Universita di Pisa; I-56100 Pisa, Italy
[2]Los Alamos National Laboratory; Los Alamos, NM 87545 USA
[3]Rice University; Houston, Texas 77001 USA
[4]Texas A&M University; College Station, Texas 77843 USA
[5]Universita di Genova; I-16100 Genova, Italy
[6]Kent State University; Kent, Ohio 44242 USA
[7]Case Western Reserve University; Cleveland, Ohio 44106 USA
[8]CERN; Geneva 23, Switzerland
[9]NASA/Ames Research Center; Moffett Field, CA 94035 USA

ABSTRACT

Theoretical approaches to gravitation abound whereas experiments in gravity are few in number. A fundamental measurement in experimental gravity that has not yet been done is the measurement of the gravitational force on antimatter. In certain extended supergravity models, specific particles have different gravitational masses from their associated antiparticles. However, as yet there has been no direct test of this prediction. We propose to test directly the equality of particle and antiparticle gravitational masses in the baryon sector with protons and antiprotons. Experimentally, we plan to use the time of flight technique pioneered by Witteborn and Fairbank in their measurement of the gravitational force on the electron. In this approach the particles are launched vertically up a drift tube. The time of flight of the particle up the drift tube together with the initial velocity gives a measure of the gravitational force acting on the particle. To realize this measurement in sensibly dimensioned equipment and with reasonable timing precision requires ultra-low velocities for the antiprotons. We propose a staged deceleration approach to achieve these velocities. In our approach, low energy antiprotons from LEAR will be decelerated in an RFQ and cyclically injected into a series of specially designed pulsed ion traps. In this series of traps, adiabatic, resistive and electron cooling will be used to lower the antiproton energy to the required thermal level. When this is achieved the antiprotons will be transferred, a few at a time, into a launching trap at the base of the drift tube. After launch, the antiprotons will be detected at the top of the drift tube with a microchannel plate. An H^- source will be used to calibrate the equipment.

PROPOSAL CONTENTS

$\bar{P}$ - acceleration

SYNOPSIS

About 375 years ago, Galileo Galilei performed one of the most famous experiments in the history of Physics. He dropped weights of wood and lead from a "high tower" in Pisa to determine their relative rate of fall. From this and other experiments, and from theoretical considerations, Galileo concluded that (but for air resistance) all bodies fall with the same acceleration. Two fundamental questions are involved in such reasoning. First, do objects with different masses fall at the same rate? Second, do objects with different compositions fall at the same rate?

Between 1889 and 1908, Eötvös performed a series of experiments addressing the second of these questions. His results verified the weak equivalence principle (universality of free-fall), in the Earth's gravitational field, to an accuracy of one part in 10^8. Then, twenty-five years ago, Dicke achieved an accuracy of one part in 10^{12} for the universality of free-fall of objects towards the Sun. However, these remarkable levels of accuracy were achieved for the free-fall of macroscopic objects, and indeed, the weak equivalence principle has only been tested to an accuracy of one part in 10^2 or 10^3 for individual elementary particles.

Modern quantum field theories which attempt to unify the gravitational interaction with the other forces of Nature predict violations of the weak equivalence principle at the elementary particle level. In particular, Zachos and Scherk have shown that certain extended supergravity models predict that leptons and baryons will fall more slowly in the Earth's gravitational field than mesons, which in turn will fall more slowly than antibaryons. The reason for this behavior is that in these models the graviton has a spin-one partner, the "graviphoton", and in some models a scalar partner as well, which in the static limit couple to mass. Therefore, in addition to conventional gravitation arising from graviton exchange, graviphoton exchange tends to repel ordinary matter from the Earth ("like charges repel"), while antimatter is further attracted.

No observationally significant deviations from general relativity occur if the new vector and scalar partners of the graviton have a small mass ($\sim 10^{-9}$ eV). However, in the Newtonian limit, there would then be experimentally detectable Yukawa terms in the gravitational potential, with a finite range. Such effects are not ruled out experimentally, and may have

already been observed in recent geophysical experiments, with exactly the repulsive nature corresponding to graviphoton exchange. Typical quantum supergravity effects are expected to be directly apparent only at the Planck mass scale (~10^{19} GeV), in particle production or in quantum loop effects. However, classical supergravity effects could be comparable to Newtonian quantities. Therefore, gravity experiments sensitive to classical (low energy) supergravity effects may well be, at present, the most direct way to test these theories.

Certain pioneering arguments which were constructed to argue for the absence of "antigravity" did not anticipate the complexities of this interaction in modern theories, and so the question is again open. Moreover, one cannot anticipate a null result on the basis of CPT symmetry, because the proof of the existence of this symmetry requires the absence of gravitational fields (flat space-time). Finally, supergravity theories may well respect CPT invariance while still predicting a non-null result. Thus, this exciting question can only be answered by experiment.

We therefore propose to perform a new version of the Eötvös experiment, in which the gravitational acceleration of antimatter towards the Earth is compared with that of ordinary matter. Specifically, we intend to measure the passive gravitational mass of the antiproton, relative to the H^- ion. No experiment of this type has yet been performed.

To measure the gravitational effect on antiprotons, the antiproton energy has to be low enough so that the time-of-flight (TOF) spectrum has sufficient particles near the cutoff time ($t_c = \sqrt{2\ell/g}$) for a significant measurement. The energy required is more conveniently measured in degrees Kelvin rather than the more familiar MeV or keV. The lowest energy beam currently available from LEAR is ~5 MeV. To execute the measurement, this energy has to be reduced by about ten orders of magnitude. We propose a series of deceleration stages involving an RFQ decelerator and several pulsed ion traps to accomplish this energy reduction. The final storage trap will store as many as 10^7 antiprotons at ~10 K or lower. Once the particles are cold enough, they will be brought, about 100 at a time, into a high precision launching trap and suddenly released. Evidently half of the particles will thus be launched vertically upward. A 1 m drift tube is located above the trap in order to isolate the rising antiproton or H^- ion from stray electric fields. The arrival times of the antiprotons relative

to the launch time are measured after a 1 m flight path. A microchannel plate is used to detect the particles. The microchannel plate was selected because of its capability to detect both H^- ions and antiprotons (with different but understandable response characteristics). This is extremely important because the H^- ion may then be used as a calibration standard, taking advantage of its near perfect simulation of antiproton intrinsic electromagnetic properties. Use of a microchannel plate enables the measurements of the H^- and antiproton TOF spectra to be made in the identical set up.

The experimental sequence starts with the extraction of a 5 MeV bunched beam from LEAR. The bunching has a macrotime structure set by the 8th harmonic buncher already in the LEAR ring. A single phase bucket of this buncher is fast extracted from LEAR and delivered to the experiment. A microtime structure matched to the operating frequency of the RFQ decelerator will also be imposed on the macroburst. This microstructure can be imposed either in or external to the LEAR ring. Bunching in LEAR makes the most efficient use of antiprotons, whereas bunching externally may have higher loss rates. In any event, this bunched beam at 5 MeV is decelerated in an RFQ, currently under design at Los Alamos and CERN, to 100 keV. An energy shifting cavity is then used to adjust the beam energy either up to 200 keV for use in other experiments or down to 20 keV for use in our gravity experiment. The 20 keV beam emerging from the energy shifting cavity will be debunched in a special cavity. This cavity will allow for a correction of the phase spread over the drift length to the first pulsed ion trap. In the drift length a provision for injecting 20 keV H^- ions into the beam line will allow for testing of the pulsed ion trap independent of LEAR operations. The drift length will also contain beam diagnostics and optics appropriate for entering the double focusing 90° bending magnet which bends the beam vertically up into the first pulsed ion trap. Located immediately before the entrance to this trap is an electrostatic deceleration stage and drift space which lowers the beam energy to 4 or 5 keV depending upon the incident beam energy spread. Initially the entrance endcap is at ground potential whereas the top endcap is at 5 kV. As the beam-burst transverses the trap and approaches the top endcap, it starts to decelerate and turn around. When the leading edge of the burst has returned to the center of the trap the potential on the entrance endcap will be quickly raised to 5

kV. This will prevent the burst from exiting the trap, i.e. the burst is "caught". In this type of electromagnetic trap (Penning trap) the particles are contained radially by a strong (6 T) magnetic field and axially by an electrostatic quadrupole potential. While in this trap the particles will be resistively cooled to ~200-300 eV. When this is accomplished, the particles will be transferred to a highly compensated harmonic trap for further resistive cooling. Although other cooling schemes have been proposed, we plan on resistive cooling at present, because it is the only demonstrated technique available. In this intermediate trap the particles will be cooled to ~5-10 K and stored in preparation for transfer, 100 at a time, into the final, launching trap. Once the launching trap is loaded, the potential will be suddenly dropped, thus releasing half of the particles upward in the drift tube. The TOF is measured using a microchannel plate at the top of the drift tube. The ion-trap-drift-tube system must operate at extremely low pressures (10^{-14} Torr) to avoid loss of antiprotons through annihilation with residual gas atoms.

To measure the gravitational acceleration of antiprotons relative to the H^- ion will require the launching of a total of 10^6 to 10^7 particles, for a 1% measurement. The same precision can be accomplished with substantially fewer particles if an externally applied electric field is used to increase the acceleration. There will be ~10^8 particles in each 8th harmonic macrobunch from LEAR. This is sufficient for one TOF spectra with some safety margin. Many TOF spectra will be required to assure reproducibility. Each antiproton run will be followed by a run with H^- ions. The H^- ions will be either internally generated in the bulk storage trap or transported from an external source.

The measurement of the gravitational mass of the antiproton is a fundamental measurement that has not yet been performed. No convincing theoretical arguments have been made to anticipate the result. This important measurement will test the principle of equivalence for antimatter, test CPT symmetry in a gravitational context, and provide a powerful constraint on modern attempts to unify gravity with the other forces of nature.

I. PHYSICS MOTIVATION: ELEMENTARY PARTICLE PHYSICS

Quantum field theory provides a mathematical framework for the description of elementary particles and their interactions, which is consistent with the requirements of causality and quantum mechanics. It is the goal of elementary particle physicists to construct a quantum field theory of all of the fundamental particles and interactions. (For twenty-five years the only such successful theory was quantum-electrodynamics.) Significant progress in this direction has been achieved in the electro-weak interactions, with the highly successful Glashow-Weinberg-Salam model, and in the strong interaction, with the candidate field theory of quantum chromodynamics. On the other hand, the gravitational field has never been successfully quantized. Considerable theoretical research efforts are presently directed at this problem throughout the world.

A. Classical Gravity-Quantum Mechanical Shortcomings

The classical effects of gravity are accurately described by Einstein's general theory of relativity. In contrast to the other three interactions, the quantum mechanical effects of gravity are not readily apparent because of the extreme weakness of the underlying interaction. This is not to say that such effects are without interest. Indeed, the gravitational influence on the quantum mechanics of ordinary matter has been observed in the C-O-W experiment.[1] Neutrons which have travelled on different paths in a gravitational potential are made to interfere, demonstrating a phase shift which arises from the gravitational contribution to their energies. Furthermore, Hawking's theoretical studies have predicted the quantum mechanical decay of black-holes.[2] However, in each of these cases the gravitational field is treated classically. A fully self-consistent treatment would require the quantization of the gravitational field itself. It is by no means apparent that general relativity and quantum field theory are compatible in their present forms. One may approach the combination of the two theories from two different directions: The study of quantum mechanical modifications of general relativistic concepts or gravitational effects on quantum field theory.

B. Quantum Mechanical Limitations of General Relativistic Concepts

Wigner[3] and others[4] have pointed out the difficulty of introducing quantum mechanical matter into general relativity. General relativity deals with the events which define the world-lines of particles. However, quantum mechanical particles do not follow definite trajectories,[5,6] and a determination of their positions involves a measurement which introduces an uncertainty into their momenta. These conceptual difficulties have their origin in the principle of equivalence, which is embodied in general relativity.[7]

Recent research has questioned the existence of the principle of equivalence at the quantum level.[8,9] Furthermore, Hawking's theoretical studies of black-holes have suggested that gravitational effects may produce violations of conventional quantum mechanics.[10] In related work, Fulling[11] has shown that the quantum field theory vacuum is not invariant under general coordinate transformations. The topology of space-time also has a profound impact on quantum mechanics. For instance if space is compact, correlations of the Einstein-Podolsky-Rosen[12] type need no longer be entirely spacelike.

Thus it is not clear that classical gravitational concepts can be successfully combined with present quantum theory.

C. Gravity and CPT Symmetry

Conventional quantum field theories are known to possess CPT invariance.[13] This symmetry systematizes the relationship between matter and antimatter, first introduced by Dirac.[14] The most familiar consequences of CPT symmetry are that for each particle there is an antiparticle with the same:

- inertial mass
- total lifetime
- magnetic moment (but opposite sign).

One of the assumptions underlying the CPT theorem is that space-time is flat. It is therefore not obvious that a quantum theory of gravity would possess CPT symmetry. Moreover, Wald[15] and others[16] have shown that the violations of quantum mechanics induced by black-holes would lead to the failure of CPT invariance, while Geroch[17] and Kiskis[18] have shown that the

topology of space-time has a direct bearing on the existence of C, P, and T symmetries in quantum field theory. Other authors have raised the possibility of CPT-violation in flat space-time.[19]

Experimentally, CPT symmetry has only been tested where gravitational effects can be ignored. Tests of this invariance principle using the inertial mass (m), lifetime (τ), magnetic moment (μ) and gyromagnetic ratio (g) are listed in Table I. It should be noted that the listed tests are normalized to either an electro-weak or a strong interaction scale as appropriate. We would not expect a CPT-violating effect due to gravity to

TABLE I-1

CPT INVARIANCE TESTS

Lepton Sector		
$(g(e^+)-g(e^-))/\text{average}$	$(2.2 \pm 6.4) \times 10^{-11}$	(Ref. 20)
$(g(\mu^+)-g(\mu^-))/\text{average}$	$(-2.6 \pm 1.6) \times 10^{-8}$	(Ref. 21)
$(m(e^+)-m(e^-))/\text{average}$	$(0.0 \pm 1.3) \times 10^{-7}$	(Ref. 22)
$(m(\mu^+)-m(\mu^-))/\text{average}$	$(0.26 \pm 1.9) \times 10^{-5}$	(Ref. 23)
$(\tau(\mu^+)-\tau(\mu^-))/\text{average}$	$(2.7 \pm 7.8) \times 10^{-5}$	(Ref. 24)
Meson Sector		
$(m(\pi^+)-m(\pi^-))/\text{average}$	$(2 \pm 5) \times 10^{-4}$	(Ref. 25)
$(m(K^+)-m(K^-))/\text{average}$	$(-0.6 \pm 1.8) \times 10^{-4}$	(Ref. 26)
$(\tau(\pi^+)-\tau(\pi^-))/\text{average}$	$(5.5 \pm 7.1) \times 10^{-4}$	(Ref. 25)
$(\tau(K^+)-\tau(K^-))/\text{average}$	$(1.14 \pm 0.93) \times 10^{-3}$	(Ref. 27)
Baryon Sector		
$(\mu(p)-\mu(\bar{p}))/\text{average}$	$(-0.8 \pm 7) \times 10^{-3}$	(Ref. 28)
$(m(p)-m(\bar{p}))/\text{average}$	$(7 \pm 4) \times 10^{-5}$	(Ref. 29)
$(m(\Lambda)-m(\bar{\Lambda}))/\text{average}$	$(7 \pm 7) \times 10^{-5}$	(Ref. 30)
$(m(\Xi^-)-m(\bar{\Xi}^+))/\text{average}$	$(1.1 \pm 2.7) \times 10^{-4}$	(Ref. 31)
$(\tau(\Lambda)-\tau(\bar{\Lambda}))/\text{average}$	$(4.4 \pm 8.5) \times 10^{-2}$	(Ref. 32)
$(\tau(\Xi^-)-\tau(\bar{\Xi}^+))/\text{average}$	(0.03 ± 0.19)	(Ref. 33)

be apparent in these tests, because of the extreme weakness of the gravitational interaction.

D. Gravitational Properties of CPT-Conjugate Matter

The principle of equivalence has only been tested for ordinary matter. For bulk matter the principle has been verified to several parts in 10^{12} by the Eötvös-Dicke experiments,[34,35,36] and more recently at the same level, on very massive bodies.[37] For free particles such as atoms,[38] neutrons,[39] photons[40] and electrons,[41] the accuracy achieved has only been one part in 10^2 or 10^3. One cannot invoke CPT symmetry to argue that antimatter also obeys the equivalence principle since it is not known if the CPT theorem holds in a gravitational field.

The experimental and theoretical situations outlined here underscore the need for a direct experimental study of the gravitational properties of elementary particles of antimatter.

Theories which attempt to unify gravity with the other forces of nature predict deviations from Newton's inverse square law.[42-45] Such effects are not ruled out experimentally,[46] and there is evidence of a repulsive Yukawa component of gravity in recent geophysical studies.[47,48] The existence of such a gravitational interaction (coupling to baryon number or hypercharge, perhaps) is supported by a re-analysis[48] of the original Eötvös experiment.[34] Presently, experiments[46,49] leave room for a massive vector field with a range of 5m to 10km. It was first noted by Zachos[50] that a component of the gravitational interaction of this type is present in certain extended supergravity theories,[44,45] where the graviton has a vector partner.[51] Scherk[45] has emphasized that a clear signal of this new interaction would be an apparent CPT violation in the gravitational masses of the proton and antiproton. (The new vector interaction would tend to repel a proton, but attract an antiproton to the earth.)

E. Indirect Tests of the Gravitational Properties of Antimatter

Although there has never been any direct test of the equivalence principle for non-CPT-self-conjugate antimatter,[52] indirect theoretical arguments have been made. The two best known arguments are due to Good[53] and to Schiff.[54] These arguments are based on the pioneering ideas of Morrison and Gold[55,56] about "antigravity", in which antiparticles rise in

the earth's gravitational field. This notion of "antigravity" is inconsistent with extended supergravity models, in which specific particles fall with different accelerations from their antiparticles.[44,45] Nevertheless, Morrison realized[56] that any form of "antigravity" would inevitably conflict with either the principle of equivalence, or with the conservation of energy. The former, however, is now recognized as a perfectly acceptable possibility.

Good argued that if K^o and $\bar{K}^o$ react oppositely to the Earth's gravitational field, then these components of the long-lived CP-eigenstate,

$$K_L = (K^o + \bar{K}^o)/\sqrt{2} \quad , \tag{1}$$

would instantly develop a phase difference, leading to regeneration of the short-lived combination,

$$K_S = (K^o - \bar{K}^o)/\sqrt{2} \quad , \tag{2}$$

of opposite CP-eigenvalue. This would occur without scattering in material, and would appear as a CP-violating effect.

Although such an (vacuum regeneration) effect has since been observed,[57] it is currently thought to be due to the weak interactions. It has been shown that conventional gravitational theory also gives this effect,[58] but with a different energy dependence than that observed. (Recently, Aronson et al.[59] have argued that there may be a tiny residium in the data that demonstrates this energy dependence.)

Good's argument depends on two major assumptions. The first is that the local, absolute gravitational potential, ϕ, must be known, for this appears in his revision of the K^o-$\bar{K}^o$ mass matrix:

$$\begin{bmatrix} m_K & o \\ o & m_{\bar{K}} \end{bmatrix} \rightarrow \begin{bmatrix} m_K(1+\phi) & o \\ o & m_{\bar{K}}(1-\phi) \end{bmatrix}, \tag{3}$$

where CPT invariance requires $m_K = m_{\bar{K}}$. Since the value of ϕ is, at best,

unknown and perhaps, as in usual gauge theories, not physically meaningful, it is difficult to draw quantitative conclusions.

More important, however, is that Good did not explore all possible new terms. The change in (3) violates the principle of equivalence, which Good was proposing to defend. Allowing all possible additional terms, we find instead

$$\begin{bmatrix} m_K & 0 \\ 0 & m_K \end{bmatrix} \rightarrow \begin{bmatrix} m_K+\phi_a & \phi_b \\ \phi_c & m_K-\phi_d \end{bmatrix}. \tag{4}$$

We note that the choice $\phi_d = -\phi_a$ (following Good[53]) has no effect on the mass eigenvalues if the condition

$$\phi_b = -\phi_c = \phi_a/2 \quad , \tag{5}$$

is also imposed. The resulting mass eigenstates are just the ordinary CP eigenstates and so there is no apparent deviation from the ordinary case. If the deviation of the ϕ's from (5) is small enough in value, the CP-violating experimental results can be reproduced also!

It should be emphasized that we do not propose the existence of a $\Delta S = 2$ component to the gravitational interaction.[60] Rather, we point out that in the absence of stringent bounds on the strength of such an interaction, Good's argument is insufficient to prove his conclusion.

Moreover, Scherk's analysis[44,45] of the gravitational interaction in extended supergravity models shows that the effects of "antigravity" in those models are not as dramatic as assumed by Good. This is because the graviton, and its vector partner, the "graviphoton", couple to the quark and gluon constituents of the neutral kaons, and not to the kaons themselves. Quark and antiquark both fall in the earth's gravitational field, in spite of the presence of "antigravity", but with the antiquark having the greater acceleration. This is in marked contrast with earlier ideas about antigravity, in which antimatter would rise in the earth's gravitational field.[55,56] Furthermore, in the models studied by Scherk, the gluons and other CPT-self-conjugate particles have conventional gravitational properties. In addition, Macrae and Riegert have pointed out[46] that by

choosing a generation-independent coupling of the "graviphoton" to fermions, the gravitational energy difference between particle and antiparticle in the neutral kaon system can be made to vanish. This also completely circumvents Good's argument, while still producing a gravitational acceleration for a baryon which is different from that for the corresponding antibaryon.

Schiff's argument is that virtual positrons* in atomic wavefunctions would influence Eötvös-Dicke[34-36] experiments if the positrons reacted anomalously to gravitation. However, as Schiff himself noted, an infinity appears in his calculation. To remedy this, he took a finite piece that should represent less than the whole effect, and used QED to calculate this part of the probability of finding a positron in an atom. From the point of view of quantum field theory, however, this argument is specious. Such an infinity is subject to a renormalization which requires an infinite subtraction. Schiff's arbitrary removal of a divergent part of the calculation does not obviously constitute a consistent renormalization. His result is therefore subject to (unknown) finite corrections within a consistent scheme.

Furthermore, Schiff took the gravitational effect to be given by the positron mass times his calculated probability. Instead, since the positron is virtual, its contribution to the stress-energy tensor is the relevant quantity in an Einsteinian formulation of the gravitational interaction. A simple estimate of this may be made directly by using the Lamb shift: The vacuum polarization contribution of 27 MHz is clearly related to the presence of virtual positrons. This represents a contribution of less than one part in 10^{16} to the gravitational interaction of a typical atom. Hence the 10^{-12} accuracy of Dicke's experiments is insufficient to draw any conclusion regarding the gravitational properties of positrons. Moreover, Schiff (like Good) assumed that the physical manifestation of "antigravity" would be a negative gravitational mass of antiparticles - they would rise in the earth's gravitational field. Scherk's analysis[44,45] of "antigravity" in certain supergravity models shows that it need not be of this extreme form: both electron and positron fall in the earth's gravitational field,

---

*In some grand unified theories, positrons are matter: electrons antimatter (Ref. 52).

with the positron having the greater acceleration. Furthermore, the "graviphoton", which is responsible for "antigravity", is massive so that its effects would not have been apparent in the Dicke[35] and Braginskii[36] versions of the Eötvös experiment, which compared the gravitational attraction of different materials to the Sun. It is only from the results of the (comparatively) less accurate original Eötvös experiments[34] that constraints can be inferred on this type of "antigravity", since these experiments compared the gravitational attraction of different materials to the earth, over laboratory distance scales.[48]

Schiff himself abandoned the attempt to study the gravitational contribution of virtual pions in the nucleus. The modern version of this would be to estimate the antiquark content of the nucleus, using QCD. However, the difference between nuclear and atomic structure (the quarks are organized into nucleons, not overall orbitals) makes their color-Lamb shift effect difficult to estimate with any reliability. Deep inelastic scattering experiments do show significant antiquark content of nuclei, but at high momentum transfer. It is not known how to continue this information to the low momentum transfer, infra-red regime. There, instead of the infinite momentum frame parton distribution, which is the measured quantity, one needs the rest frame constituent distribution. It is even more difficult to make reliable estimates of the variation with atomic species, which is needed to apply the Eötvös-Dicke results.

The Pound-Rebka[40] experiments have tested the principle of equivalence for CPT-self-conjugate elementary particles: photons. Left- and right-circularly polarized photons, which are CPT-conjugate states, were both found to be red-shifted by the same amount in these experiments. One cannot infer the gravitational properties of non-self-conjugate antiparticles from these experiments since the relation between the photon (a gauge particle) and such particles is, at best, model dependent. For instance, an exact supersymmetry would allow the conclusion that photinos, the partners of photons, behave as expected under gravity, but these are still CPT-self-conjugate. Even if a larger symmetry could extend the results to non-self-conjugate matter, the supersymmetry itself is known to be violated (if it exists at all). Moreover, this symmetry breaking is thought to be related to the structure of spacetime, and so, to gravity. Thus, the negative (in our terms) Pound-Rebka result makes the test of

non-self-conjugate matter all the more critical. In the extended supergravity models analyzed by Scherk[44,45] the gravitational interaction of CPT-self-conjugate particles, such as photons, is conventional, and hence these models are in perfect accord with the Pound-Rebka experiments.[40]

F. Direct Tests of the Gravitational Properties of Antimatter

The only direct test of the gravitational properties of non-self-conjugate antimatter was attempted by Witteborn and Fairbank.[41] By sending pulses of electrons from a hot cathode up a shielding, low temperature vertical drift tube and measuring their transit time from the centroid of broad distributions, they found

$$g_{e^-} = (0.09 \pm 0.10)\, g \quad , \tag{6}$$

where g is the local acceleration due to the Earth's gravity. The expected result is zero because of the Schiff-Barnhill effect[61] (sagging of the electrons in the drift tube material, which creates an electric field along the vertical axis of the tube). Therefore, (6) represents a 10% accuracy in the measurement of the gravitational response of the electron, after correction for this "background" effect. The expected result for positrons in this apparatus is

$$g_{e^+} = 2\, g \quad , \tag{7}$$

so that 5% accuracy would seem feasible. Unfortunately, a sufficient supply of slow (cold) positrons, comparable to the electron supply, was not achieved.

Thus no direct experimental test has ever been made of the gravitational properties of non-self-conjugate antimatter, and so it is simply not known whether theories of gravity based on the equivalence principle are compatible with CPT symmetry. The experiment proposed here uses the factor of 1836 between the masses of the antiproton and the positron to suppress the Schiff-Barnhill effect. (The electric field in the drift tube is unchanged, and so the more massive antiproton receives a

smaller acceleration from this field.) This reduces the "background" correction to the 10^{-3} to 10^{-4} level, leaving an unambiguous and highly accurate test of the gravitational properties of antimatter.

The availability of low energy antiprotons from LEAR, which we will cool further, makes this experiment feasible. It also allows a more accurate and precise test of the gravitational properties of antimatter than is possible with positrons.

G. Theoretical Prospects

It is clear that there is presently a great deal of ferment in the area of quantum gravity. Current theoretical research at Los Alamos is directed towards understanding the range of possible CPT violation in theories of gravity, and towards the study of quantum modifications of the principle of equivalence.

Modern quantum field theories which attempt to unify gravity with the other three interactions introduce extra dimensions to space-time. These extra dimensions have to be compactified in order to reduce the observable dimensionality to four. We are studying the possibility of introducing interactions in the extra dimensions, which would induce an apparent violation of CPT symmetry in the observable four dimensions of space-time.

Another line of research concerns the study of quantum field theories from a non-inertial viewpoint. One of us,[62] together with J. S. Bell and J. M. Leinaas,[63] has shown how the failure of general coordinate invariance of the quantum field theory vacuum, discovered by Fulling[11] and by Unruh,[64] is connected with CPT symmetry. By studying such behavior, we hope to determine if CPT symmetry exists in a non-inertial (and, by inference, gravitational) setting, and also to study possible quantum modifications of the principle of equivalence.

H. Conclusions

At the present time there is neither a direct nor an indirect experimental or theoretical determination of the gravitational properties of antimatter. The measurement of the gravitational mass of the antiproton at any reasonable level of precision will remedy this situation. It will directly test the principle of equivalence for antimatter, test CPT symmetry in a gravitational setting, and provide a powerful test of the gravitational

interaction predicted by the extended supergravity models analyzed by Scherk.[44,45] The ratio of apparent CPT-violating quantum effects to inertial quantities is expected to be small (~ inertial mass/Planck mass). However, the ratio of apparent CPT-violating classical gravitational quantities to inertial quantities could be of order one in supergravity theories. This would be similar to our experience with parity violating effects relative to the strong and electroweak interactions. On the one hand, the results of a direct test could provide a striking demonstration that current theoretical prejudices are correct, just as Aspect's experiments[65] have verified Bell's inequalities[66] in quantum mechanics. On the other, the outcome might be as significant as the Michelson-Morley experiment.[67] In any event, these are so few experimental tests of gravity that any additional information is of vital importance, and, moreover, the results could prove invaluable in the further reconciliation of gravity with quantum mechanics.

REFERENCES FOR SECTION I

1. R. Collella, A. W. Overhauser and S. A. Werner, Phy. Rev. Lett. 34, 1472 (1975).

2. S. W. Hawking, Nature 248, 30 (1974); Comm. Math. Phys. 43, 199 (1975).

3. E. P. Wigner, Rev. Mod. Phys. 29, 255 (1957); Bull. Am. Phys. Soc. 24, 633 (1979).

4. H. Salecker and E. P. Wigner, Phys. Rev. 109, 571 (1958); A. Peres and N. Rosen, Phys. Rev. 118, 335 (1960); P. G. Bergmann and G. J. Smith, Gen. Rel. Grav. 14, 1131 (1982); M. B. Mensky in Proceedings of the Third Seminar on Quantum Gravity, eds. M. A. Markov, V. A. Berezin and V. P. Frolov, World Scientific, Singapore (1985).

5. R. P. Feynman and A. R. Hibbs, Quantum Mechanics and Path Integrals, McGraw-Hill, New York (1965).

6. L. F. Abbot and M. B. Wise, Am. J. Phys. 49, 37 (1981).

7. M. P. Haugan, Ann. Phys. (NY) 118, 156 (1979); R. H. Dicke in Relativity, Groups and Topology, eds. C. DeWitt and B. DeWitt, Gordon and Breach, New York, 1964; C. M. Will in General Relativity, eds. S. W. Hawking and W. Israel, Cambridge University Press, Cambridge, 1979; P. C. W. Davies and J. Fang, Proc. Roy. Soc. (London) A381, 469 (1982).

8. P. Candelas and D. W. Sciama, Phys. Rev. D27, 1715 (1983).

9. J. F. Donoghue, B. R. Holstein and R. W. Robinett, Phys. Rev. D30, 2561 (1984); Gen. Rel. Grav. 17, 207 (1985).

10. S. W. Hawking, Phys. Rev. D14, 2460 (1976); Comm. Math. Phys. 87, 395 (1983).

11. S. A. Fulling, Phys. Rev. D7, 2850 (1973).

12. A. Einstein, B. Podolsky and N. Rosen, Phys. Rev. 47, 777, (1935).

13. J. Lüders, Kgl. Dan. Vid. Sel. Mat. Fys. Medd. 28, No. 5 (1954); J. S. Bell, Proc. Roy. Soc. (London) A231, 479 (1955).

14. P. A. M. Dirac, Proc. Roy. Soc. (London) A126, 360 (1930).

15. R. M. Wald, Phys. Rev. D21, 2742 (1980).

16. D. N. Page, Phys. Rev. Lett. 44, 301 (1980); Gen. Rel. Grav. 14, 299 (1982).

17. R. Geroch, in General Relativity and Cosmology, Proceedings of the International School of Physics "Enrico Fermi," Course 47, ed. B. K. Sachs, Academic, New York (1971).

18. J. Kiskis, Phys. Rev. D17, 3196 (1978).

19. I. I. Bigi, Z. Phys. C12, 235 (1982); I. T. Todorov in Nobel Symposium8 ed. N. Svartholm, Wiley, New York (1968).

20. P. B. Schwinberg, R. S. Van Dyck, Jr., and H. G. Dehmelt, Phys. Rev. Lett. 7, 1679 (1981).

21. J. Bailey, et al., Nucl. Phys. B150, 1 (1979).

22. P. B. Schwinberg, R. S. Van Dyck, Jr., and H. G. Dehmelt, Bull. Am. Phys. Soc. 24, 1203 (1979).

23. F. G. Mariam, et al., Phys. Rev. Lett. 49, 993 (1982);G. Feinberg and L. M. Lederman, Ann. Rev. Nucl. Sci. 13, 431 (1963).

24. G. Bardin, et al., Phys. Lett. 137B, 135 (1984).

25. D. S. Ayres, et al., Phys. Rev. D3, 1051 (1971).

26. W. T. Ford, et al., Phys. Lett. 38B, 335 (1972).

27. Particle Data Group, Rev. Mod. Phys. 56, (1984), p. s97.

28. ibid., p. s122.

29. ibid., p. s120, s121.

30. ibid., p. s125.

31. ibid., p. s131, s132.

32. ibid., p. s126.

33. ibid., p. s132.

34. R. v. Eötvös, D. Pekár and E. Fekete, Ann. Phys. (Leipzig) 68, 11 (1922).

35. P. G. Roll, R. Krotkov and R. H. Dicke, Ann. Phys. (NY) 26, 442 (1964); R. H. Dicke, Sci. Am. 205, 84, December 1961.

36. V. B. Braginskii and V. I. Panov, Sov. Phys. JETP 34, 463 (1972).

37. J. G. Williams et al., Phys. Rev. Lett 36, 551 (1976); I. I. Shapiro, C. C. Counselman and R. W. King, Phys. Rev. Lett. 36, 555 (1976).

38. I. Estermann, O. C. Simpson, and O. Stern, Phys. Rev. 71, 238 (1947).

39. A. W. McReynolds, Phys. Rev. 83, 172 (1951); 83, 233 (1951); J. W. T. Dabbs, J. A. Harvey, D. Paya and H. Horstmann, Phys. Rev. 139, B756 (1965); L. Koester, Phys. Rev. D14, 907, (1976).

40. R. V. Pound and G. A. Rebka, Jr., Phys. Rev. Lett. 4, 337 (1960); R. V. Pound and J. L. Snider, Phys. Rev. 140, B788 (1965).

41. F. C. Witteborn and W. M. Fairbank, Phys. Rev. Lett. 19, 1049 (1967); Rev. Sci. Inst. 48, 1 (1977); Nature 220, 436 (1968).

42. Y. Fujii, Nature Phys. Sci. 234, 5 (1971); Gen. Rel. Grav. 6, 29 (1975); J. O'Hanlon, Phys. Rev. Lett. 29, 137 (1972).

43. A. Zee, Phys. Rev. Lett. 42, 417 (1979), 44, 703 (1979); K. I. Macrae, Phys. Rev. D18, 3737, 3761, 3777 (1978).

44. J. Scherk, La Recherche 8, 878, (1977); Phys. Lett. 88B, 265 (1979).

45. J. Scherk in Unification of the Fundamental Particle Intaractions, eds. S. Ferrara, J. Ellis and P. van Nieuwenhuizen, Plenum, New York, (1981).

46. G. W. Gibbons and B. F. Whiting, Nature 291, 636 (1981); P. Hut, Phys. Lett. 99B, 174 (1981); K. I. Macrae and R. J. Riegert, Nucl. Phys. B244, 513 (1984).

47. S. C. Holding and G. J. Tuck, Nature 307, 714 (1984) F. D. Stacey, G. J. Tuck, S. C. Holding, A. R. Maher and D. Morris, Phys. Rev. D23, 1683 (1981); F. D. Stacey in Science Underground, eds. M. M. Nieto et al., A.I.P., New York (1983).

48. E. Fischbach, D. Sudarsky, A. Szafer, C. Talmadge, and S. H. Aronson, Phys. Rev. Lett. 56, 3 (1986).

49. J. W. Beams, Physics Today 24, 34 (May 1971); D. R. Long, Phys. Rev. D9, 850 (1974); D. R. Mikkelsen and M. J. Newman, Phys. Rev. D16, 919 (1977); Y. T. Chen, A. H. Cook and A. J. F. Metherell, Proc. Roy. Soc. (London) A394, 47 (1984); V. K. Milyukov, Sov. Phys. JETP 61, 187 (1985).

50. C. K. Zachos, Phys. Lett. 76B, 329 (1978).

51. P. Fayet, Phys. Lett. 95B, 285 (1980).

52. T. Goldman and M. M. Nieto, Phys. Lett. 112B, 437 (1982).

53. M. L. Good, Phys. Rev. 121, 311 (1961); see also, W. Thirring, in Essays in Physics, ed. G. K. T. Conn and G. N. Fowler, Academic, New York, 1972, Vol. 4, p. 125.

54. L. I. Schiff, Proc. Nat. Acad. Sci. 45, 69 (1959); Phys. Rev. Lett. 1, 254 (1958).

55. P. Morrison and T. Gold, Essays on Gravity (Gravity Research Foundation, New Boston, NH, (1957); P. Morrison and T. Gold, On the Gravitational Interaction of Matter and Antimatter, (1956).

56. P. Morrison, Am. J. Phys. 26, 358 (1958).

57. J. H. Christenson, J. W. Cronin, V. L. Fitch, and R. Turlay, Phys. Rev. Lett. 13, 138 (1964).

58. J. Leitner and S. Okubo, Phys. Rev. 136, B1542 (1964).

59. S. H. Aronson, G. J. Bock, H.- Y. Cheng and E. Fischbach, Phys. Rev. D28, 476, 495 (1983).

60. J. Bernstein, N. Cabibbo and T. D. Lee, Phys. Lett. 12, 146 (1964); J. S. Bell and J. K. Perring, Phys. Rev. Lett. 13, 348 (1964); O. Nachtmann, Acta. Phys. Austriaca, Suppl., ed. P. Urban, Springer, Berlin, 1969, Vol. VI, p. 485.

61. L. I. Schiff and M. V. Barnhill, Phys. Rev. 151, 1067 (1966).

62. R. J. Hughes, Ann. Phys. (NY) 162, 1, (1985).

63. J. S. Bell, R. J. Hughes and J. M. Leinaas, Z. Phys. C28, 75 (1985).

64. W. G. Unruh, Phys. Rev. D14, 870 (1976).

65. A. Aspect, P. Grangier and G. Roger, Phys. Rev. Lett. 47, 460 (1981).

66. J. S. Bell, Physics 1, 195 (1965).

67. A. A. Michelson and E. W. Morley, Am. Sci. 34, 333 (1887).

II. THE GRAVITY MEASUREMENT

A. The Measurement Scale

It is common knowledge that the gravitational force is the weakest of the forces in nature. To measure the effect of gravity on antiprotons, all sources of non-gravitational force must be controlled at a level sufficient for the gravitational effects to be dominant. Because antiprotons are charged and have a magnetic moment, we can expect that the electromagnetic forces will be the principal source of difficulty. We can expect no contribution from the weak and strong interactions because of their very short range. We will now establish the scale of the electromagnetic forces relevant to the gravity measurement.

The scale of the electric fields that must be controlled can be estimated from the quantity

$$E = \left[\frac{m_p g}{e}\right] = 1.03 \times 10^{-7} \text{ V/m} . \tag{1}$$

Stray electric fields in the experiment need to be substantially less than this to observe the gravitational effects on antiprotons. The pioneering work of Witteborn and Fairbank[1] on the gravitational properties of electrons showed that with some effort stray electric fields could be controlled at the level of 10^{-11} V/m.

The scale of magnetic fields that needs to be controlled, or more precisely their gradients, can be estimated by observing that the force on a magnetic moment μ from a magnetic field is given by

$$\underset{\sim}{F} = (\underset{\sim}{\mu} \cdot \underset{\sim}{\nabla})\, \underset{\sim}{B} . \tag{2}$$

If the magnetic field is uniform in all directions but the z-direction, then

$$F = \mu_z \frac{dB}{dz} , \tag{3}$$

which acts along z. For an antiproton in a uniform magnetic field, the effective magnetic moment will be given by[2]

$$\mu_z = 2\mu_N \left(n + \frac{1}{2} \pm \frac{g_s s}{2} \right) , \tag{4}$$

where n is the orbit quantum number, μ_N is the nuclear magneton, g_s is the antiproton g-factor, and $s = \pm 1/2$. The average orbital quantum number will be set by the energy of the antiprotons and can be estimated as

$$\bar{n} = \frac{kT}{\hbar\omega_c} , \tag{5}$$

where k is Boltzmann's constant, T is the temperature, and ω_c is the cyclotron frequency

$$\omega_c = \frac{eB}{mc} . \tag{6}$$

We are assuming here equipartition of energy among the three translational degrees of freedom. For antiprotons at temperatures greater than 1 K, the n value is large compared to the other terms in Eq. 4. We have therefore that if $mg = \mu_z \, dB/dz$ then

$$\frac{\Delta B}{B} \frac{1}{\Delta z} < \frac{g\hbar e}{2\mu_N ckT} \tag{7}$$

$$\simeq 1.19 \times 10^{-3} \frac{1}{T} \, (m^{-1}) ,$$

where T is in K and Δz is in meters. The $\Delta B/B\Delta z$ we need to be concerned with then are of order 10^{-3} to 10^{-4} m^{-1} for 1 - 10 K antiprotons. For higher temperatures, still more stringent requirements will be placed on the magnetic gradient.

To set the energy scale for the measurement, we note that the gravitational potential energy difference for a distance L is given by

$$U = mgL \tag{8}$$

for L = 1 m, then the energy involved is

$$\begin{aligned} U &= 1.6 \times 10^{-26} \text{ joules} \\ &= 1.03 \times 10^{-7} \text{ eV} \\ &= 1.19 \times 10^{-3} \text{ K} \end{aligned} \tag{9}$$

This amount of energy is very small, but not unmeasurable, as we will see.

In the sections that follow, the techniques required to control the stray electric and magnetic fields are described, as well as the approaches to the measurement that enable this energy change to be determined.

B. The Time-of-Flight Technique

The time-of-flight (TOF) technique for the measurement of the gravitational properties of matter can be traced back to Aristotle[3] who erroneously reported that heavier bodies fall faster than light ones-- some systematic error in observation or theoretical prejudice, no doubt. More recently G. Galilei reported[4] the currently accepted results on the same experiment. In the modern era, the time-of-flight technique has been used by Witteborn and Fairbank[1,5-6] to measure the gravitational properties of electrons. In their approach to this technique, electrons with thermal velocities are launched vertically up a copper drift tube. The arrival at the top of the drift tube was detected by a 14-stage electron multiplier and the time of flight was recorded. Because the initial velocity of the electrons was thermally distributed, what they measured through many repetitions was the distribution function for the time of flight given a distribution of initial velocities. They also ran several measurements using externally applied electric fields which they analyzed in a similar way.

Let us consider what the TOF spectrum for particles launched vertically would be under ideal circumstances. In general, for a particle with initial velocity v_o, the time of flight either up (upper signs) or down (lower signs) a drift space of length L will be

$$t = \int_o^L \frac{dz}{\left[v_o^2 \mp 2gz\right]^{1/2}} = \frac{v_o}{g}\left(\pm 1 \mp \left[1 \mp \frac{2gL}{v_o^2}\right]^{1/2}\right) . \tag{10}$$

We know from timing considerations alone (Eq. 9) that the energies, hence the velocities, involved here for meter-like values of L must be very low. Evidently then, the value of v_o will not be a fixed value, but will be distributed according to a Maxwell-Boltzmann (MB) distribution. Assuming as before, an equipartition of energy among the three degrees of freedom, the one-dimensional distribution can be written as

$$dN(v) = \left[\frac{m}{2\pi kT}\right]^{1/2} \exp\left[-\frac{mv^2}{2kT}\right] dv , \tag{11}$$

where the velocities range from $-\infty < v < \infty$ and the distribution over this range is normalized to 1.0. We define an average velocity, v_m, in one direction as

$$\frac{1}{2} m v_m^2 = \frac{1}{2} kT , \tag{12}$$

To rewrite Eq. 11 as

$$dN(v) = \left(\frac{1}{2\pi}\right)^{1/2} \frac{1}{v_m} \exp\left[-\frac{v^2}{2v_m^2}\right] dv . \tag{13}$$

This distribution for $v \geq 0$ is plotted in Fig. II-1 for several temperatures between 2 and 10 K. The range of velocities in these distributions increases with increasing temperature whereas the likelihood for low velocities decreases. The number of particles at low velocities is an important parameter in the TOF spectrum because of the increased sensitivity to gravitational effects. Thus we can expect, generally, the lower the temperature, the better.

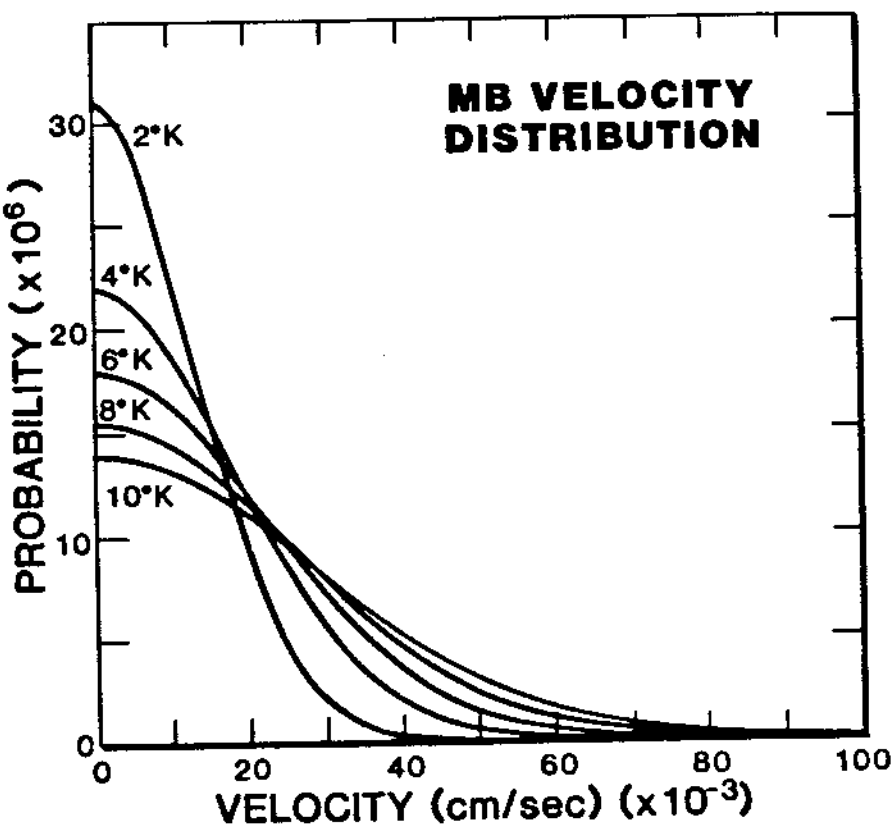

Fig. II-1. Maxwell-Boltzmann (MB) distribution of velocities for temperatures as indicated (see text also.)

The TOF spectrum resulting from a Maxwell-Boltzmann distribution of velocities can be derived by using Eq. 10 to relate t to v and dt to dv. Let us consider the TOF distribution for upward launching first. Making the appropriate substitutions, we have that

$$dN(t) = \left(\frac{1}{2\pi}\right)^{1/2} \frac{1}{v_m} \left[\frac{L}{t^2} - \frac{g}{2}\right] \exp\left[-\frac{1}{2v_m^2}\left(\frac{gt}{2} + \frac{L}{t}\right)^2\right] dt \,. \qquad (14)$$

The characteristics of this distribution can be seen by physically considering the situation: we toss a particle upward with some initial velocity; we measure how long the particle takes to rise to an elevation, L. For very large initial velocities, this time is very short. For these very short times, the above distribution is sharply peaked, as shown in Fig. II-2. In the figure, the distribution of arrival times at an elevation L = 1 m is plotted for several values of temperature between 2 and 10 K. The mean value in time (t_m) for these distributions corresponds

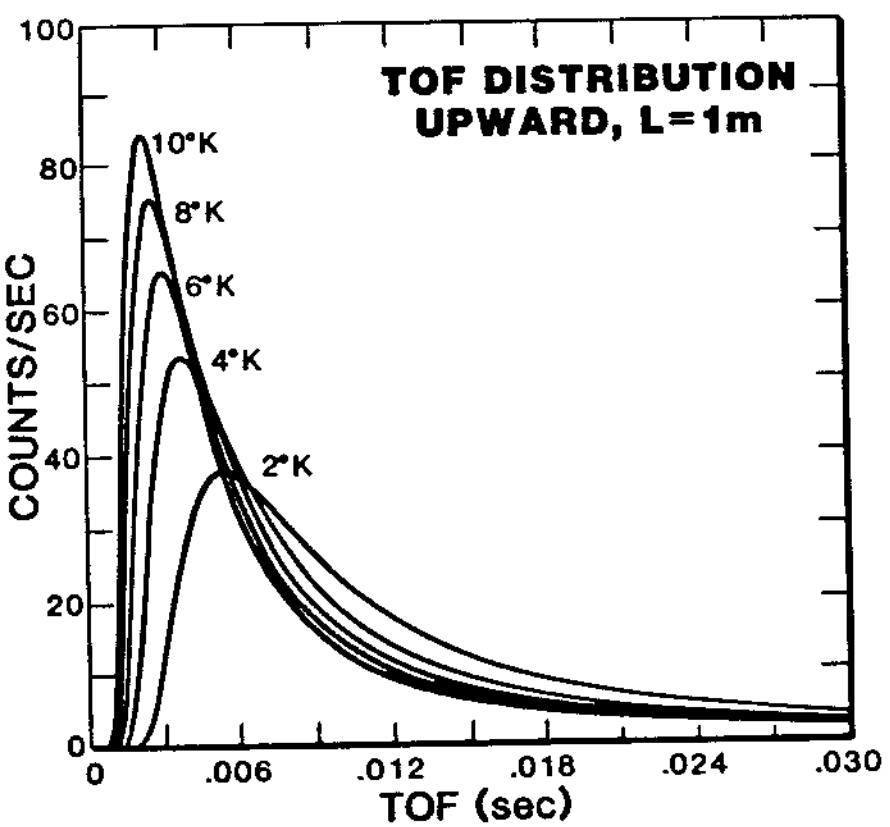

Fig. II-2. TOF distribution for upward launch using a Maxwell-Boltzmann distribution of initial velocities. The early time part of the spectrum is shown for temperatures as indicated. The drift length is L = 1 m.

approximately to the TOF for the initial velocity of v_m, the mean value of the Maxwell-Boltzmann velocity distribution. The shape of this early time peak is very insensitive to the effects of gravity, but it does allow a determination of the velocity distribution function, hence, the temperature of the launched particles.

The long tails toward late times shown in the figure arise from the low velocity component of the Maxwell-Boltzmann distribution. As the initial upward velocity of our tossed particle decreases, the time of arrival at L increases until eventually the initial velocity is just enough to make the particle reach L before it turns around and falls back down. This cutoff velocity is given by

$$v_c = (2gL)^{1/2} \quad . \tag{15}$$

Using Eq. 10, the time required to reach L is given by

$$t_c = \left(\frac{2L}{g}\right)^{1/2} \quad . \tag{16}$$

Looking back at Eq. 14, we see that at $t = t_c$ the distribution of arrival times vanishes. There are no more arrivals after $t = t_c$ because the initial velocity was insufficient to reach L. The TOF distribution function near the cutoff time is shown in Fig. II-3 for L = 1 m and several temperatures. From the figure we see that the lower the temperature, the more steeply the distribution function approaches the cutoff. For higher temperatures, there are fewer and fewer low velocity particles (see Fig. II-1 and II-2), and the distribution flattens at the cutoff. How many particles then don't make it up to the elevation L? This quantity will give an idea as to the number of particles near the cutoff point. This quantity can be calculated from the distribution function by noting that its norm for L = 0 is 0.5 as expected but decreases with increasing L to

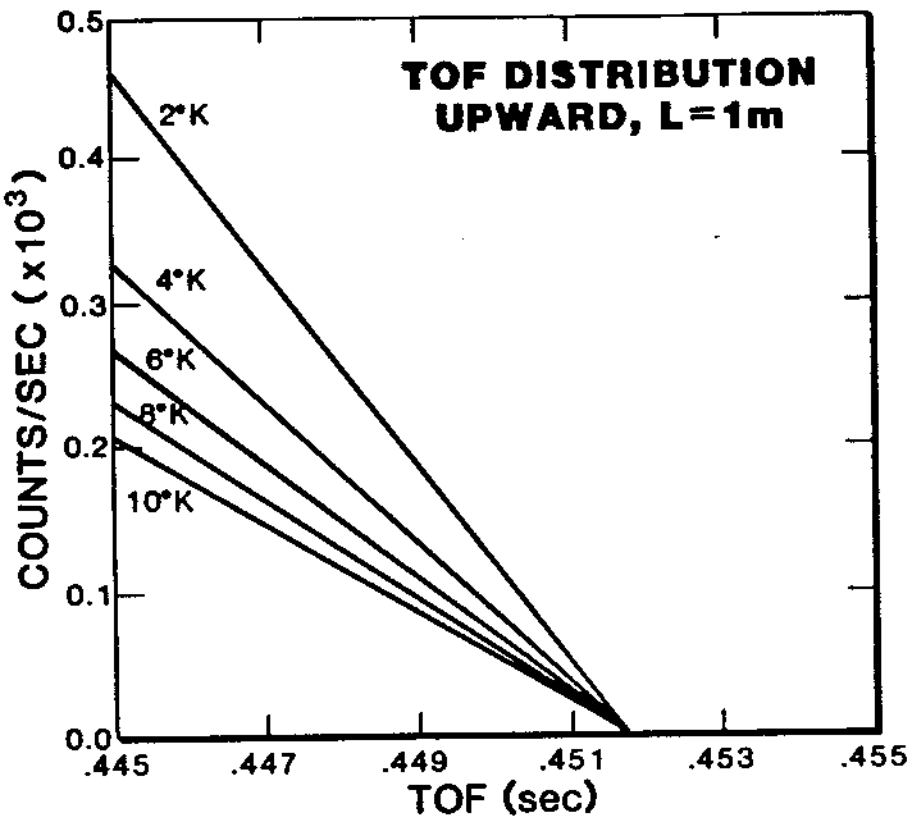

Fig. II-3 Late-time TOF distribution for upward launch using a Maxwell-Boltzmann distribution of initial velocities for temperatures as indicated. Note cutoff (see text also).

account for the lost particles. The fraction of particles going up not reaching L = 1 m is plotted in Fig. II-4 as a function of temperature. For temperatures less than 10 K, 0.5% or more of the original number of particles launched vertically do not get to L = 1 m. This is a substantial number if we start with 10^6 particles at the outset.

Let us now consider a downward launch. Making the appropriate substitutions we have that

$$dN(t) = \left(\frac{1}{2\pi}\right)^{1/2} \frac{1}{v_m}\left(\frac{L}{t^2} + \frac{g}{2}\right) \exp\left[-\frac{1}{2v_m^2}\left(\frac{L}{t} - \frac{gt}{2}\right)^2\right] dt \,. \quad (17)$$

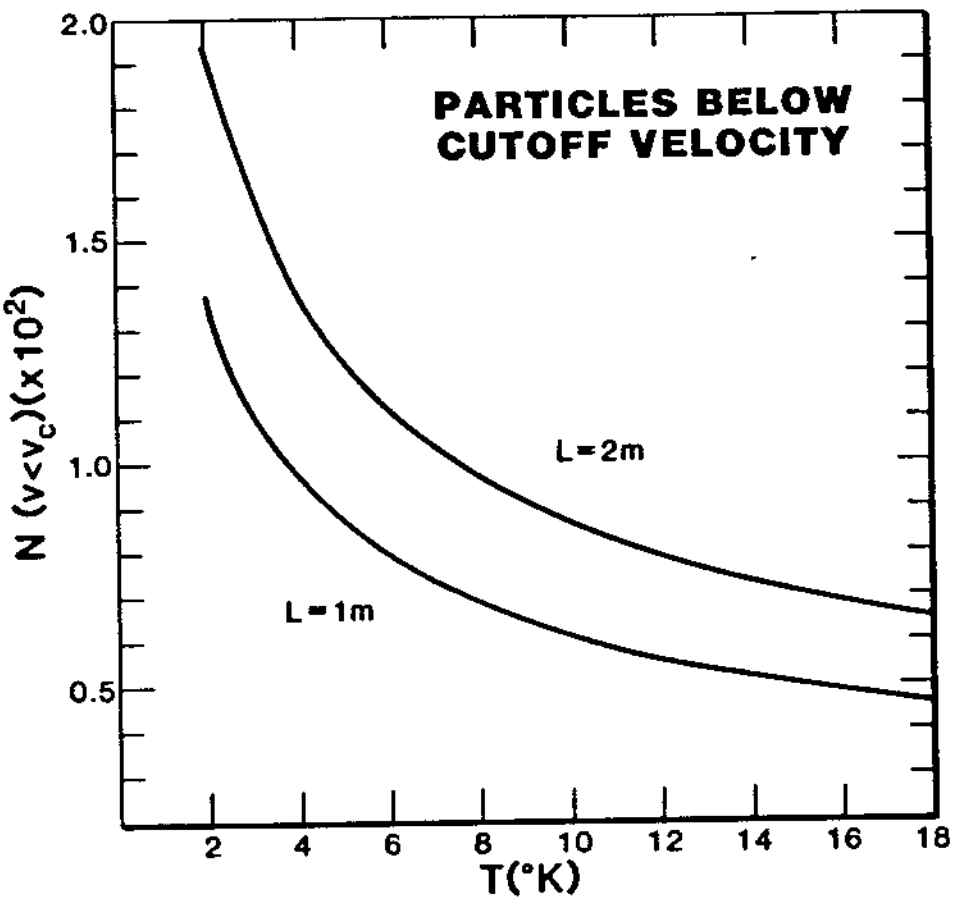

Fig. II-4. Number of particles not reaching L = 1 m launched vertically as a function of the temperature of the initial velocity distribution.

This distribution exhibits the same sharp peak at early times as before. This is shown in Fig. II-5. Once again, the distributions are highly skewed towards late arrival times, getting less so with increasing temperature. Once again, the shape of these early time distributions is very insensitive to gravitational effects, but is characteristic of the temperature of the initial Maxwell-Boltzmann velocity distribution.

The late time behavior of the downward launch TOF spectrum is very different from the behavior at late times for upward launch. For downward launch, the latest-arriving particles started at z = 0 with an initial velocity v = 0. We ignore for the moment those particles that started upward with very low velocity and turned around to fall eventually to z = L = 1 m. For the particles with v = 0 at z = 0, the TOF downward will be

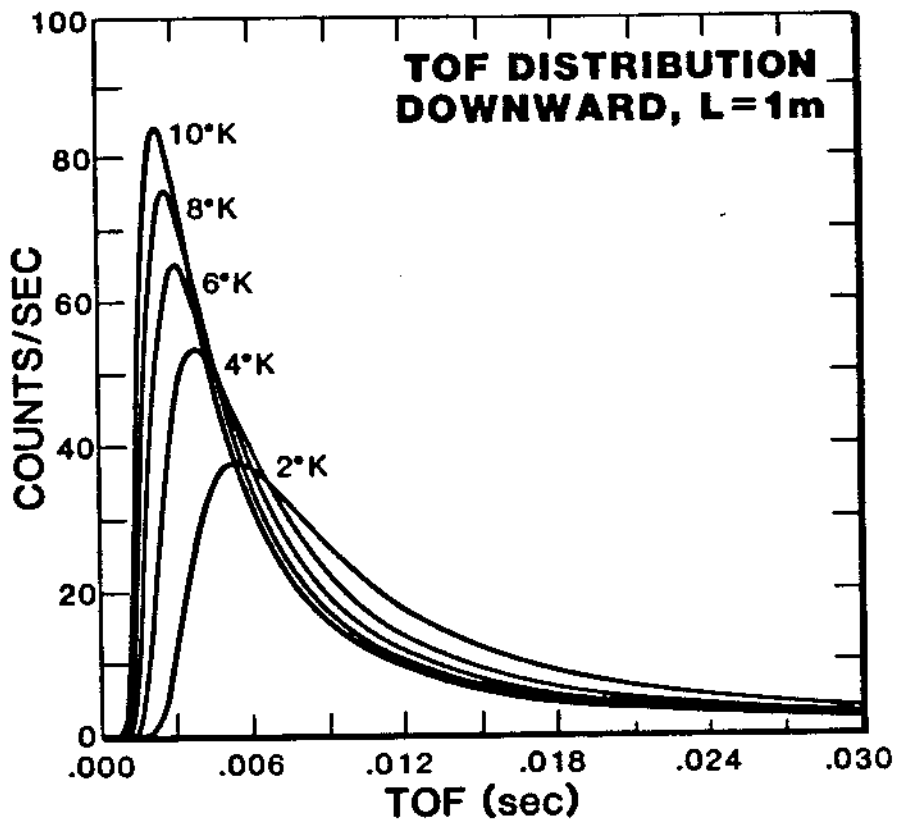

Fig. II-5. TOF distribution for downward launch using a Maxwell-Boltzmann distribution of initial velocities. The early time part of the spectrum is shown for temperatures as indicated. The drift length is L = 1 m.

$$t_c = \left(\frac{2L}{g}\right)^{1/2} \quad . \tag{18}$$

The cutoff time is the same as in the vertical spectrum but the character of the distribution at the cutoff is very different from before. The late-time behavior of the downward TOF spectrum is shown in Fig. II-6 for several temperatures of interest. In this case, the distribution flattens out at an amplitude decreasing with increasing temperature, and abruptly drops to zero at the cutoff time. For all temperatures, the particles that rose briefly and turned around to arrive at z = L sometime later will

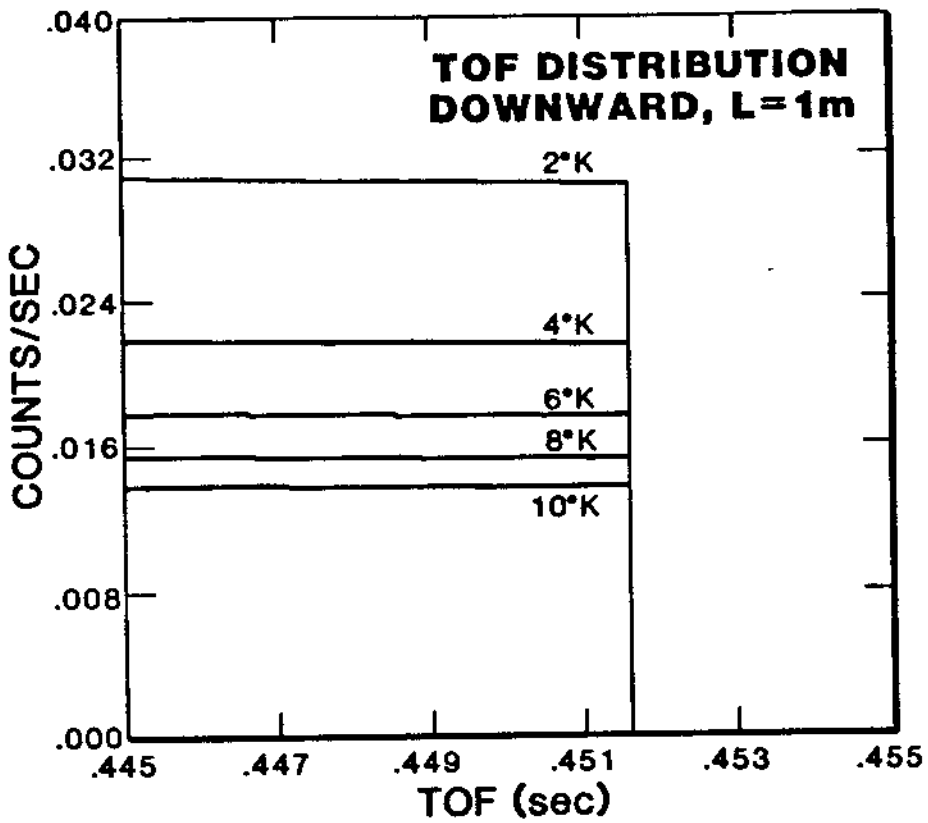

Fig. II-6. Late-time TOF distribution for downward launch using a Maxwell-Boltzmann distribution of initial velocities for temperatures as indicated. Note cutoff (see text also).

extend this cutoff by a calculable small amount, and are an additional concern with the downward launch approach. However, this is a controllable quantity in the experimental design.

In the TOF approach with a Maxwell-Boltzmann distribution, one is looking at endpoints of TOF distributions where the sensitivity to the gravitational effect is most pronounced. Let us consider now, alternatives or modifications of this approach. Witteborn and Fairbank modified the TOF spectrum by applying a current through the length of their copper drift tube. A similar approach could be used for the antiprotons. The potential in the case of antiprotons that just balances the force of gravity is of order 10^{-7} V/m (see Eq. 1). For a 1-m copper drift tube, a resistance of

$\sim 10^{-7}$ Ω can be obtained at 4.5 K (Ref. 1). The current then needed to sustain such a potential drop over this distance is given by

$$I = \frac{V}{R} \simeq 1 \text{ A} \quad . \tag{19}$$

A current of 1 A or even a 10^{-3}-A current can be regulated to very high precision. Thus, the net acceleration can be changed at will by applying this external current with very good precision.

The effect of this externally applied force can be seen by rewriting Eq. 10 to include the externally applied field (considering upward launch only)

$$t = \int_0^L \frac{dz}{\left[v_o^2 - 2 \left(g \pm \frac{qE}{m} \right) z \right]^{1/2}} \quad . \tag{20}$$

In this equation we have assumed that $V(z) = \pm zE$ where E is a fixed electric field value. By adjusting the magnitude and direction of E, the net acceleration can be reduced to zero or can be made so large that few particles will reach an elevation of 1 m. The effect of increasing the net acceleration by 50% in the TOF distribution for upward launch is shown in Fig. II-7 for late times. The net effect of this is to cut off the distribution earlier than under normal circumstances. The character of the distribution is the same as with only gravity, but the slope of the distribution function coming into the cutoff is steeper (see Fig. II-3 for comparison). In principle, the electric field can be adjusted to increase significantly the effective force. This will be useful in the calibration and the measurement because the current can be regulated with adequate precision.

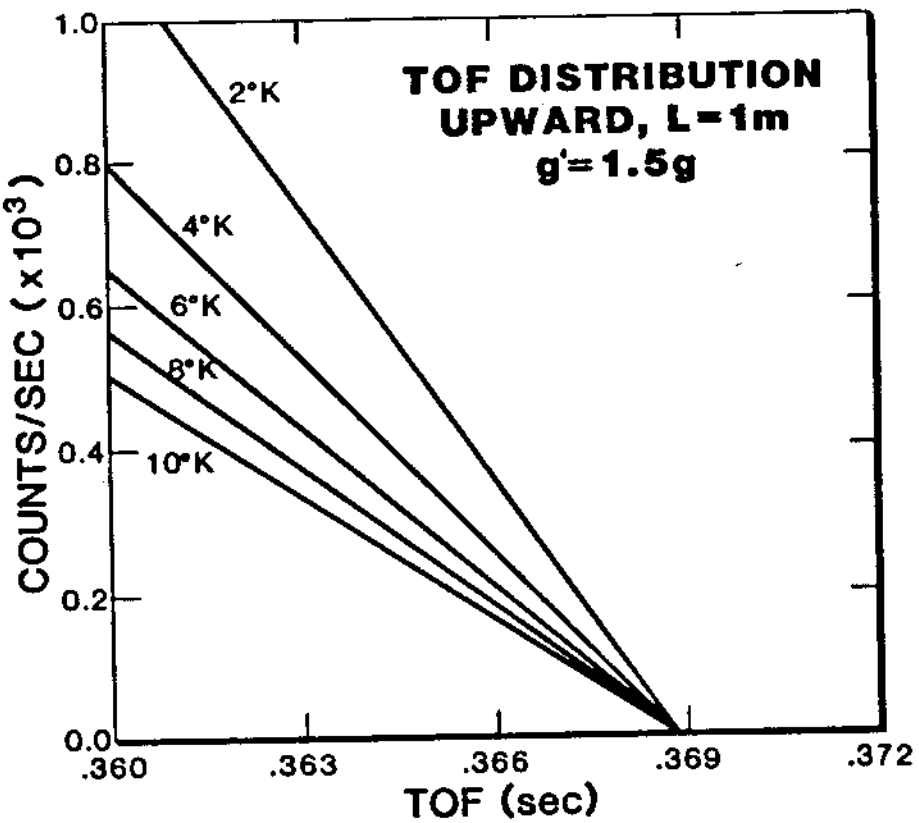

Fig. II-7. Late-time TOF distribution for upward launch using a Maxwell-Boltzmann distribution of initial velocities for temperatures as indicated. The net force is increased by 50% due to an externally applied electric field (see text also).

C. Calibration with an H^- and Proton Source

Absolute measurements of gravitational effects, although important, are not among the goals of our experiment. Rather, we propose to test the universality of free fall for antiprotons relative to protons. Supergravity theories are presently unable to predict absolute values of gravitational acceleration for elementary particles, but they do predict that antiprotons will fall faster in the Earth's gravitational field than will protons (by as much as three times faster in theories with both vector and scalar partners to the graviton). This is, in essence, a relative statement. We propose, then, to calibrate our equipment using protons or H^- particles. An input parameter in this calibration process will be the local gravitational acceleration at CERN[7]

$$g = 980.735 \text{ cm/sec}^2 \quad .$$

With this advance knowledge, the TOF spectrum of these particles can be measured and used to determine all non-gravitational effects in the apparatus. Naturally, these effects need to be controlled in the experimental design as much as possible. However, their net effect on antiprotons can be determined using "other particles." This is true to the extent that these "other particles" simulate the interaction of the antiprotons with the non-gravitational effects. To preserve the comparison of baryon and antibaryon, these "other particles" should be baryons so that the gravitational effects are calibrated for baryon-like interactions. But for non-gravitational effects, these "other particles" should mimic antiprotons identically. Because these non-gravitational effects are electromagnetic in character, the "other particles" should have the same charge and magnetic moment as the antiproton. Naturally, such a particle, other than the antiproton itself, cannot exist. However, the H^- ion, fortunately, has the same charge and nearly the same magnetic moment as the antiproton. The reason for the charge similarity is obvious; the reason for the magnetic moment similarity is somewhat subtle. The two electrons in the H^- ion are coupled to spin zero, but because of the coulomb repulsion between them, they are anti-correlated in their orbits. This anticorrelation leads to diamagnetism for the H^- ions (and helium also).[8] Thus, the magnetic moment arising from the electrons in the H^- ion is an induced effect which increases linearly with increasing magnetic field strength. The total effective magnetic moment of the H^- ion in a magnetic field is given by:

$$\mu_I = 2\mu_N \left(n + \frac{1}{2} + \frac{g_p s_p}{2} \right) + s g_e \mu_e$$

$$= \left(1.384 \times 10^{-16} \frac{T}{B} + 1.65 \times 10^{-30} B \right) \frac{\text{ergs}}{\text{Gauss}} \quad . \qquad (21)$$

If we take T ~ 10 K and B = 6×10^4 Gauss, this gives

$$\mu = (2.3 \times 10^{-20} + 9.9 \times 10^{-26}) \ \frac{\text{ergs}}{\text{Gauss}} \ . \qquad (22)$$

Evidently, the orbital contribution involving the nuclear moment dominates over the electron contributions for all n values.

The H^- ion will mimic the behavior of the antiproton in electric and magnetic fields, allowing us to calibrate these effects fully. Additionally, D^- or other negative ions with different masses can be used in the calibration process as a further check on the electromagnetic effects present in the drift space. Further calibration tests are available by using positive ions with behavior we should be able to predict if we understand the negative ion behavior, and the process for changing polarities in the trap/detector systems. Once the electric effects are solidly understood, it should be possible to again check the magnetic gradient effects.

In addition to being the calibration standard for the drift space, H^- ions can also be used to test the low-energy beam line and ion trap system. Thus, we can tune these systems for maximum transmission before antiprotons are used. We propose, therefore, to incorporate in our experimental setup, an H^- ion source with the appropriate energy to test the beam line and ion trap systems. However, because we feel at present that a possible electron cooling stage could strip the H^- ion, rendering it neutral, we propose also to have the capability to produce H^- ions at low temperatures internal to one of the traps in the system. These particles can then be used to test the drift space, independent of the low-energy beam line.

Finally, we need to consider the detection of H^- ions and antiprotons. Naturally, it is important to detect these particles in the same device so that the stray field effects on the drift time are the same. Because of their very low velocity, the H^- ions will not be detectable in devices such as scintillators, although antiprotons could be readily detected in this way. The device of choice, we feel, is the microchannel plate (MCP). This device has very high gain and extremely fast time response as well as being relatively insensitive to magnetic fields. MCPs can detect low-energy H^-

ions as well as antiprotons. In addition, specially designed MCPs have detection efficiencies near 100%.

D. Sources of Systematic Errors

We emphasize again that the experiment we propose is a relative measurement of the gravitational force on the antiproton using the H^- ion, as a calibration standard. Thus, systematic effects that will lead to errors in the measurement arise from the constancy of effects over the measurement interval including the calibration period. A very precise knowledge of the time dependence of these effects is also required. Nevertheless, the experimental design must be laid out carefully enough so that the gravitational effects are measurable. This means, in essence, that the stray electric and magnetic effects must be controlled at levels indicated in Section II-A. In this section we discuss the methods and options we will use in our final experimental design.

1. Electrostatic Effects. The gravitational force acting on an antiproton at the Earth's surface is equivalent in magnitude to the electrostatic force between two antiprotons separated by 12 cm or to the force between an antiproton and its image charge in an infinite conducting plane 6 cm away. This is in contrast to the case for the electron where distances involved are 5 m and 2.5 m, respectively.

We plan to use a grounded cylindrical conducting tube to shield the drift space from stray electric fields.[9] On the axis of an ideal drift tube of infinite extent, there are no electric fields. Because the drift tube we will use is of order 1 to 2 m in length, the effect of the closed ends needs to be considered in its design. The electric field due to the presence of these closed ends can be found using standard Green's function techniques for solving Laplace's equation in cylindrical coordinates.[10] Assuming that the length of the drift tube, h, is larger than its diameter, 2a (it is a tube, after all), the electric field on axis is given by

$$E(z) = \frac{q}{\pi\varepsilon a^2} \sum_{i=1}^{\infty} \frac{1}{\left[J_1(u_i a)\right]^2} \left[e^{-2u_i z} - e^{-2u_i (h-z)} \right] , \qquad (23)$$

where the quantity $u_i a$ is the i^{th} zero of J_o ($J_o(u_i a) = 0$). A plot of this electric field versus distance from one end is shown in Fig. II-8 for 2-cm and 4-cm tube diameters. From the figure, it is evident that, for distances greater than about a tube diameter, the drift space is essentially field free. The end effects will, however, slightly shift the TOF distribution cutoff. This slight shift will be the same for H^- ions and antiprotons and can be calibrated out.

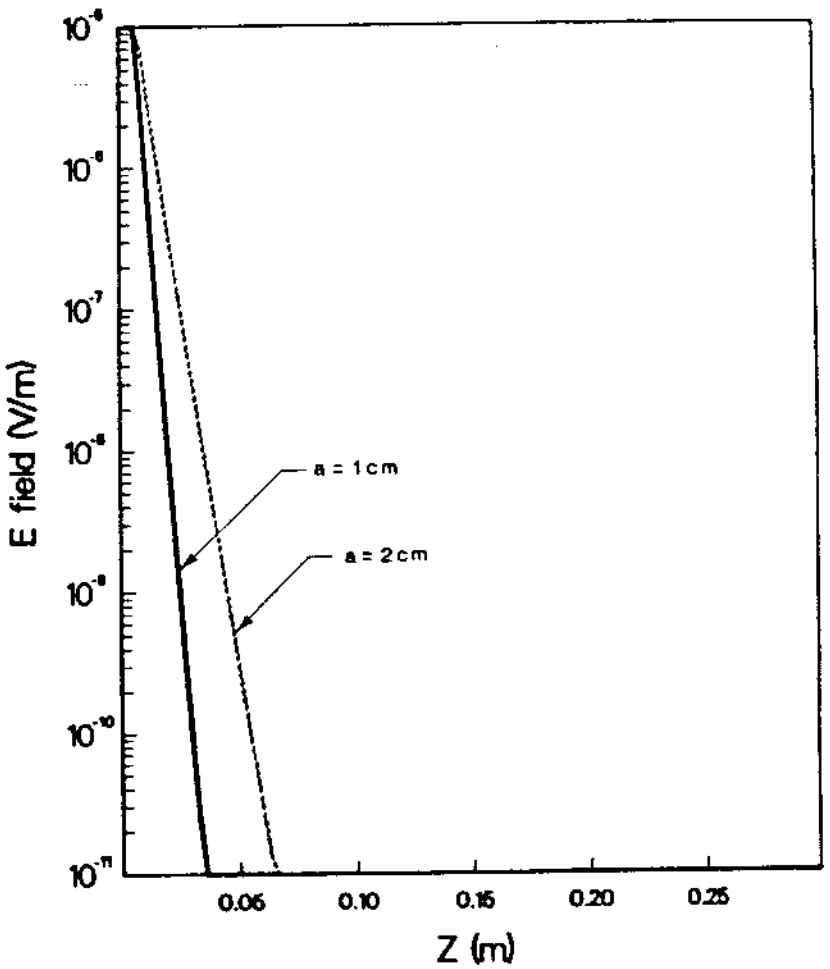

Fig. II-8. The electric field felt by a unit charge in a 1-m drift tube with closed ends as a function of distance from one end. The tube diameters are as indicated. The field is symmetric at the other end (z ~1 m).

Having only closed ends at the end of the drift tube is an idealized situation. In practice, the ends of the drift tube may not be at the same potential as the walls. This is due in part to contact potentials, but, more importantly, to the field penetration from the rather high electric field sources at the ends of the drift tube, the trap, and the MCP detector. Depending upon the launching technique, the ion trap in practice could be at zero potential. Let us concentrate then on the MCP end. The field penetration can be estimated by modelling the MCP as a charged conducting disc placed at the end of an otherwise grounded, closed, conducting cylinder. Taking the voltage on this disc to be V_b and its radius to be b, the additional electric field felt by a unit charge a distance z away from the disc is given by

$$E_e(z) = \frac{2V_b b}{a^2} \sum_{i=1}^{\infty} \frac{J_1(u_i b)}{\left[J_1(u_i a)\right]^2} e^{-u_i z} , \qquad (24)$$

where $u_i a$ and $u_i b$ are the i^{th} zeros of J_0 as before, and a is the drift tube radius. The effect of the closed end at z = h is vanishingly small at z ~ 0 and has been eliminated in the above expression. This additional electric field is plotted in Fig. II-9 for b = 1 mm and V_b = 10 V. From the figure it is evident that the field penetration needs to be controlled at the MCP end of the drift tube. This can be accomplished with specially designed MCPs incorporating a shielding grid. In any event, the MCP operating voltage will be controlled to high precision in the experimental setup and will be the same for the H^- ion and the antiproton. Thus, it can be calibrated out of the system.

We have presumed thus far that the H^- ion or antiproton has been precisely on the axis of the drift tube. The particle can, in principle, be guided away from the axis by the guide magnetic field lines if there is a misalignment or by the residual transverse momentum from the magnetron motion at launch time. To determine the effect of such a deviation, it is necessary to calculate $\Delta v/\Delta r$ where Δr is the distance of the particle from the axis. The calculation of $\Delta v/\Delta r$ from the Green's function in cylindrical cordinates involves a double infinite summation over products

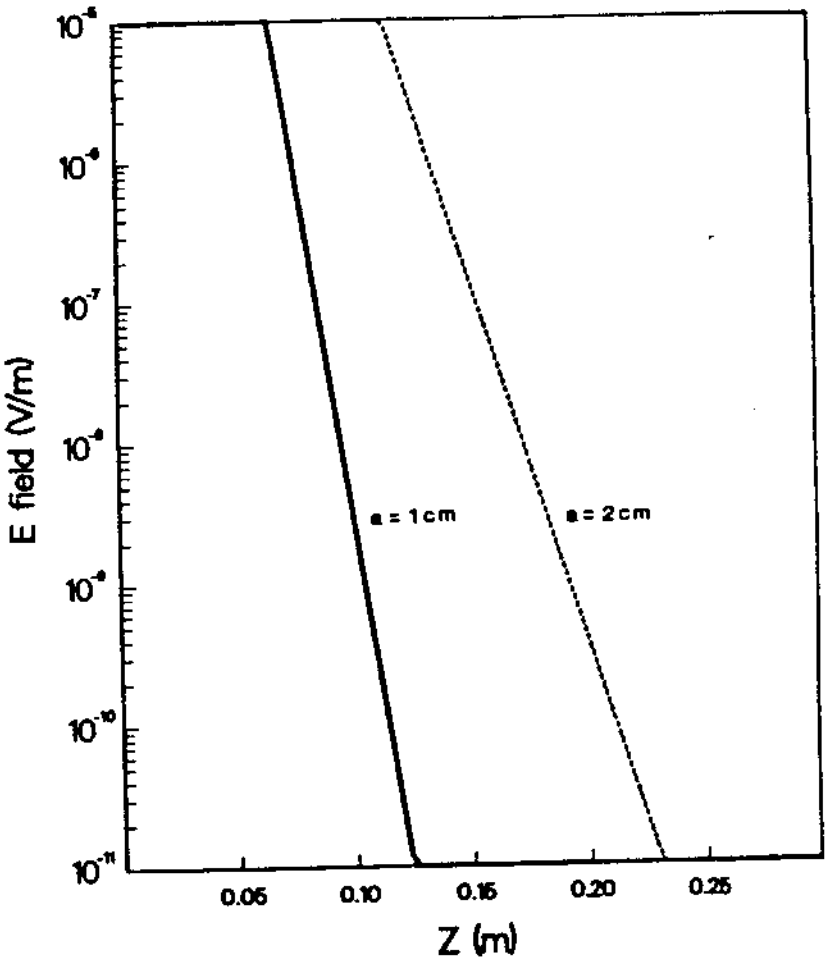

Fig. II-9. The additional electric field felt by a unit charge due to field penetration simulated by a 1-mm disk at 10 V as an example (see text also).

of Bessel functions and requires the removal of the singularity resulting from the point charge itself. This calculation, along with accurate field modeling of all electrostatic effects, is underway. Let us for the moment set the scale of this quantity ($\Delta v/\Delta r$) by calculating the work required to displace a unit charge a distance r from the center of a sphere of radius a. This is readily done using the method of images to give

$$W = \frac{qr^2}{8\pi\varepsilon a^3} \quad . \tag{25}$$

For a 2-cm-diameter drift tube, this estimate shows that $r \leq 0.4$ cm is required to keep the electrostatic effects less than 10% of the gravitational ones. For a 4-cm diameter drift tube, r must be less than 1.1 cm. These dimensions are still larger than the active size of the detector by some factor. Therefore, this effect is of little consequence to the measurement. However, once again, it will be the same for H^- ions as antiprotons and can be calibrated out of the system.

If the tube diameter varies, the particle will be attracted to the smaller-diameter sections and repelled from the larger-diameter ones. If the H^- ion or antiproton passed from a very long cylinder of radius a to a slightly larger one of radius (a + da), the resulting change in potential energy would be aproximately

$$\Delta W = \frac{qda}{8\pi\varepsilon a^2} \quad . \tag{26}$$

To keep this change less than the gravitational effect over 1 m requires that, for a 2-cm-diameter drift tube, $da \leq 1.5$ cm. Because the anticipated precision for the drift tube diameter is better than 2×10^{-2} cm, this effect only contributes less than 1% and again can be calibrated with H^- ions.

The last electrostatic effect we consider here is the influence on each other of antiprotons travelling in the drift tube. If we consider the antiprotons arrayed in a line on the axis of the drift tube, then this effect can be estimated from the expression for the electric field a distance z_1 from a point charge on the axis of a cylinder:

$$E_p = \frac{q}{2\pi\varepsilon a^2} \sum_{i=1}^{\infty} \frac{e^{-u_i z_1}}{\left[J\,(u_1 a_i) \right]^2} \quad . \tag{27}$$

To keep this effect a small fraction of the gravitational one, $z_1 > 2.5a$ where a is the drift tube radius. This effect then suggest that the tube radius be as small as possible so that bunches of particles can be accommodated. We will develop several drift tubes and launching techniques and will study this effect in some detail. In any event, as long as the linear density of H^- ions and antiprotons are the same, this effect can be calibrated out. A uniform launching technique can assure this.

2. Magnetostatic Effects. Magnetic fields are used to supply the transverse restoring force in the ion traps. Additionally magnetic fields will be used to guide the orbits of the launched particles to remain on the axis of the drift tube. We plan to use persistant superconducting magnets for the entire ion trap/drift tube system. These magnets once energized and disconnected from the power supply have a persistance of $\Delta B/B\Delta t = 10^{-8}$ per hour. This is a more than adequate time stability, but additionally the time dependence is well known and can be corrected for if necessary.

The more important magnetic effect arises from field gradients. As discussed earlier (see Section II-A), the degree to which the antiprotons or H^- ions will couple to these gradients depends upon the cyclotron orbit level for the particle. In Section II-A, a relationship between field gradients and temperature was established (Eq. 7), assuming that the resulting force should be less than the gravitational force. From that relationship, for a 10 K antiproton, the field gradients need to be controlled to the level

$$\frac{\Delta B}{B\Delta z} < 1.2 \times 10^{-4} \ (m^{-1}) \ . \tag{28}$$

However, commercially available solenoids can be tuned using shim coils to be uniform to $\Delta B/B \sim 5 \times 10^{-5}$ over essentially any length.[11] This is about ten times less than the field gradient in Eq. 28. The effect is then far less than the effect of gravity.

Nevertheless, the residual field gradients will modify the TOF distributions discussed in Section II-B. The degree of modification will depend upon the cyclotron orbit level of the antiproton or H^- ion. Because the populations of these levels are statistically distributed, for each

value of the axial velocity, hence for each TOF value, the magnetic effects will be distributed according to the cyclotron level population. Thus, each TOF value will be smeared out slightly. The net effect of this is to change the shape of the TOF distributions at the endpoints.

Let us estimate the magnitude of this distribution effect. Assuming that the cyclotron levels are in thermal equilibrium, the distribution function can be written as

$$P(n,s) = \frac{1}{Z_{ROT}} \exp\left[\frac{-2\mu_N B}{kT}\left(n + \frac{1}{2} + \frac{g_s s}{2}\right)\right], \qquad (29)$$

where

$$Z_{ROT} = \frac{\exp\left[\frac{-\mu_N B}{kT}\left(1 + \frac{g_s s}{2}\right)\right] + \exp\left[\frac{-\mu_N B}{kT}\left(1 - \frac{g_s s}{2}\right)\right]}{1 - \exp\left[\frac{-2\mu_N B}{kT}\right]} \qquad (30)$$

In the above expressions Z_{ROT} is the rotational part of the partition function, μ_N is the nuclear magneton, B is the applied magetic field, T is the equilibrium temperature, s is the spin state $\pm 1/2$, and $g_s = 2.79$ for antiprotons. For H^- ions there is an additional term as discussed in Section II-A due to the incomplete cancellation of the electron spins. This is a small effect, as discussed earlier and can be corrected for. This distribution function for several temperatures between 1 K and 10 K is shown in Fig. II-10. The ambient magnetic field in the figure is 50 kG. From the figure, it is evident that the lower the equilibium temperature, the narrower the distribution of n values. For all temperatures the importance of spin up or spin down is only apparent for very low n values.

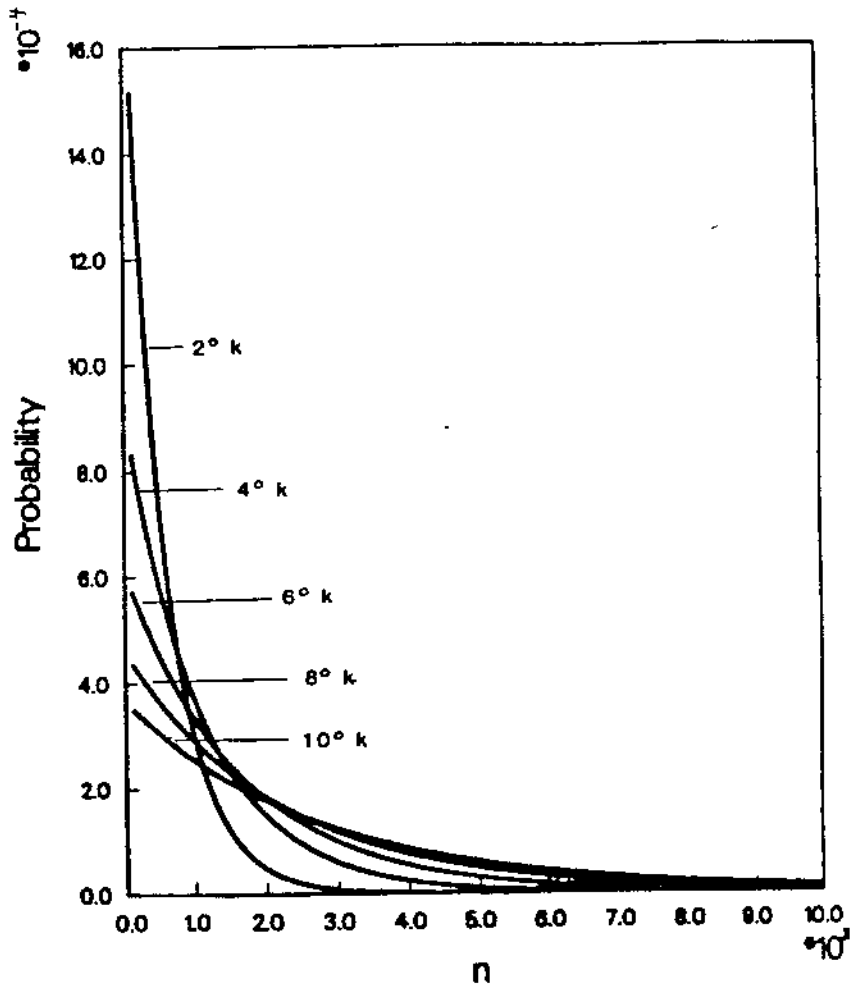

Fig. II-10. The distribution function for cyclotron levels in a 50-kG field for temperatures as indicated. The spin states have been averaged.

Figure II-11 displays the distribution function at 10 K for several values of the magnetic field as indicated. From this display it is evident that the higher the magnetic field, the narrower the distribution of n values.

The smaller the range of n values involved in the measurement, the smaller the effect on the endpoint of the TOF distribution function. The range in n values can be reduced by going to lower temperatures or higher ambient magnetic fields (see Figs. II-10, II-11). Getting to low temperatures is a priority in the experiment for many reasons, including the magnetic effects.

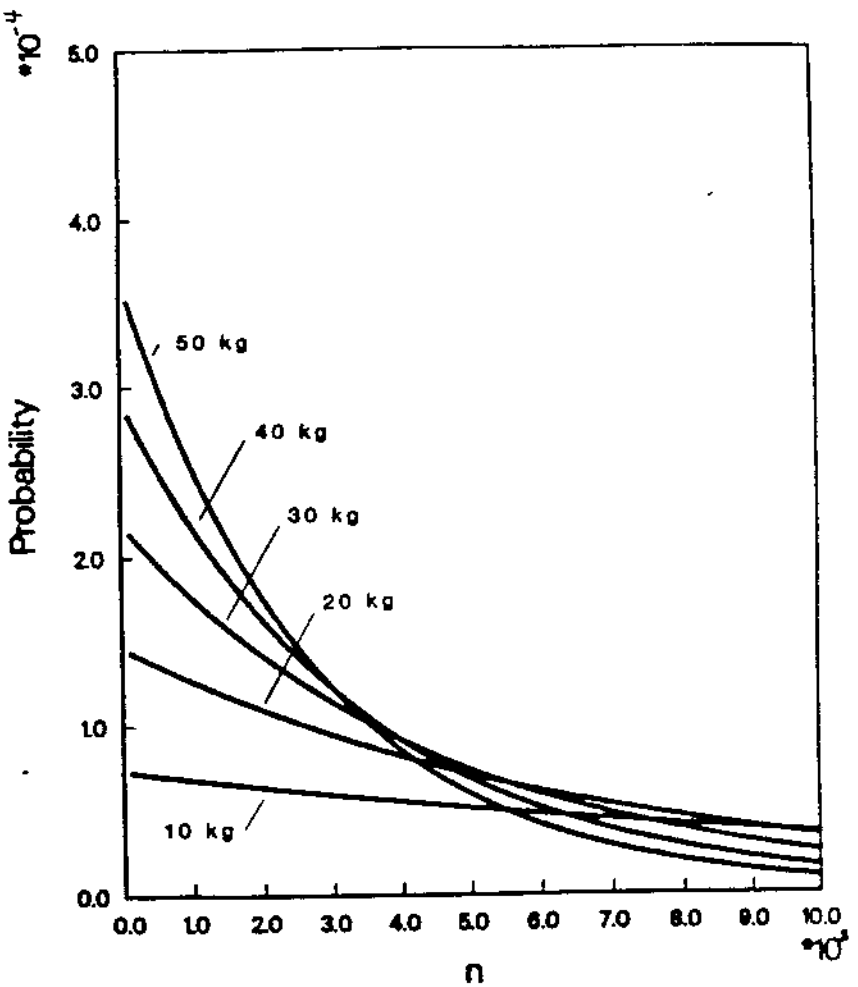

Fig. II-11. The distribution function as 10 K for ambient magnetic fields as indicated.

The effect of the cyclotron level distribution function on the TOF endpoint for upward launch over a 1-m flight path is shown in Fig. II-12. In the figure the equilibrium temperature was taken to be 10 K and the ambient magnetic field was 60 kG. The TOF distribution with no gradient effect is also shown. From the figure it is seen that the magnetic gradient effects change the shape of the TOF distribution at the endpoint, whereas the slope of the TOF distribution approaching the endpoint region

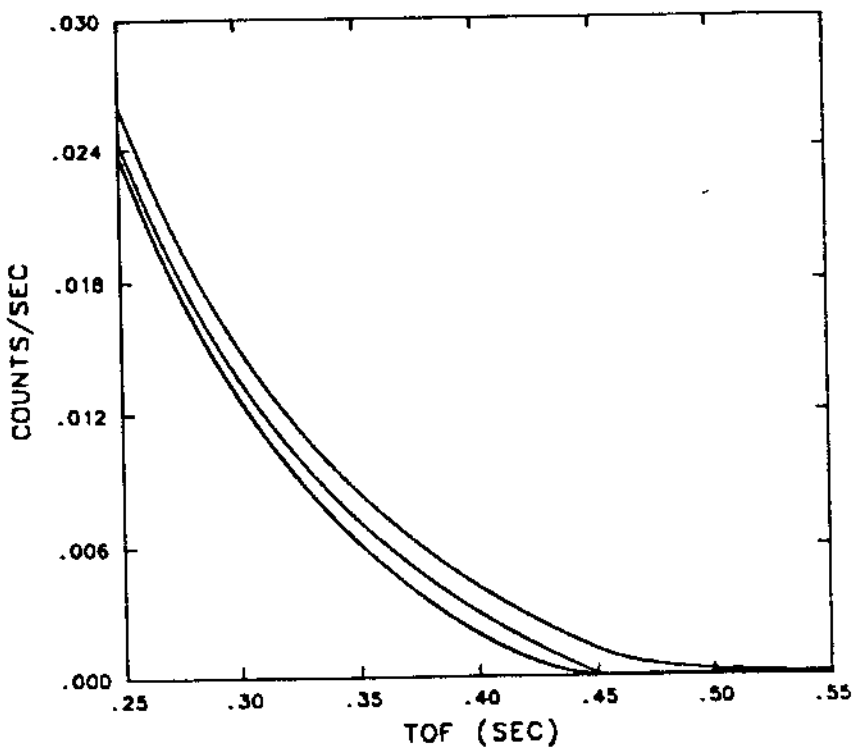

Fig. II-12. The TOF distribution function for upward launch over a 1-m flight path. The endpoint region is shown for no magnetic gradient (central line) and $\Delta B/B = 4.0 \times 10^{-5}$ pointng upward (top line) and downward (bottom line). The equilibrium temperature of the particles is 4 K in a 60-kG ambient field.

is only slightly affected. Because of this feature, because the field gradients can be mapped out to very high precision (~2 Gauss) and because the H^- ion is the calibration standard, it is possible to unfold or deconvolute the gradient effects in the analysis of the TOF distribution data. This deconvolution approach and its dependence on temperature, ambient field, drift length, and the H^- ion correction factor is currently under study using Monte Carlo techniques.

Because of the capability to map the field gradients and to unfold the effects in the final analysis the magnetostatic effects can be controlled at a suitable level for the gravity measurement.

3. The Patch Effect. Although the drift tube discussed thus far has been considered to be a good conductor, the surface of even the best of conductors is not everywhere at the same potential. The surface of metallic conductors (usually) is composed of tiny crystal faces or "patches" which can have contact potential differences of V ~ 0.1 V (Ref. 12). These differences can be interpreted in terms of a dipole layer of charge according to the theory of Bardeen.[13] Let us consider then, that only two patch potentials exist: +0.1 V and -0.1 V. We first assume that the two kinds of patches are present in about equal numbers but with local statistical fluctuations. Out of N patches randomly chosen from the two possible types, the probable excess of one type over the other is $\sqrt{N}$. Consider a group of N_1 patches at equal distances r_1 from a test charge. The potential from each patch is either $+\phi(r_1)$ or $-\phi(r_1)$. The probable difference of the potential from the average (i.e. zero) is just $\pm\sqrt{N_1}\phi(r_1)$. Let N_i be the number of patches at distance r_i from the test charge. The probable fluctuation in the total potential felt by the test charge as is moves along is given by

$$\Delta\phi = \left[\sum_i N_i \phi^2(r_i) \right]^{1/2} = \left[\int \phi^2(r)\, dN(r) \right]^{1/2} . \qquad (31)$$

Further, let A be the area of each patch, τ be the surface dipole moment, a be the radius of the drift tube, and z be the distance along the drift tube axis. For ϕ due to dipole double layers we have

$$\phi = \frac{Aa\tau}{4\pi\varepsilon\left(a^2 + z^2\right)^{3/2}} . \qquad (32)$$

The number of patches between z = 0 and z = z is $N(z) = 2\pi az/A$, so

$$dN(z) = \frac{2\pi a}{A}\, dz . \qquad (33)$$

Thus the total fluctuation change felt by the test charge is:

$$\Delta\phi^2 = \frac{3A\tau^2}{8\varepsilon^2 a^2} \tag{34}$$

Where Eqs. 33 and 34 have been substituted in Eq. 32. In annealed OFHC copper, typical crystal sizes are about 4.5×10^{-5} m (Ref. 14). Using a 1-cm radius drift tube and taking $\tau/\varepsilon_o = 0.1$ V yields $\Delta\phi = 2.76 \times 10^{-4}$ V: a substantial potential variation on the gravitational scale. However, taking the above patch size does not take advantage of the enormous progress made in thin film deposition techniques and surface physics since the original study of the patch effect by Witteborn and Fairbank in 1968. Process techniques have been developed that will reduce the crystal size for metallic surface coatings to less than the lattice constant.[15] Thus, truly amorphous coatings of metal are possibe. These new coating techniques take advantage of collisional cascade effects on surface coating growth.[16] These effects arise in ion beam deposition of material when a second beam of inert and non reactive ions is also incident on the substrate to be coated.[17] The collisional cascades thus induced suppress crystal formation. In the light of this new coating process, which we will use in the construction of the drift tube for the gravity experiment, we estimate the fluctuations to be at the $\Delta\phi = 5.5 \times 10^{-10}$ V, where we have taken the patch size to be equal to the lattice constant for copper, 3.6×10^{-10} m, and the drift tube radius is 2 cm. At this level the fluctions are small compared to gravity.

Thus far we have estimated the patch effect based on a random distribution of dipole elements. If these elements were arrayed in an orderly pattern an analysis based on the work in Ref. 12 shows that the fluctuations will be given by

$$\phi_{max} - \phi_{ave} = \frac{0.1}{2\pi} \exp\left[\frac{-2\pi z\sqrt{2}}{x}\right] \text{ V} , \tag{35}$$

where x is the dimension of the patch and z is the distance above the plane of patches. We have that for z = 1 cm, x = 0.1 cm (a <u>very</u> large patch)

$\Delta\phi = 4 \times 10^{-41}$ V. It is unlikely that the patches could be completely periodic but any periodicity would enormously reduce the effect.

Yet another effect that reduces the importance of the patch effect is the adsorption of gases on the surface of the drift tube. This includes effects from condensation of gases at cryogenic temperatures[18] as well as chemical combinations on the surface due to oxide formation.[19] The measurements accomplished by Lockhart, Witteborn and Fairbank[18] indicating patch effect contributions plummeting at ~7 K is indeed suggestive of the condensation mechanism for suppression. In that work they report an ambient field of $\sim 10^{-10}$ V/m at 4 K. For the antiprotons, this is small compared to gravity. However the patch effect will influence the H^- ion in the same way as the antiproton. Thus the effect can be calibrated out of the system using the H^- ion. The patch effect will be studied by our collaboration as part of the drift tube development (see Section III-F).

4. The Electron Sag Effect. The notorious "Electron Sag" effect that came to light after Witteborn and Fairbank had started their measurement of the gravitational effect on electrons,[1,5,6] is the least problematical of the systematic effects for the antiproton measurement. This effect was first reported by Schiff and Barnhill[20] in 1966 shortly after F.C. Witteborn had passed in his thesis. In this work it is pointed out that the electrons in the conduction band of a copper drift tube will "sag" toward the bottom due to gravity. The resulting redistribution of charges in the copper will generate an electric field that would move an electron on the drift tube axis with an acceleration equal and opposite to that of gravity. Thus the net force felt by an electron in the drift tube would be zero. For a positron, the force would be twice that of gravity. In general, in the drift tube a charged particle will experience an acceleration

$$g_{eff} = g\left(1 - \frac{Qm_e}{eM}\right), \tag{36}$$

where Q and M are the charge and mass of the particle. Whereas for electrons this is a 100% correction, for antiprotons this effect is a 5×10^{-4} correction.

5. The Lattice Sag Effect. After the electron sag effect was pointed out, it was observed that the lattice of the metal would also sag under the gravitational force. A strain-induced change in the work function was hypothesized[21] and later observed under special conditions.[22] This lattice sag hypothesis was the result of requiring charge neutrality in the metal in addition to the Schiff-Barnhill sagging of the electrons. Consider a column of metal standing vertically in a gravitational field. The metal at the base of the column is compressed due to its support of the overlying weight of metal. Most of this weight is due to the atomic lattice and not the electrons. Thus the lattice spacing is smaller due to compression at the base. This would set up an enormous electric field if it were not for the conduction band electrons that redistribute themselves so as to preserve charge neutrality. In Ref. 21 the expression for the electric field just outside a metallic conducting surface is found to be

$$E = \frac{1}{e} \left[\gamma M g - m g \right] , \tag{37}$$

where M is the atomic mass, m is the electron mass, and γ is a quantity that characterizes the relative compressibility of the electrons and the neutral lattice. This quantity, γ, is calculable from the modulus of hydrostatic compressibility, and some assumptions related to the deformation of the lattice (see Ref. 21 and the review article by Herring and Nichols, Ref. 12, and also Ref. 23). In any event, the quantity γ is in the range 1 - 0.01 for copper. Thus the dominance of the lattice sag effect is assured in all metals over the electron sag effect. How then is it possible that Witteborn and Fairbank[1] did not observe this lattice sag effect, but rather observed only the Schiff-Barnhill effect, even in subsequent measurements[18,24] designed to seek it out? To date there has not been a satisfactory explanation of the experimental data. Nevertheless, in Ref. 23 Herring points out that the only part of the conductor that generates the gravitationally induced external field is the top few atomic layers on the surface. These layers are the only ones involved in defining the work function. The experimental data presented in Ref. 18 indicated a temperature-dependent shielding effect where the

ambient electric field in the drift tube dropped from ~5 x 10^{-7} V/m to ~10^{-10} V/m right near 7 K where residual gases would be frozen out on the tube walls. This coating would change the work function just as it would change the influence of the patch effect. Several models attempt to deal with this "coating" effect [25,26] and under the right assumptions, account for the experimental results. An independent measurement by Craig[22] showed that a metallic dust coating on the surface of the metal would eliminate the strain-induced change in the work function. All of these results showed that when the surface of the conductor is coated so as to disconnect it from the supporting lattice, the strain-induced change in the work function is not significant at the level of the electron sag effect.

The lattice sag effect, although important for an absolute measurement, is not an important effect in our relative measurement on H^- and antiprotons. To assure this, we will study the reproducibility of the TOF results using H^- ions so that the boundaries of the lattice sag effect will be well known to us in our apparatus. The lattice sag effect can be calibrated out of the system using H^- ions.

6. Thermal Effects. A homogeneous metal with no applied voltage may still have a potential difference from one part to another if these parts are at different temperatures. The potential difference, ΔV_T, varies with temperature according to

$$\Delta V_T = \sigma_T \Delta T \ , \tag{38}$$

where σ_T is the Thompson coefficient. For metals it is usually a few microvolts per degree. Measurements have been made of σ_T for copper at 4.2 K, but the coefficient changes drastically with the purity and the history of the sample.[27] For the Thompson voltage to be less than the gravitational potential over 1 meter, the temperature gradient needs to be approximately

$$\Delta T < 3.6 \times 10^{-2} \text{ K} \ . \tag{39}$$

If the drift tube were in direct contact with the liquid helium cooling bath, a temperature gradient of up to 0.34 K/m would exist because of variation in the liquid helium boiling point with pressure.[28] There are two options for controlling this effect: 1) Have the drift tube in contact with the bath at only one point. 2) Use a superconducting drift tube. The Thompson coefficient of a superconductor is zero.[30]

The second method would solve the problem most conclusively, but introduces several difficulties. First, the magnetic field in the drift tube would be more troublesome to vary because the tube itself would have to be driven normal in order to change the field. Second, the surface texture of available superconducting materials could not be as carefully controlled as for copper. Finally, the walls of the drift tube would have zero dc resistance. Thus, it would be impossible to set up an axial electric field by running current through the drift tube, as discussed in Section II-B.

The first method would solve the problem by connecting the drift tube to the heat bath at one end and otherwise insulated by vacuum along its entire length. Because of the low heat capacity of copper at 4 K, the temperature over a 1-m length of drift tube would equilibrate in tenths of a second to the $\sim 10^{-5}$ K level for an initial 10^{-1} K gradient over its length. A gradient can also be present if there is a heat leak. Careful design and fabrication can assure the absence of such unwanted thermal contacts. This is the design we will implement in our experiment.

Finally, if the helium bath is maintained below the λ- point (2.17 K), it becomes an extremely good conductor and presumably would allow the drift tube temperature to stay uniform to far less than 10^{-2} K. This would be a possibility if very long drift tubes (several meters) were the option we chose.

The last thermal effect we put to rest is the presence of thermal fluctuations in the electric field along the axis of a 4.2 K drift tube. An early calculation of this effect showed that 10^{-7} V/m was the level of the fluctuation.[30] In an erratum[31] the fluctuations were determined to be of order 10^{-14} V/m and are of no consequence.

Thermal effects can be controlled with careful experimental design at a level well below that of importance to the antiproton experiment. Once again, however, residual effects can be calibrated out using H^- ions.

7. Vacuum Effects. The particle concentration of background gases in the drift tube needs to be low enough so that collisions that affect the orbits of antiprotons or ions at the level of 10^{-7} eV are very unlikely. In addition, the background gas concentrations in the rest of the deceleration and trapping system need to be low enough to ensure very low loss rates of antiprotons before they can be used in the measurement. One of the central reasons for maintaining the low energy part of the system at 4.2 K was to reduce the out gassing from the walls, thus greatly reducing the background gas pressure. In addition, the vacuum walls serve as a pump by condensing out all gases except helium and hydrogen. These gases can be condensed out also by operating part of the system at temperatures lower than 4.2 K. The hydrogen can be pumped very effectively using pumps of special design. The vacuum system for the experiment will incorporate these pumps.

The electrostatic interaction of greatest importance in determining the vacuum in the drift tube region is the attraction of the antiproton to the induced dipole moment of the helium atom. The dielectric strength, K, of helium gas is about 1.000065. The polarizability, α, is given by

$$\alpha = \frac{(K-1)\varepsilon}{n_o} , \tag{40}$$

where $n_o = 2.69 \times 10^{25}$ is Loschmidt's number. For helium $\alpha \simeq 0.21 \times 10^{-40}$ Farad$\cdot$m^2. The electric field due to the antiproton is given by

$$E = \frac{q}{4\pi\varepsilon r^2} . \tag{41}$$

The induced dipole moment will be

$$p = \alpha E = \frac{\alpha q}{4\pi\varepsilon r^2} \quad . \tag{42}$$

The potential arising from this dipole is given by

$$V = \frac{p \cos\theta}{4\pi\varepsilon R^2} \quad . \tag{43}$$

Using Eq. 42 in the above and taking $\theta = 0$, $R = r$, we have that the potential energy of an antiproton near a helium atom will be

$$U = - \frac{\alpha q^2}{(4\pi\varepsilon)^2 r^4} \quad . \tag{44}$$

This quantity exceeds 10^{-7}eV when $r < 7.2 \times 10^{-7}$ cm. Thus the cross-section for undesirable collisions is given by $\sigma < 1.64 \times 10^{-12}$ cm^2. For a 1-m mean free path $\ell = 1/\rho\sigma$, the density needs to be $\rho < 6.10 \times 10^{9}$ cm^{-3}. This corresponds to a pressure of 2.64×10^{-9} Torr at 4.2 K. This pressure is far greater than is commonly achievable in a cryogenic vacuum system and several orders of magnitude above the pressure needed to keep the loss rate due to annihilation low. Thus induced dipole interactions will not interfere with the gravity measurement.

8. Overall Assessment. In this section we have discussed the electrostatic, magnetostatic, and condensed matter effects that are of concern in the gravity experiment we propose. Unlike the experiment of Witteborn and Fairbank on the electron, we propose to execute a relative measurement of antiprotons with respect to H^- ions. Electrostatically these particles are identical, being of the same charge. Thus all electrostatic effects can be calibrated out of the system. Magnetostatically, these particles are very similar due to the nearly complete cancellation of the electronic magnetic moments and the dominance of the effective hadronic moment due to the high cyclotron levels involved. Once again, the magnetostatic effects can be calibrated out. With careful

experimental design all the electro- and magnetostatic effects can be controlled at a level well below that of gravity. Thus we depend on the calibration process to deal with residual effects only.

The hadronic contribution to the inertial mass of the H^- ion and the antiproton are the same to within 0.1%. The leptonic component in the H^- inertial mass could contribute differently (in principle) to the gravitational mass. Thus it will be difficult to draw definitive conclusions at a level of better than 0.1% on the gravitational effect on matter compared to antimatter in the hadronic sector. The anticipated precision of our experiment is consistent with this limit.

The key feature that simplifies the measurement of the gravitational effect on antiprotons is the availability of a normal matter counterpart with very nearly the same mass and magnetic moment, and the same charge: the H^- ion. This calibration standard will allow for a relative measurement of the gravitational acceleration of antiprotons compared to protons at the level of 0.5 - 1%, provided that statistical effects and uncertainties in the calibration procedure are treated with the care we intend.

E. Sources of Statistical Error

Regardless of what technique is used to measure the gravitational force on antiprotons, the measurement will rely on accumulating many measurements of individual antiprotons, i.e. the measurement is a statistical one. For the TOF approaches discussed in Section II-B a spectrum of particles with different arrival times is measured. For both upward and downward launch, the late time parts of the spectra are most sensitive to the gravitational effects. The measurement in this approach is of the end point of the spectrum. This can be extracted by a fitting procedure of the late time spectrum.

Let us consider then the late time spectrum of particles launched vertically up a drift tube of length L. The spectrum is cut off at

$$t_c = \left(\frac{2L}{g} \right)^{1/2} . \qquad (45)$$

For times near this cutoff the exponential term in the TOF distribution function (Eq. 14) is very near 1.0. Thus the distribution function can be rewritten as

$$dN(t) \simeq \frac{1}{(2\pi)^{1/2}} \frac{1}{v_m} \left[\frac{L}{t^2} - \frac{g}{2} \right] dt \quad , \tag{46}$$

where v_m is defined in Eq. 12. This expression for the late-time TOF distribution is of the form

$$dN(t) = \left[a_o - \frac{a_2}{t^2} \right] dt \quad , \tag{47}$$

which can be readily solved for the cutoff time yielding

$$t_c = \left[\frac{a_2}{a_o} \right]^{1/2} \quad . \tag{48}$$

We have fit a function of the form of Eq. 47 to a Monte Carlo simulation of the late-time part of the TOF spectrum to test the sensitivity of the measurement to statistical and other effects. A typical fit is shown in Fig. II-13 for 2×10^6 stored antiprotons at an average temperature of 10 K launched upward in a 100-cm drift tube. The goodness-of-fit criterion used is the conventional chi-squared test which enables a simple matrix inversion solution to a fit using Eq. 47. In the analysis of the experimental data we plan to use a fit criterion based on Poisson distributed data,[32] rather than chi-square which is designed for Gaussian distributed data. Nevertheless, the simplified version is adequate for our purposes now.

Using the fit results for the standard deviations for the coefficients in Eq. 47, Eq. 48 for t_c, and a simple error analysis, allows the calculation of the standard deviation for the measurement of g. Because

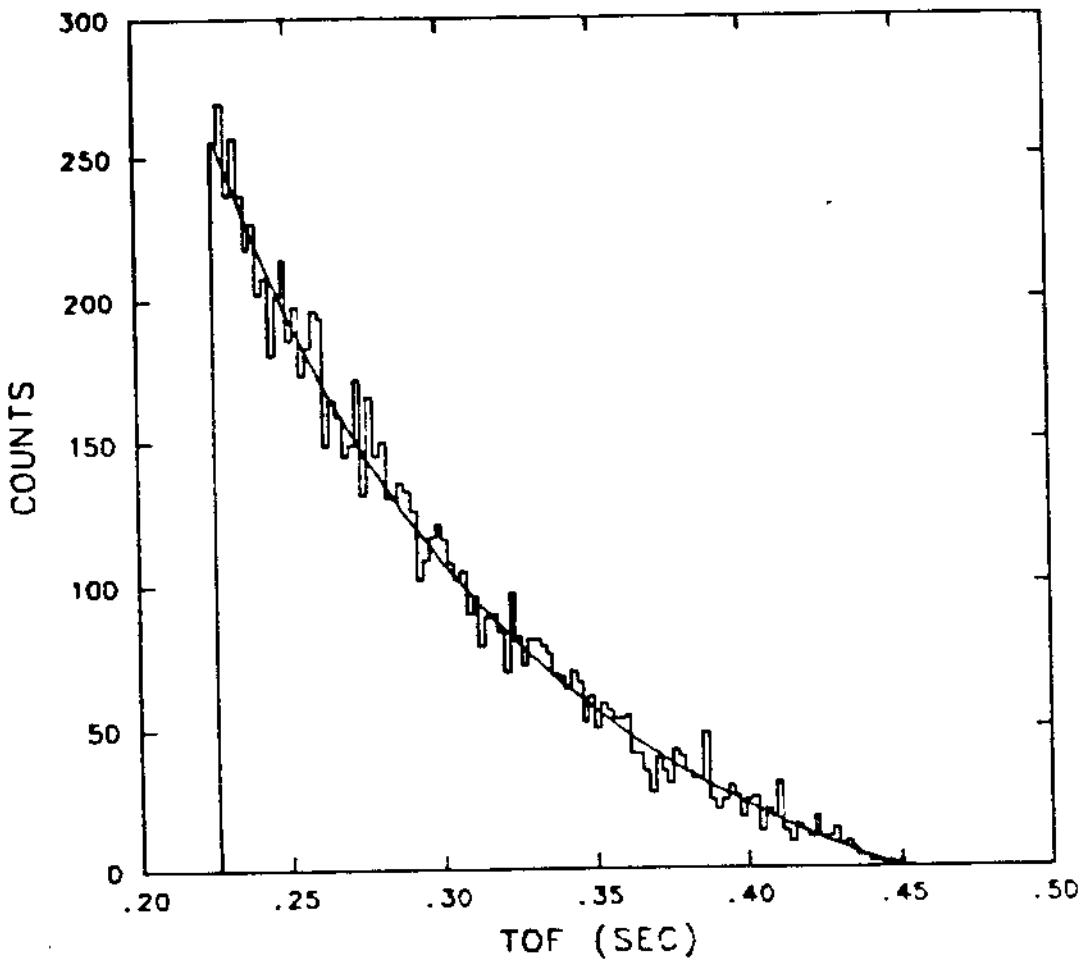

Fig. II-13. Typical fit to a Monte Carlo simulation of the late time TOF spectrum. The data represent 2 x 10^6 stored antiprotons at an average temperature of 10 K launched upward in a 100-cm drift tube.

the error in g also involves the uncertainty in the drift length L, we have included an estimate of this uncertainty as

$$\sigma_L = 0.1 \text{ cm} \quad , \tag{49}$$

which is a reasonable estimate of this quantity based on the launching ion trap design. Figure II-14 displays the relative error, σ_g/g, for the gravity measurement versus the total number of stored antiprotons in the

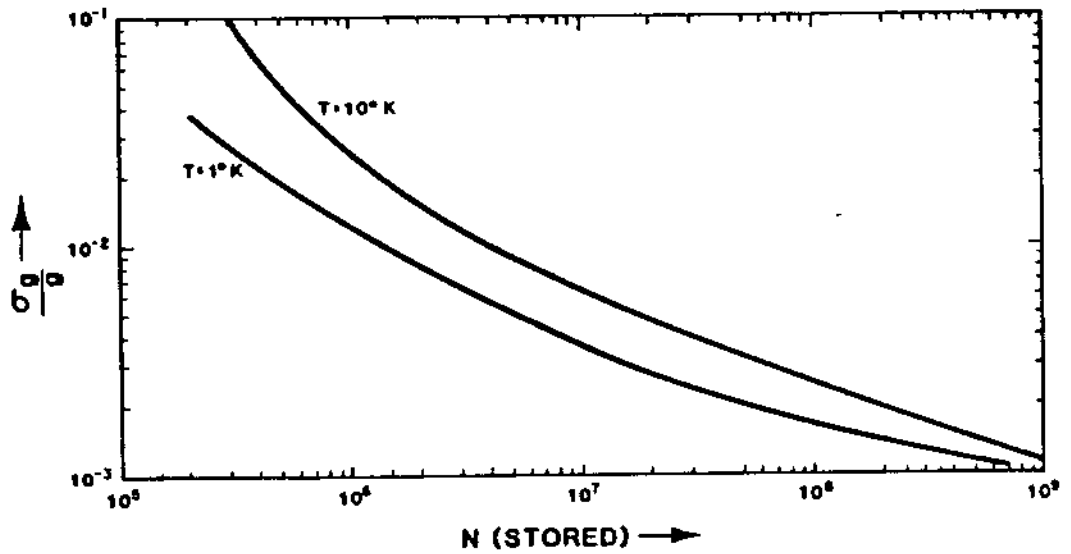

Fig. II-14. Relative error in the acceleration σ_g/g versus the total number of antiprotons involved in the measurement of g. The results for two average temperatures as indicated are shown. The drift length is 100 cm (see text also).

measurements. Shown in the figure are the results for a 100-cm upward drift length and two average temperatures as indicated. From the figure it is evident that for a 10^6 particle measurement the error in g will be between 1 and 3% for the temperatures shown. In actual fact it will be 1.5 to 2.0 times larger due to the relative nature of the measurement. For a 10^7 particle measurement the error will be between 0.4 - 0.6%, a substantial gain in precision. For 10^8 particles and up, the error starts to be dominated by the error in the drift length, σ_L (see Eq. 49), but a 0.1 - 0.3% measurement would be possible with this many particles. The dominance of σ_L for precisions in the range 0.1 - 0.3% suggests using a longer drift tube. Calculations show that using a longer drift tube (200 cm) does improve precision for measurements using 10^9 particles and up.

As discussed in Section II-B, it will be possible to pass a highly regulated current through the drift tube to set up an electric field that can either increase or decrease the total acceleration (see Eq. 20). By

applying a suitable current the total effect can be enhanced 10 or 100 times. This has a most dramatic effect on the statistical error for the gravitational acceleration. This is illustrated in Figure II-15, where the result with no electric field is shown for comparison. As is evident in the figure, by increasing the net effect tenfold, an order of magnitude

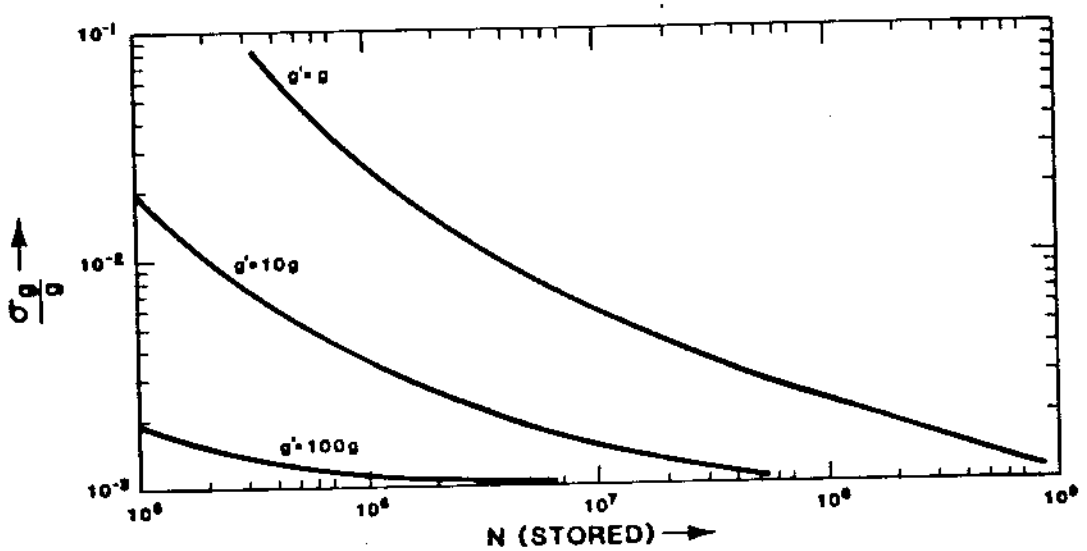

Fig. II-15. Relative error in the acceleration σ_g/g versus the total number of antiprotons involved in the measurement of g. The results for gravity, 10x, and 100x increased acceleration are shown (see text also).

improvement in the accuracy is possible. For 10^6 particles a 0.35% measurement could be accomplished. If the acceleration were increased 100 fold, such an accuracy would be possible with 10^5 particles. At these levels of accuracy the error is dominated by the error in the drift length. Naturally, the current through the drift tube can be regulated with some finite precision, and hence the axial electric field in the drift tube is known to this precision. This has not been included in the error estimates presented in Figure II-15. However, these contributions will be very small because of the high level of regulation possible ($\Delta I/I = 10^{-5}$ or 10^{-6}). Using an axial electric field to increase the net effect is an important technique for improving the accuracy of the gravity measurement for low

particle numbers. It is important that this axial field be the same to within the regulation precision for both a measurement with H^- ions and antiprotons. This requirement and the general use of an axial electric field for the measurement is under study by our collaboration.

The effect of the spread in cyclotron levels is an additional effect that can be dealt with through a fitting procedure. Using a theoretically parameterized resolution function for this effect, it is possible to deconvolute this effect from the measured TOF spectrum. The importance of this effect and its contribution to the error can be minimized with careful experimental design and also through the calibration procedure with H^- ions whose response will be nearly identical to antiprotons.

In summary, the statistical effects associated with fitting the end point of the TOF spectrum suggest that 10^6 to 10^7 antiprotons will be required for a 1% measurement of the acceleration of gravity. By using an axially applied electric field a ~0.2% measurement could be possible with the same number of particles. The effect of the error in the drift length dominates the measurement precision at the 0.1% level.

REFERENCES FOR SECTION II

1. F.C. Witteborn and W.M. Fairbank, Rev. Sci. Inst. 48, 1 (1977).

2. I.I. Rabi, Z. Phys. 49, 507 (1928); M.H.Johnson and B.A. Lippmann, Phys. Rev. 76, 828 (1949); W.-Y. Tsai and A. Yildiz, Phys. Rev. D4, 3643 (1971); T. Goldman and W.-Y. Tsai, ibid. p. 3648.

3. Aristotle, De Caelo 2.13.294^{b} 3-6; Physica 4.8.215^{a} 25-31; see The Works of Aristotle by J.L. Stocks, W.D. Ross, ed., Oxford University Press (1922).

4. G. Galilei, De Motu (~1590) (see Le Opere Di Galileo Galilei, Edizione Nationale 1. 262-3); Discorsi e Dimostrazioni Matematiche Intorno a Due Nuove Scienze Attenenti alla Mecanica e i Movimenti Locali .... Leyden (1638); (see Ed. Naz. 8.108-9).

5. F.C. Witteborn and W.M. Fairbank, Phys. Rev. Lett. 19, 1049 (1967); Nature 220, 436 (1968).

6. W.M. Fairbank, F.C. Witteborn, J.M.J. Madex, and J.M. Lockhart, in Experimental Gravitation, B. Bertotti, ed., Academic Press, New York (1974) P. 310.

7. Based on the international gravity formula, Handbook of Geophysics, MacMillan, Co., New York (1961), p. 12-68.

8. H.J. Bethe and E.E. Salpeter, Quantum Mechanics of One and Two Electron Atoms, Academic Press, New York (1957) p. 227.

9. F.C. Witteborn, Thesis, Stanford University, 1965 (unpublished).

10. J.D. Jackson, Classical Electrodynamics, Wiley and Sons, New York (1962).

11. D. Wallace and G. Ekstrom, American Magnetics Corp., Oak Ridge, Tenn., Private Communication.

12. C. Herring and M.H. Nichols, Revs. Mod. Phys. 21, 185 (1949).

13. J. Bardeen, Phys. Rev. 49, 653 (1936).

14. W.H. Munse and N.A. Weil, ASTM Proc. 51, 996-1022 (1951).

15. R.N. Castellano, M.R. Notis, and G.W. Simmons, Vacuum and Thin Film Technonogy, I. Yarwood and F. Andersson, eds., (Pergammon, Oxford, 1978) p. 109.

16. P.K. Haff and Z.E. Switkowski, Jour. App. Phys. 48, 3383 (1977).

17. C. Weissmantel, H.J. Erler, and G. Reisse, Surf. Sci. 86, 207 (1979).

18. J.M. Lockhart, F.C. Witteborn and W.M. Fairbank, Phys. Rev. Lett. 38, 1220 (1977).

19. A.R. Hutson, Phys. Rev. B17, 1934 (1978).

20. L.I. Schiff and M.V. Barnhill, Phys. Rev. 151, 1067 (1966).

21. A.J. Dessler, F.C. Michel, H.E. Rorschach, and G. T. Trammell, Phys. Rev. 168, 737 (1968).

22. P.P. Craig, Phys. Rev. Lett. 22, 700 (1969).

23. C. Herring, Phys. Rev. 171, 1361 (1968).

24. F.C. Witteborn and M.R. Pallesen, Phys. Rev. Lett. 19, 1123 (1967).

25. G.T. Trammell and H.E. Rorschach, Phys. Rev. B2, 4761 (1970).

26. R.S. Hanni and J.M.J. Madey, Phys. Rev. B17, 1976 (1978).

27. A.V. Gold, D.K.C. MacDonald, W.B. Pearson, and I.M. Templeton, Phil. Mag. 5, Ser. 8, 765 (1960).

28. R.T. Swim, Advances in Cryogenic Engineering, 5, K.D. Timmerhaus, ed., (Plenum, New York, 1960), p. 262.

29. H.M. Rosenberg, Low Temperature Solid State Physics, (Oxford, Clarenden Press, 1963), p. 276.

30. H.J. Maris, Phys. Rev. Lett. 33, 1177 (1974).

31. H.J. Maris, Phys. Rev. Lett. 33, 1594 (1974).

32. M.V. Hynes, J. Kelly, B.A. Peterson, and B.E. Norum, Los Alamos Document, LAUR-84-149.

III. EXPERIMENTAL DESIGN

A. Experimental Overview

To measure the gravitational effect on antiprotons, the antiproton energy has to be sufficiently low for the TOF spectrum (discussed in Section II-B) to have sufficient particles near the cutoff time ($t_c = \sqrt{2\ell/g}$). As presented in Section II-B, the energy required is better measured in degrees Kelvin, rather than the more familiar MeV or keV. The lowest energy beam currently available from LEAR is ~5 MeV (Ref. 1). To perform the measurement, this energy has to be reduced by about ten orders of magnitude. We propose a series of deceleration stages involving an RFQ decelerator and several pulsed electromagnetic ion traps to accomplish this energy reduction. The final ion trap will store up to 10^7 antiprotons at ~10 K or lower. Once the particles are cold enough, they will be brought, ~10^2 at a time, into a high precision launching trap and suddenly released into a drift tube. After a 1 m flight path, the arrival times of the antiprotons relative to the launch time are measured using a microchannel plate to detect the particles.

A schematic view of the experimental setup is shown in Fig. III-1. In

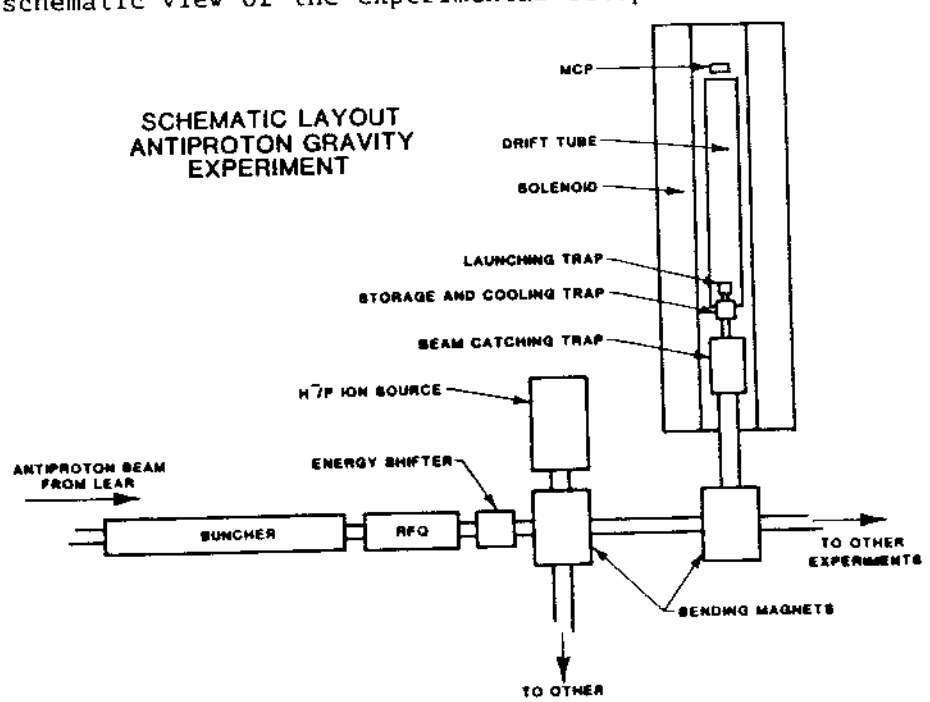

Fig. III-1. Schematic view of the experimental setup indicating major equipment items (see text also).

the figure, a bunched beam is extracted from LEAR at 5 MeV. The beam in LEAR has a macrotime structure set by the 8^{th} harmonic buncher already in the LEAR ring. A single phase bucket out of the 8 circulating is fast extracted from LEAR and delivered to the experiment. A microtime structure that is matched to the operating frequency of the radio frequency quadrupole (RFQ) decelerator will also be imposed on the macroburst. This microstructure can be imposed by a buncher system either in the LEAR ring or externally. Bunching in LEAR makes the most efficient use of antiprotons whereas bunching externally has higher loss rates. In any event, this bunched beam at 5 MeV is decelerated in an RFQ, currently under design at Los Alamos and CERN, to 100 keV. An energy shifting cavity is then used to adjust the beam energy up to 200 keV for use in other experiments or down to 20 keV for use in our gravity experiment. In the drift length, a provision for injecting 20 keV H^- ions into the beam line will allow for testing of the pulsed ion trap independent of LEAR operations. The drift length will also contain beam diagnostics and optics appropriate for entering the double focusing 90° bending magnet which bends the beam vertically up into the first pulsed ion trap. Located immediately before the entrance to this trap is an electrostatic deceleration stage and drift space which lowers the beam energy to 4 or 5 keV depending upon the incident beam energy spread. Initially the entrance endcap is at ground potential and the top endcap is at 5 kV. As the beam burst traverses the trap and approaches the top endcap it starts to decelerate and turn around. When the leading edge of the burst has returned to the center of the trap the potential on the entrance endcap will be quickly raised 5 kV, which will prevent the burst from exiting the trap, i.e. the burst is captured. In this type of electromagnetic trap (Penning trap) the particles are contained radially by a strong (6 T) magnetic field and axially by an electrostatic quadrupole potential. While in this trap the particles will be resistively cooled to ~200-300 eV. When this is accomplished, the particles will be transferred to a highly compensated harmonic trap for further resistive cooling. Although other cooling schemes have been proposed,[2,3] we plan at present on resistive cooling because it is the only demonstrated technique available. In this intermediate trap the particles will be cooled to ~5-10 K and stored in preparation for transfer, 10^2 at a time, into the final, launching trap.

Once in the launching trap, the potential will be suddenly dropped, thus releasing half of the particles upward. Above the launching trap we locate a 1-m drift tube for isolating the rising antiproton from stray electric fields. The TOF is measured using a microchannel plate at the top of the drift tube. This same device can be used to detect H^- ions used in the calibration runs. The ion traps must operate at extremely low pressures ($< 10^{-14}$ Torr) to avoid loss of antiprotons through annihilation with residual gas atoms.

To measure the gravitational acceleration of antiprotons relative to the H^- ion will require the launching of a total of 10^6 to 10^7 particles for a 1% measurement (see Section II-E). This same precision can be achieved with fewer particles if an externally applied electric field is used. There will be $\sim 10^8$ particles in each 8^{th} harmonic macrobunch from LEAR. This is sufficient for one TOF spectrum with some safety margin. Many TOF spectra will be required to verify reproducibility and to study systematic errors. Each antiproton run will be followed by a run with H^- ions either internally generated in the bulk storage trap or transported from the H^- source.

In the subsections that follow, each of the major pieces of experimental equipment is discussed in some detail. Finally, we conclude this section with a discussion of the experimental development program that we are now executing. In particular we present the technical milestones that are required before the experiment can be performed. Several of these milestones have already been achieved.

B. The LEAR Facility

1. Low Energy Operation. Recently, LEAR has been successfully operated at 5 MeV kinetic energy. Although it is hoped that lower energy operation will be possible, we will plan our beam line design based on 5 MeV extracted energy from LEAR. The beam characteristics at 5 MeV are summarized in Table III-1. The beam line design for the gravity experiment is discussed in Section III-C. The lifetime of the beam in the LEAR ring at 5 MeV is currently ~1 hr. We understand that this lifetime could be extended by the addition of new power supplies for the steering and focusing elements in the ring. We will maintain our close contact with the operations personnel working on the low energy operation at LEAR.

Table III-1

LEAR LOW ENERGY PARAMETERS

Energy	5.0 MeV
Momentum	97.0 MeV/c
ε_x(unnormalized)	3π·mm·mrad
ε_y(unnormalized)	3π·mm·mrad
$\Delta p/p$ (Full)	2.0×10^{-4}

2. Bunching. The beam entering the RFQ is required to have a microtime structure that is matched to the operating frequency of the RFQ. In addition to the microtime structure, our experiment requires a macrotime structure that corresponds to the 8^{th} harmonic of the bunching system that already exists in the LEAR ring. This macrotime structure will provide our experiment with a pulse length, at the decelerated energy, that will match the length of our first pulsed ion trap. It is required then that a buncher for the microtime structure be built. In principle this buncher can be inserted either in the LEAR ring or externally in the beam line just preceding the RFQ. Insertion in the LEAR ring can be accomplished in one of the long straight sections of the ring. The cavity itself can be quite short and can be designed so that it will not interfere with normal LEAR operation. Bunching in the ring is done adiabatically over a period of time that is very long compared to the circulation time around the ring. Bunching in such a mode can be accomplished with low antiproton losses. The microtime structure can also be imposed without interfering with the macrotime structure imposed by the existing buncher in LEAR. However, if one bunches in LEAR one must preserve this time structure during extraction and transport to the RFQ, which may require additional cavities.

Bunching externally in the beam line just preceding the RFQ, is also a possibility. Two possible schemes are discussed in Section III-C-b. The first scheme will bunch 75% of the extracted beam from LEAR into the acceptance of the RFQ with relatively good longitudinal emittance (good energy resolution). The difficulty is that it requires about 25 meters of floor space and several elements to be implemented. The second external bunching scheme we have considered (see Section III-C-b) will bunch 50% of the beam from LEAR into the RFQ acceptance with fairly good longitudinal emittance. This design requires 13 meters of beam line.

3. Extraction. Our experiment requires the fast extraction of a single bunch assembled by the 8^{th} harmonic buncher already in the LEAR ring. To minimize particle losses the fast extraction kicker needs to be fully energized and de-energized in between the 8^{th} harmonic phase buckets. This requirement can be satisfied by the existing kicker system. Thus fast extraction can be accomplished with no particle losses.

4. Vacuum Isolation. The beam line we propose tó build as part of our experiment will inherently have a vacuum of $<10^{-11}$ Torr. The deceleration system itself will be the most problematic source of vacuum contamination. Therefore we will have several stages of vacuum isolation to maintain $<10^{-11}$ Torr on both entrance and exit apertures of the deceleration system. All beam line elements will be bakeable to 250° C, and built according to standard ultra-high vacuum practice. We will always maintain a better or equal vacuum at the interface of our beam line with LEAR than in LEAR itself. We will take extra precautions and care in the design of our vacuum system because of the inherent ultra-high vacuum requirement of our experiment and because we wish to eliminate the vacuum window conventionally used in experimental beam lines. At the very low energy we plan on extracting from LEAR, a window of any thickness will severely degrade the beam quality and reduce the number of particles available for our measurement. This issue is currently under study by the collaboration. Our estimates thus far indicate that a window cannot be used. We will design our vacuum system accordingly. (See also Section III-H.)

C. The RFQ Decelerator

1. Introduction. The RFQ as a particle accelerator originally was proposed by Kapchinskii and Teplyakov.[4] Outside the Soviet Union, the development of RFQ technology has been led by the Los Alamos National Laboratory. The work at Los Alamos has led to the widespread application of RFQ structures for the solution of the low-velocity problems that are inherent to many accelerator systems.[5] Several comprehensive reviews of RFQ's are available (see Refs. 6-8).

Figure III-2 displays a schematic view of a 4-vane RFQ resonator. Currents transverse to the RFQ axis provide + - + - polarities on the vanes (poles) which result in a transverse quadrupole electric field. This quadrupole field configuration produces focusing in one transverse plane and

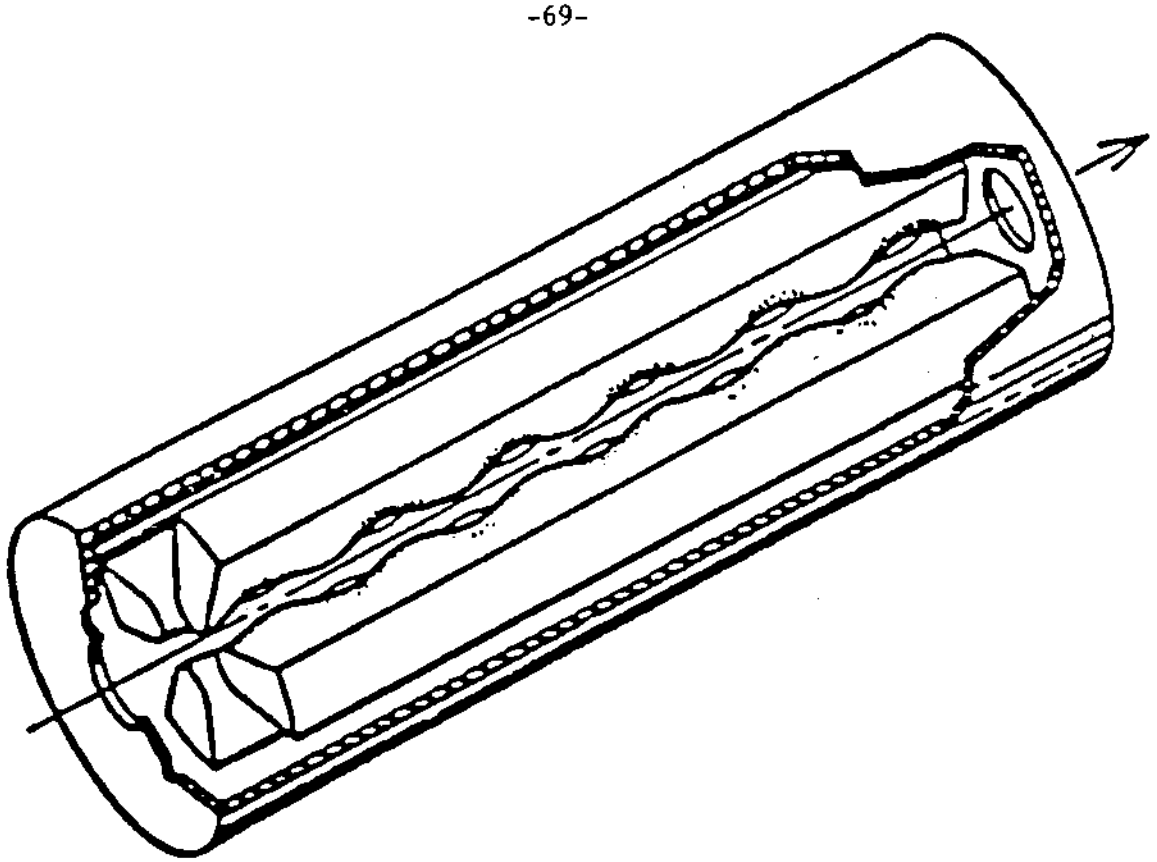

Fig. III-2. Sectional schematic view of a 4-vane RFQ resonator. Note the sinusoidal-like variation of the vane radius (see text also).

defocusing in the other. One half rf cycle later these focusing forces reverse sign to produce an overall strong focusing effect. Pole tips with a constant unmodulated radius produce a radial focusing force only. Pole tips with a sinusoidal-like variation in radius, as shown in Fig. III-2, have longitudinal accelerating fields as well as transverse focusing fields.

In conventional drift-tube linacs the focusing force, which is obtained from magnetic quadrupoles within the drift tubes, becomes too small at low velocities to counteract the tendency of a finite emmittance beam to diverge. The RFQ can operate at a velocity below that of conventional linacs because the focusing is obtained from the velocity-independent electric force. The strong focusing in an RFQ permits acceleration while maintaining good beam quality. In comparison with a d.c. accelerator the RFQ frequently offers the advantage of a reduced size. For this application the overall length of the RFQ may not be much more than a few meters. The

RFQ is relatively simple to operate as compared with most other accelerators.

Our proposal to use an RFQ as a decelerator has no precedent. We are confident, however, that it can be done. The particles are injected into the RFQ when the longitudinal field is decelerating rather than accelerating.

The output values one tries to achieve in the deceleration system must correspond to experimental requirements. Important parameters include the final energy, transverse emittance, and energy spread. In the reference design described here we consider final energies between 20 and 200 keV. Although it may be possible to reach energies lower than 20 keV with the rf deceleration system, one also has the option of further deceleration with a dc potential to achieve ultra-low antiproton energies. In our design, we have also attempted to preserve the beam quality by keeping the growth of both transverse and longitudinal emittance low. Small longitudinal emittance implies that either a small energy spread or a small phase spread is potentially available.

2. Basic Considerations. To preserve beam quality, one must work in a sufficiently narrow region of the longitudinal phase coordinate to minimize nonlinear effects. In general, the input beam is not matched to the RFQ in longitudinal phase space unless a longitudinal matching element is placed between LEAR and the RFQ. The matched beam parameters in the longitudinal phase plane at the input to the RFQ (high energy end) are related to the RFQ parameters by

$$\frac{\Delta W}{\Delta \phi} = \frac{1}{2}(emc^2\beta^2\gamma^3 AV|\sin\phi_s|)^{1/2}, \qquad (1)$$

where β and γ are relativistic factors, A is the accelerating efficiency (which depends on the amount of vane-tip modulation in the RFQ), V is the intervane voltage, W the kinetic energy and ϕ_s is the synchronous phase.*

*We use the linac convention for the phase in which ϕ=0 is at the positive peak of the wave form.

Another formula, useful for the design of an RFQ decelerator, relates approximately the output and input phase spreads:

$$\frac{\Delta\phi_{out}}{\Delta\phi_{in}} = \left[\frac{(AV|\sin\phi_s|\beta^2)_{in}}{(AV|\sin\phi_s|\beta^2)_{out}}\right]^{1/4} . \qquad (2)$$

If one works in the linear region where the longitudinal emittance is conserved, the final energy spread can also be obtained from Eq. (2).

Equations (1) and (2) together with the usual set of RFQ formulae[6] have been used to choose appropriate RFQ parameters.

3. Reference Design for the rf Deceleration System. The reference design presented here assumes that a single 8^{th} harmonic bunch at 5 MeV is extracted from LEAR. Using fast extraction, the energy spread is expected to be small, on the order of ±1 or 2 keV. Two buncher cavities will place a reasonable fraction (~50%) of the beam into the longitudinal phase space required by the RFQ. The RFQ will decelerate the beam from 5 MeV to 0.1 MeV. A separate rf cavity ("energy shifter") will reduce the beam energy to around 20 keV. This same cavity could be used to vary the energy between 20 and 200 keV to satisfy the needs of other experiments.

The 5 MeV injection energy is the dominating factor in the design of the deceleration system. Bunching at 5 MeV requires long distances. The acceleration (or deceleration) efficiency of RFQ's decreases with increasing particle energy. A Drift Tube Linac (DTL) is normally used for energies above 2 or 3 MeV. Also, the difficulty of tuning an RFQ increases with $(L/\lambda)^2$, where L is the length of the RFQ and λ is the free-space wavelength of the rf. However, we consider one relatively long RFQ to be a simpler system than a DTL-RFQ combination.

a. Design of the RFQ. A major consideration is to minimize the length of the RFQ. The acceleration rate, and therefore the length, depends on the intervane voltage, the vane modulation, and the synchronous phase by

$$\frac{d\omega_s}{dz} = \frac{\pi qAV}{\beta\lambda}\cos\phi_s , \qquad (3)$$

where ω_s is the kinetic energy of the synchronous particle and z is the longitudinal distance along the RFQ. Both A and $\cos\phi_s$ are limited to be less than unity, so V must be large to shorten the RFQ. However, if V is large, the mean aperture radius r_o must also be large to prevent an excessively high electric field on the vane-tip surface. But r_o cannot be arbitrarily large. A good rule of thumb is that $r_o < \ell$, where $\ell = \beta\lambda/2$ is the length of the shortest cell in the RFQ. For 100 keV protons, β = 0.0146. Consequently, r_o should be less than 0.007λ.

In the RFQ design, we have restricted the maximum surface field to

$$E_s = \kappa V/r_o \leq 1.65\ E_K \quad , \tag{4}$$

where E_K is the Kilpatrick limit, and κ is a field enhancement factor that depends on the vane-tip geometry. We have assumed vane tips having a constant transverse radius of curvature $\rho = 0.75\ r_o$ in order to minimize κ. The above considerations have led us to the RFQ parameters summarized in Table III-2.

The matched input in the longitudinal phase space has a $\Delta W/\Delta\phi$ = 5.65 keV/degree. Assuming a total emittance of 100 π·keV·deg (a value we have found to be readily achievable by a buncher system), a matched ellipse would have semi-axes of 4.2 deg and 24 keV. We have assumed the 5 MeV beam to

Table III-2

REFERENCE RFQ PARAMETERS

Parameter	Value
Frequency (MHz)	200
Initial energy (MeV)	5.0
Final energy (MeV)	0.1
Number of cells	84
Intervane voltage (kV)	177
Mean aperture radius r_o (cm)	1.04
Peak surface field (MV/m)	24
Modulation parameter at 5 MeV	2.8
Modulation parameter at 0.1 MeV	1.1
Synchronous phase 5 MeV (deg)	-162
Synchronous phase 0.1 MeV (deg)	-142
Length (cm)	315
Peak power (kW)	535

have a transverse unnormalized emittance of 3 π·mm·mrad, although the transverse acceptance of the RFQ is much larger.

The results of simulations of the matched beam passing through the RFQ are shown in Figs. III-3 through III-5. The beam width, phase spread, and energy spread at each cell are shown in Fig. III-3. The 5 MeV input characteristics are shown in Fig. III-4. In this figure the phase and energy spectra, the x-y coordinates, and the longitudinal coordinates surrounded by the separatrix enclosing the region of longitudinal stability are shown. These same characteristics at the exit of the RFQ (100 keV) are shown in Fig. III-5.

b. Design of the Buncher System. Using two buncher cavities, one operated at 200 MHz and the other at 400 MHz, it is possible to place about 75% of a continuous beam into the matched 100 π·keV·deg ellipse. Unfortunately, the distance required at 5 MeV is about 25 meters. However, it is possible to bunch 50% of the beam into a smaller phase spread in a distance of about 13 meters. This beam is not longitudinally matched to the RFQ, but approximates a vertical line in longitudinal phase space. By slightly adjusting the intervane voltage, this line can be made almost

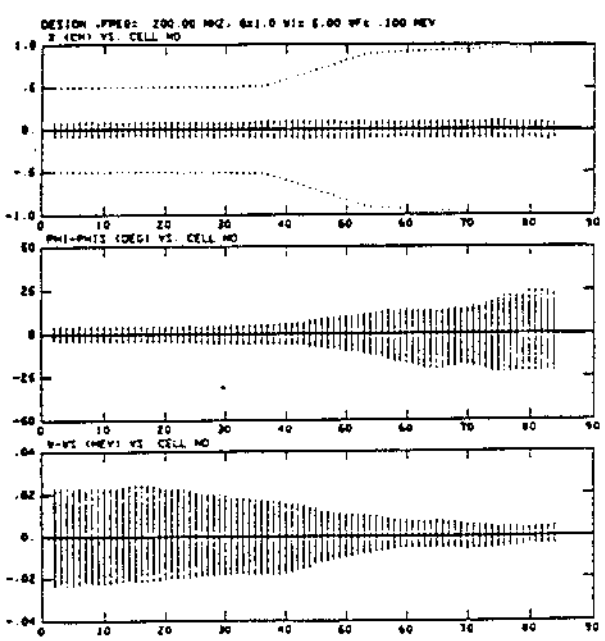

Fig. III-3. Horizontal profiles (top) phase spread (center), and energy spread (bottom) of a matched beam passing through the RFQ. The dots on the top graph indicate the minimum vane aperture along the structure.

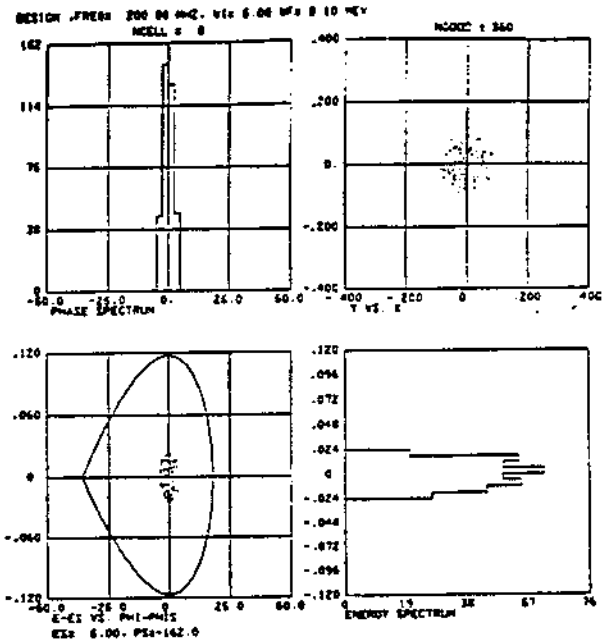

Fig. III-4. Phase spectrum (upper left), x-y coordinates upper right), longitudinal coordinates enclosed within the separatrix (lower left), and energy spectrum (lower right) of a matched beam at the entrance to the RFQ decelerator.

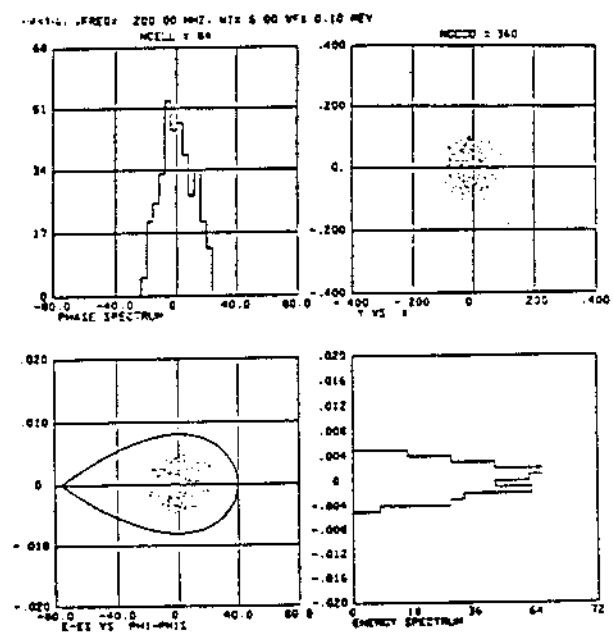

Fig. III-5. Characteristics of a matched beam at the exit of the RFQ decelerator.

horizontal at the exit of the RFQ, which means that the beam can have a small energy spread.

An example of a transport system between the buncher cavities and the RFQ is shown in Fig. III-6. At the upper left is shown the x-x′ and the y-y′ phase space ellipses at the buncher, and at the upper right are these ellipsis at the entrance to the RFQ. At each end are two matching quadrupoles, between which are four doublets separated by 2 meters. The horizontal and vertical profiles of the beam in the transport system are shown at the bottom of Fig. III-6.

We have simulated the behavior of the beam as it passes through the buncher system, RFQ, and the energy-shifter cavity. At the bunchers, the beam is assumed to be continuous with a ±1 keV energy spread. The beam characteristics at the entrance to the RFQ are shown in Fig. III-7. Most of the phase width of the beam is caused by the ±1 keV energy spread at the buncher. After passing through the RFQ and 5 cm beyond, the beam characteristics are as shown in Fig. III-8. An energy shifter cavity at this location could reduce the energy to around 20 keV. The simulated

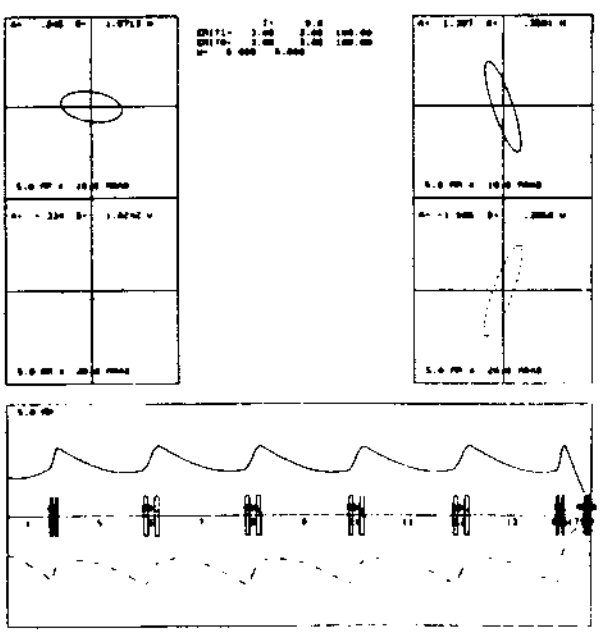

Fig. III-6. Beam characteristics in the 5 MeV bunching line. Horizontal and vertical phase-space ellipses at the buncher are shown at the upper left, and at the RFQ at the upper right. Horizontal and vertical profiles in the transport system are shown at the bottom.

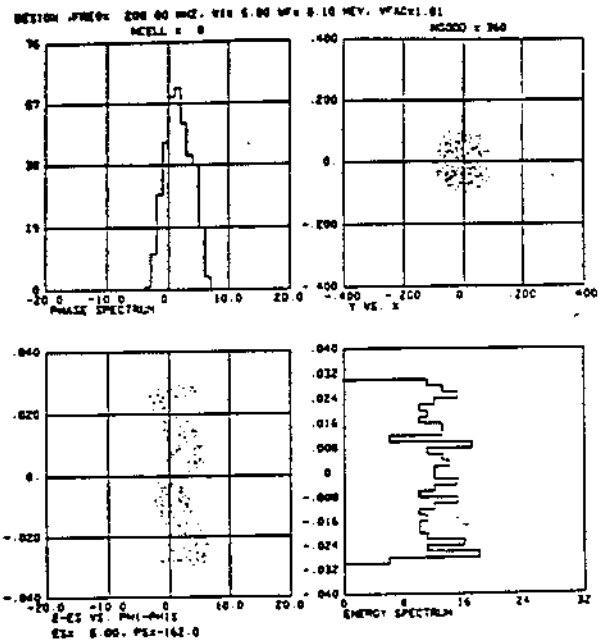

Fig. III-7. Beam characteristics at the entrance to the RFQ assuming a continuous beam at the buncher having a ±1 keV energy spread.

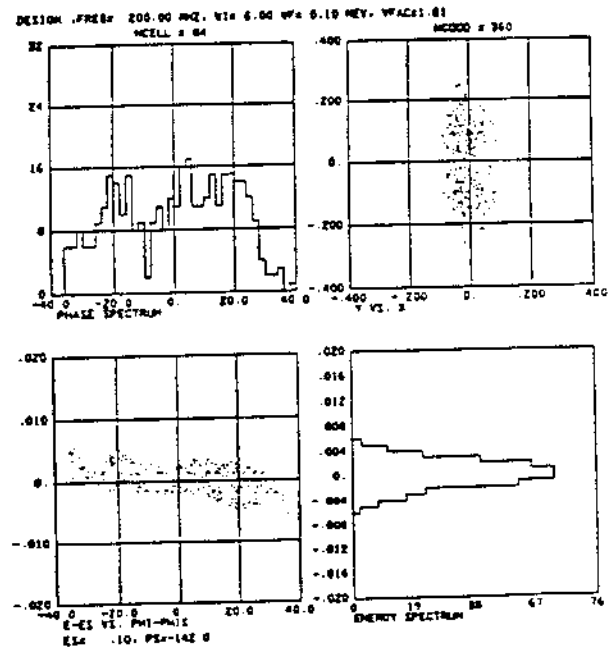

Fig. III-8. Beam characteristics 5 cm after the exit of the RFQ decelerator, before the energy shifter.

results are shown in Fig. III-9. Most of the beam lies within a ±10 keV energy spread, and a good fraction lies within ±4 keV. The increased energy

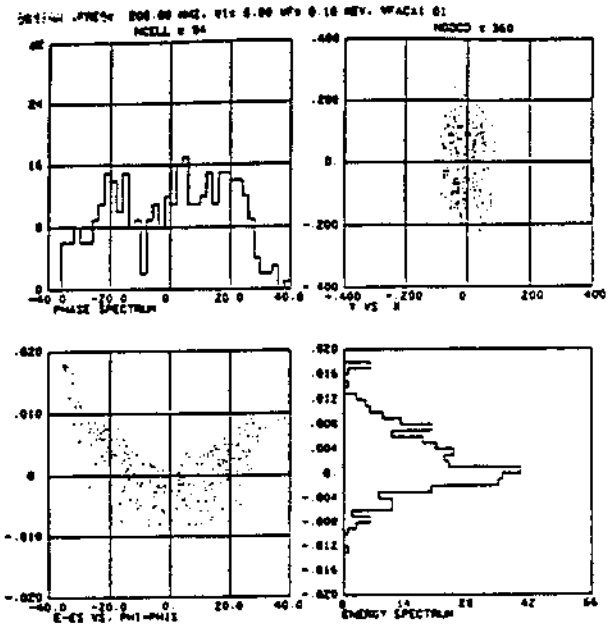

Fig. III-9. Beam characteristics after an 80 keV energy shifter cavity.

spread in the central region is caused by the off-axis particles being decelerated more than the on-axis particles.

These simulations indicate what might be expected from a deceleration system. More detailed calculations are needed, especially for the energy-shifter cavity. Final design calculations for the entire deceleration system would necessarily be done in coordination with the needs of the low-energy transport line (see Section III-D), the antiproton Penning trap, and with the detailed characteristics of the LEAR beam.

It is tantalizing to hope one could simply use a degrading foil and obtain significant quantities of antiprotons at the necessary low energies for acceptance into a trap. Unfortunately, little if any data exists for transmitted, degraded antiproton numbers at 10 keV energies from bombarding a foil (~235 μm) with the lowest energy beams (5 MeV) from LEAR. Indeed, a search through the literature reveals no data on proton stopping powers below 10 keV. This data is necessary for accurate estimation of the number of degraded transmitted protons versus energy. Moreover, the antiproton will behave differently at low energy than protons (no electron capture and the annihilation process).

Our conclusion is that a degrading foil will not permit us to use 10^7 to 10^8 antiprotons in a single measurement, which we would like to repeat a number of times to obtain a high precision determination of $\bar{g}/g$. Further the RFQ decelerator just described could also form the cornerstone for future experiments requiring a low energy ($\lesssim$ 200 keV) antiprotons and as such is attractive in itself.

D. Low Energy Beam Transport

1. Antiproton beam line. An important link in the success of this project is the ability to transport low-energy (20 keV) antiprotons ($\bar{p}$) from the RFQ decelerator system into the Penning trap. To avoid $\bar{p}$ losses this transport must be done with high efficiency and with no degradation of the ultra-high vacuum (at least 10^{-14} Torr) in the trap region.

A sketch of our plan for the low-energy system is shown in Fig. III-10. This consists of a direct-extraction, duoplasmatron ion source and a system of electrostatic lenses, magnets, and apertures. Other elements that are not shown are valves, Faraday cups, beam steerers, and pumps. The five long, narrow apertures shown are cylindrical tubes and act as throttles

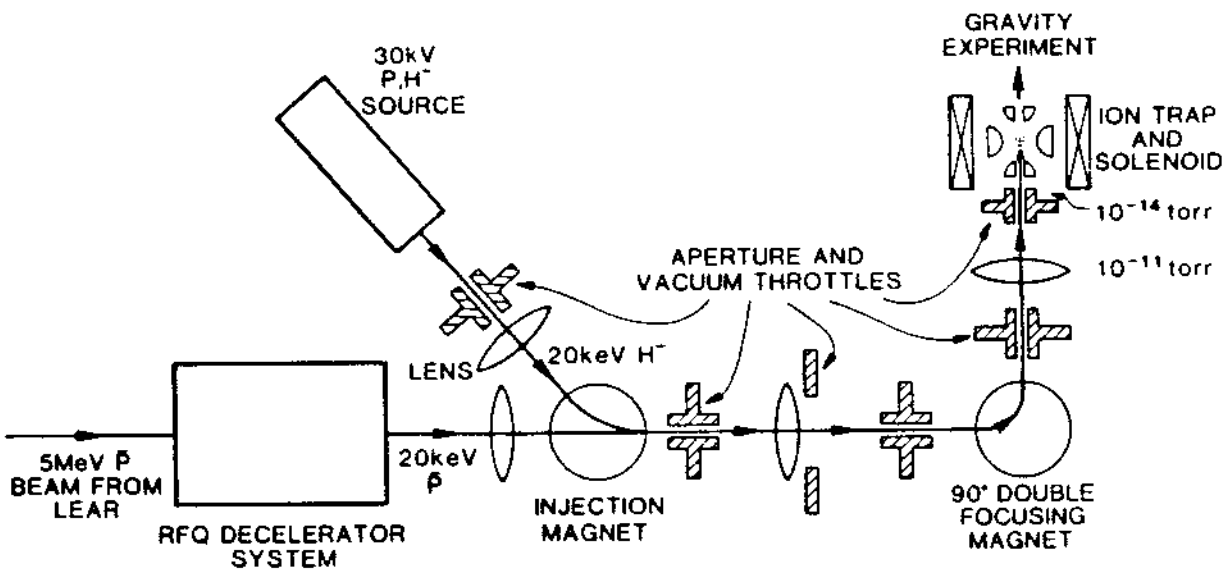

Fig. III-10. Layout (plan view except for the ion trap and solenoid vertical line, which is a side view) emphasizing the 20 keV beam transport. The ion trap in our present test system has a 3 mm diameter entrance aperture.

to separate different vacuum regions. They are positioned at minima in the beam's transverse dimensions (waists) and serve to transport the beam across vacuum regions that could differ in pressure by a factor of 100 or more. The waists are formed by either the electrostatic einzel lenses or the 90° double-focusing magnet. The system will be constructed using all metal seals, stainless steel beam pipes, and other elements capable of baking to attain high vacua. We expect that the pressure in the decelerator system will be about 10^{-10} Torr when the H^- source is valved off and that the pressure just below the last throttle will be about 10^{-11} Torr for all running conditions. The final reduction in pressure in the trap region, necessary for long $\bar{p}$ lifetimes, will be accomplished by operating that region in a 4 K environment. We plan to use a cold shutter arrangement to isolate the trap environment from the rest of the system when beam is not being injected. The trap design allows a 30 cm length of beam to be compressed and trapped with high efficiency. This 30 cm is the beam length that is planned to be injected by the RFQ system into the low-energy beam line. The energy spread in the beam at that point, however, will propagate into a longitudinal spatial spread as the beam moves the approximately four meters to the trap. For example, a beam energy width of 4 keV at 20 keV will spread spatially at a rate of 10 cm per meter traversed. Such an energy width is not unreasonable from the point of view of the RFQ design; however, we would like to keep the spatial extent of the beam at the trap as close to 30 cm as possible. To this end we are studying the possibility of including a debuncher as an element in the RFQ system and of shortening the path length traversed by the low energy beam. As of January, 1986, we have constructed at the Los Alamos Ion Beam Facility a low-energy beam test line approximating most of the plan of Fig. III-10, except that the RFQ system is not present and the trap is operated at room temperature. Our experience with the test system is described in Section III-H.

2. Calibration source. A separate source of 20 keV protons and H^- ions is necessary for two reasons. First, the negative ion beam will be used to adjust the low-energy system and trap to be ready for $\bar{p}$ injection. Second, p or H^- will be trapped and launched into the gravity drift tube to test the properties of the gravity-measurement apparatus and to calibrate this apparatus for the $\bar{p}$ gravity measurement.

An ion source designed for our application is available commercially and would provide approximately 50 μA of H^- or D^- ions, and even more current of protons or deuterons. The energy spread of this beam would be only several tens of eV. Suitably forming the phase space to be compatible with transport to the trap would reduce the useful current to the order of 10 μA. To prevent undue heating and consequent pressure rise in the trap region from extraneous beam, we will provide for chopping of the cw beam from the source so that only a short burst will be sent to the trap.

E. The Ion Trap System

1. Introduction. Of the different possible schemes to electromagnetically confine charged particles the Penning trap[9] is the most promising approach for our applications. Compared to the radio frequency quadrupole trap,[10] where the particles are weakly but continuously heated by the external RF-fields controlling their macromotion,[11] and the Kingdon trap,[12] which relies on a high transverse angular momentum for stability, the Penning trap allows the lowest possible kinetic energy of the confined particles. In the Penning trap, confinement is achieved by a combination of electrostatic and magnetic fields. A cross section of the electrodes of

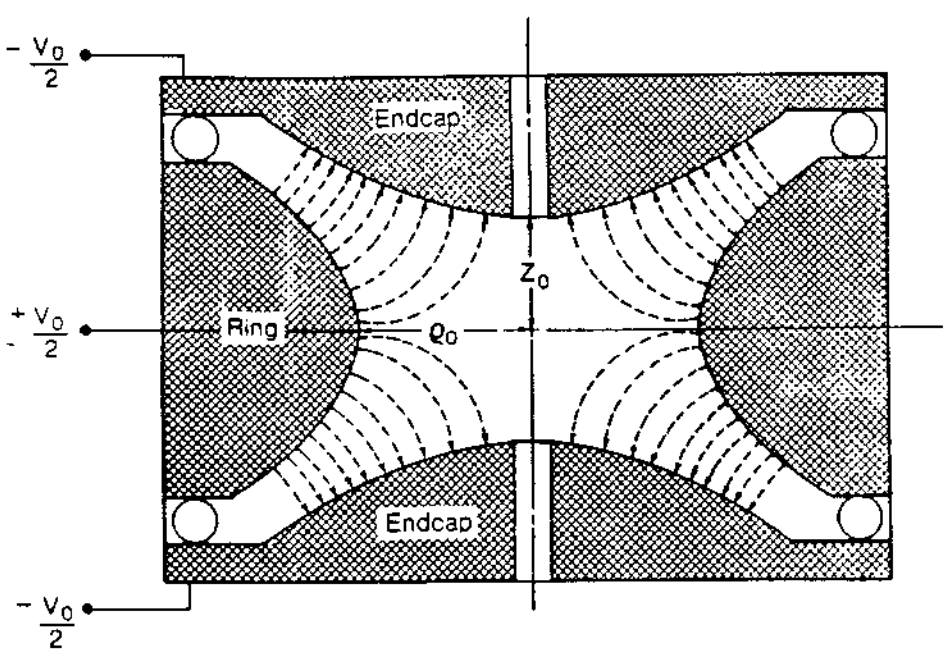

Fig. III-11. Cross sectional view of an asymptotically symmetric Penning trap. The dashed lines represent the electric field lines.

such a trap is shown in Fig. III-11. The top and bottom electrodes (endcaps) have hyperbolic curvature. The third electrode (ring electrode), also hyperbolic in curvature, is cylindrically symmetric about the vertical axis. The electric field produced by this configuration, when properly biased, will confine a negatively charged particle located near the center of the trap along the vertical axis but will repel the same particle towards the ring electrode in the horizontal plane. The superimposed magnetic field will force any transverse motion into a combination of cyclotron and magnetron (ExB drift) orbits. With an appropriately adjusted B field these orbits can be kept small compared to the transverse dimensions of the trap structure.

In an ideal Penning trap an electrostatic quadrupole potential

$$V = V_o \frac{z^2 - \rho^2/2}{2d^2} \quad , \tag{5}$$

and a homogeneous magnetic field along the vertical axis

$$\vec{B} = B_o \hat{z} \quad , \tag{6}$$

are superposed.

The quadrupole potential is commonly produced by placing electrodes along equipotential surfaces of V. The two branches of the hyperboloids of revolution

$$z^2 = z_o^2 + \rho^2/2 \quad , \tag{7}$$

represent the end caps, and the hyperboloid of revolution

$$z^2 = 1/2 \, (\rho^2 - \rho_o^2) \quad , \tag{8}$$

is required for the ring electrode. z_0 and ρ_0 are the minimum axial and radial distances from the trap center to the electrodes, and the characteristic trap dimension is defined by

$$d^2 = 1/2\ (z_0^2 + \rho_0^2/2) \quad . \tag{9}$$

In an asymptotically symmetric trap these quantities are connected by the relation

$$z_0^2 = \rho_0^2/2 \quad , \tag{10}$$

which places the electrodes at potentials $\pm V_0/2$, and leaves the center of the trap at ground. Other combinations of ρ_0 and z_0 are possible without disturbing the harmonic properties of the trap if appropriate electric potentials are applied to the caps and ring electrodes. For a ratio α of ρ_0 to z_0 the potentials applied to the electrode are related by

$$V_{Ring}/V_{Caps} = \frac{\rho_0^2}{2z_0^2} = \frac{\alpha^2}{2} \quad . \tag{11}$$

Because all electrode structures have to be truncated at some point the ideal quadrupole potential is only realized near the center of the trap, but additional electrodes (guard rings) can be used to correct, to some extent, the anharmonicity.[13] Harmonicity of the electric potential is not a stringent requirement for the confinement of the particles, but is desirable for most of the detection and cooling schemes described below. If the basic requirement of harmonicity can be lifted, virtually any geometric design and a wide choice of electric potentials is possible as long as the magnetic field overcomes the radially defocusing effects of the electric field.

In an ideal (harmonic) Penning trap the motion of a charged particle decouples into an axial motion independent of the magnetic field, which is a simple harmonic motion with frequency

$$\omega_z^2 = \frac{eV_o}{md^2} \quad , \tag{12}$$

and a radial motion, composed of the rapid cyclotron motion at the frequency

$$\omega_+ = \frac{\omega_c}{2} + \left(\frac{\omega_c^2}{4} - \frac{\omega_z^2}{2}\right)^{1/2} \quad , \tag{13}$$

where $\omega_c = \frac{e}{m} B$ is the cyclotron frequency in the absence of electrostatic fields, and a slow $\vec{E}x\vec{B}$ drift motion (magnetron motion) with frequency

$$\omega_- = \frac{\omega_c}{2} - \left(\frac{\omega_c^2}{4} - \frac{\omega_z^2}{2}\right)^{1/2} \quad . \tag{14}$$

The stability criterion can be stated in the form

$$\omega_c >> \omega_z \quad , \tag{15}$$

with the minimum requirement $\omega_c = \sqrt{2}\omega_z$ which reflects the dominance of the magnetic over the electric forces in the radial direction. Because the motions are harmonic, the system can be described quantum mechanically as three quantized harmonic oscillators.[14] However, for hadrons the quantum numbers are so large that a classical description is adequate, and the quantum mechanical description will be alluded to only in particular circumstances.

2. System Design. As will be discussed below, the optimum trap for antiproton capture following deceleration by the RFQ decelerator, and the optimum traps for cooling to 4 K temperatures, or for launching antiprotons for the gravity experiment, are not necessarily the same. Thus a system composed of more than a single trap, and the transfer of antiprotons from

one trap to another, must be considered. The strong uniform magnetic field required for trapping facilitates the transfer of charges from one trap to another with minimal loss. Consequently, a contiguous sequence of harmonic traps is envisioned. The operations of ion injection, cooling, transfer, and ejection at low energy can all be tested with H^- ions or protons, rather than antiprotons.

An important consideration with low-energy antiprotons is the vacuum necessary to prevent annihilation upon contact with matter. To obtain an estimate of the maximum pressure tolerable the cross sections for $\bar{p}$ + H annihilation from reference 15 can be used. The results of this estimate are given in Section III-G (see Fig. III-14), where contours of constant annihilation rate are plotted as a function of antiproton temperature and residual gas pressure. Pressures of 10^{-15} Torr at the temperature of 10 K keep the loss rate below 10^{-6} sec^{-1} per particle. This is not achievable with conventional room temperature vacuum techniques. However, cryogenic vacuum using liquid helium cooling is significantly more effective in producing these low pressures. Thus, we expect that the final trap, to be used for cooling the antiprotons to 4 K, and subsequent ejection, will be cryogenically cooled, as will the walls of the adjacent vacuum system. A graphite matrix will be used on the walls to provide enhanced pumping speed in the region of this trap. A slightly higher pressure is tolerable in the initial, or "injection" trap, which may be operable at room temperature. Weak coupling between the regions of pressure differing by up to a factor of 1000 can be easily maintained by a baffle and a small tube, through which the charged particles will be transferred.

The system we propose is composed of an elongated "injection" trap which is matched to the pulse of antiprotons emerging from the RFQ decelerator, and a set of two more conventional "precision" traps for final cooling and for particle ejection. The operations to be performed with this system consist of injection of antiprotons from the RFQ and pre-cooling, transfer of the antiprotons to the storage trap at moderate energy (tens of eV), final cooling to 10 K, and transfer to the launching trap for ejection at very low energy into the drift tube. Several different cooling mechanisms are available to reduce the antiproton energy. These mechanisms, and the inter-trap transfer technique, are discussed in some detail below.

3. Injection. In the framework of the current (preliminary) design, the RFQ decelerator output will provide us with a bunch of antiprotons at 20± 4 keV kinetic energy with a physical length of 30 cm. The goal is to transfer the entire bunch into a first trapping structure which is sufficiently large to accept all the particles provided by the RFQ without significant loss, and still maintain basic harmonicity to allow some initial cooling. After the phase space has been sufficiently compressed, the bunch will be transferred into a second trap which is better suited for further cooling and preparation for the experiment. Figure III-12 shows a preliminary set up which is currently under investigation at LANL. The 20 keV antiprotons are focused by an einzel lens (not shown) to match the magnetic field lines of the fringe field of the superconducting solenoid. This is necessary to minimize the transverse energy and the growth in longitudinal energy spread due to the mirror effect in the inhomogeneous region of the magnetic field. It also provides an upper bound to the possible increase in longitudinal energy once the particle is trapped, due to the coupling between the radial and axial degrees of freedom in this somewhat anharmonic trap structure. Antiprotons at this relatively low energy are strongly bound to the magnetic field lines and the size of the

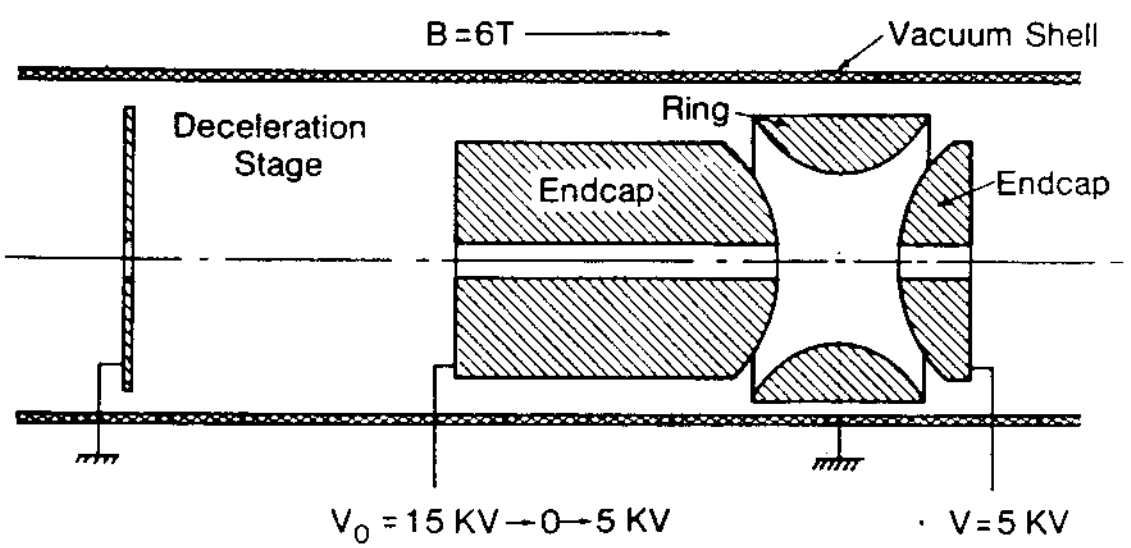

Fig. III-12. Schematic view of the catching trap currently used at the Los Alamos National Laboratory.

beam spot is drastically reduced once the particle enters the high field region (B>1 T) as shown in Fig. III-16. Here the ions enter an electrostatic deceleration section which reduces the longitudinal energy from the initial 20 keV to a value limited by the intrinsic energy spread of the bunch. At the same time the physical length of the bunch is compressed by the square root of the ratio of initial to final energy; in our case from 30 cm to approximately 15 cm. While the particles are drifting through the field-free region inside the front endcap, the potential can be lowered to zero before the bunch emerges into the trap. The downstream endcap is held at a retarding potential so that the particles eventually come to a stop and turn around. At this time the upstream endcap is pulsed up to a potential high enough to close off the potential well, thereby trapping the particles at a kinetic energy reduced by a significant factor from the initial energy (20 keV to 2.5 keV in this specific example).

To trap the entire bunch of 15 cm length and to allow for some spread in the drift region a trap structure with length $z_o = \rho_o/\sqrt{2}$ cannot be used. The trap structure we plan to use is designed with $z_o = 5\ \rho_o$. In order to place the center of the trap at $V_{cap}/2$ during the catching period the ring electrode has to be set to $V_{Ring} = +.48\ V_{cap}$. After capture is completed the voltages can be changed to $V_{Cap}/2$ for the endcaps and $-.02\ V_{Cap}$ for the ring electrode to adjust the center of the trap to zero volts for the subsequent transfer to the compensated trap.

After the antiprotons have been cooled to some moderate energy of the order of a few tens of eV, using one or several of the cooling techniques described in the next paragraph, we can either transfer the particles to a second trap which is better suited for further cooling or repeat the filling and precooling cycle with the next macropulse from LEAR, this time lowering the upstream endcap only to a few hundred volts. This will prevent the previously stored particles from escaping from the trap but still allow the injection of higher energy particles from the RFQ system. Repeating this cycle, the first storage trap may be filled to some fraction of the space charge limit, which for the dimensions and field values we plan to use is on the order of 10^{10} to 10^{11} cm^{-3}.

4. Cooling. After the energy of the antiprotons has been lowered from 20 keV to about 3 keV by the previously described injection technique, several different cooling mechanisms can be used to reduce the energy

further to the subthermal temperatures required by subsequent experiments. To understand the cooling systems to be presented, it is necessary to consider the relaxation of the confined bunch of particles produced by ion-ion collisions or by anharmonicities in the trapping potential. The time scales set by this relaxation determine the types of cooling which can be expected to be effective. To cool completely the stored charge cloud, it is necessary either to cool the cyclotron and axial degrees of freedom, or to have rapid coupling between the cyclotron and axial oscillations. The magnetron motion is largely decoupled and has low kinetic energy. Coupling between the axial and the cyclotron motion can occur either by collisions, or by anharmonicities in the potential. Ion-neutral collisions are negligible, by virtue of the low ambient pressure maintained in the trap. The leading anharmonicity of the potential which couples the axial and radial motions has the form[16]

$$V = -3V_o \beta z^2 \rho^2 / 2d^4 \qquad (16)$$

where $\beta = 10^{-3}$ or less in typical traps. Since the cyclotron and axial oscillation frequencies differ by about a factor of 100, this coupling will transfer energy only slowly - in times not less than the order of seconds based on studies using trapped ion clouds. The only other mechanism is ion-ion collisions within the trapped cloud of charges. For this relaxation time constant, we turn to plasma physics. The Spitzer self-collision time[17] for a group of antiprotons with charge e, mass m_p, interacting with each other at an absolute temperature T is given by

$$t_c = \frac{7.8 \times 10^6 \, (\frac{kT}{e})^{3/2}}{n \, \ln\Lambda} \qquad (17)$$

where n is the density in cm^{-3}, and $\ln\Lambda$ is a shielding constant, with a value near 20 for ions in a trap. Figure III-13 shows the relaxation of a trapped cloud of about 10^5 protons interacting with themselves at a temperature (kT/e) ~ 0.33 eV. Energy is pumped parametrically into the

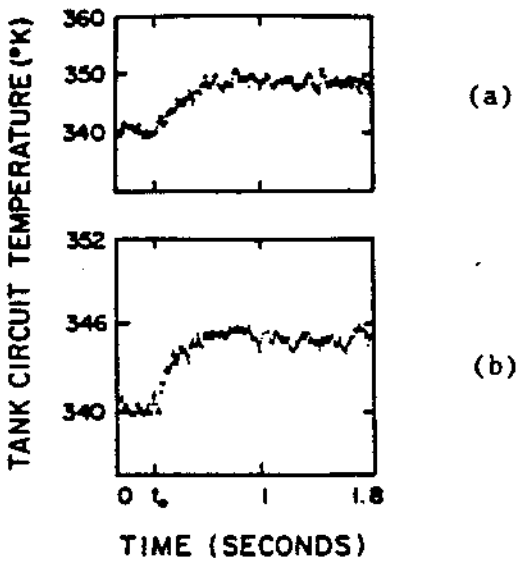

Fig. III-13. Relaxation of a trapped cloud of about 10^5 protons after the energy is increased by (a). 75%, and (b). 40%.

radial motion at time t_0, and scatters into the axial motion. The energy is monitored with a tuned "tank" circuit, which has an effective temperature (measured by Johnson noise fluctuations) proportional to the ion temperature. In Figure III-13(a) the temperature of the cloud is increased by 75% and in III-13(b) by about 40%. One sees clearly the faster relaxation at the lower temperature in (b), as predicted by Spitzer theory. The magnitudes, based on the measured ion parameters, differ only by a factor of two from the theory, while the ratio of the measured and calculated relaxation times are in agreement. These relaxation times are relatively rapid; however, if the mean ion temperature were increased to 10^6 K (=86 eV), one estimates $t_c \approx 5 \times 10^3$ sec, if the other parameters are kept constant. Thus, ion-ion collisional relaxation is unimportant except for temperatures corresponding to a few eV or less, unless higher densities than $10^5/cm^3$ are maintained. We now return to cooling. Several different cooling mechanisms are available, each having its place at a certain stage. The commonly used technique for cooling stored ions is the damping with an external resistor, sometimes in earlier publications also referred to as radiative cooling (not to be mistaken for cooling by synchrotron radiation which has a prohibitively long time constant for heavy particles but works

quite well for electrons and positrons). Imagine a proton with mass m and charge e oscillating at a frequency ω_z between two infinite plates at distance $2z_0$ connected by an external resistor R. The current $i = ev_z/2z_0$ induced by the oscillating motion of the ion will dissipate energy due to Joule heating of the resistor and damp the motion with a time constant.

$$t = 2mz_0^2/e^2R \qquad (18)$$

until the temperature of the resistor and the motion of the particles come to equilibrium. In practice the two infinite plates are replaced by the two endcaps of the trap whose capacitance is tuned out by an inductor L. In this case the resistor R is given by the quality factor of the tuned circuit as $R = Q/\omega C$ and is for typical circuits of the order of 10^6 Ohms, setting the time constant in the traps we are using to the order of tens of seconds. This time is valid for a single particle as well as for an ensemble of particles in a completely incoherent motion and could be drastically reduced if coherence could be introduced to the motion along the z-axis without increasing the energy. The resistive damping time constant for large traps and antiprotons is long: for typical parameters about 100 seconds. But it is short compared to expected particle storage times under ultra-high vacuum conditions. For example, cooling ions from 500 eV to 1 eV requires about 6.2 time constants or about 10 minutes. Thus, with superior vacuum, the particle loss should be minor even during this long cooling period. Also, in the actual experiment the time constant for direct cooling of the cyclotron motion using a split ring design could be significantly shorter than the collisionally coupled cooling, depending on the geometrical factors defining the coupling between the particles and the external circuit. Experiments to investigate these possibilities are currently under way at Texas A&M University and at LANL.

A very rapid initial cooling can be achieved by the technique of adiabatic cooling. As described in the first part of this section, the axial motion of the trapped particles can be described by a harmonic oscillator with energy eigenvalues

$$E_z = (n_z + \frac{1}{2})\,\omega_z \qquad (19)$$

proportional to the square root of the applied external potential. If this potential is reduced adiabatically, the quantum number remains constant and the energy is reduced by the square root of the ratio of initial to final well depth. The adiabatic requirement calls for a time constant large compared to a period of the z-motion, which in our case is in order of several microseconds. A limitation to this technique is given by the requirement that the final well depth must still be larger than the final kinetic energy of the particles to maintain trapping conditions.

A cooling technique common in accelerator rings but not yet established for trapped particles is the method of electron cooling. In accelerator rings the "transverse hot" antiprotons are merged with a beam of "transverse cool" electrons, both occupying the same longitudinal phase space. Through Coulomb collisions the transverse motions are brought to thermal equilibrium, thereby cooling the transverse motion of the antiproton beam. Even though the conditions are vastly different in a Penning trap it is a method worthwhile looking into since first estimates yield time constants comparable or shorter than the radiative cooling technique[3]. Penning traps can confine particles of the same sign of charge, e.g. antiprotons and electrons or protons and positrons. We now consider the collisional transfer of energy from the hot heavy particles to cooler, light particles held near a low temperature. For dissimilar masses, e.g. electrons and antiprotons, Spitzer[17] has given an expression for the equipartition time constant to equilibrate the initially different temperatures T_e and T_p. This is given by

$$t_{eq} = \frac{5.87}{1836\, n_e\, \ln\Lambda}\,(T_p + 1836 T_e)^{3/2} \qquad (20)$$

where n_e is the electron density and $dT/dt = (T_f - T)/t_{eq}$. Due to their small mass, electrons will rapidly come to equilibrium with themselves at temperature T_e. Likewise, the protons will come to equilibrium with

themselves with a time constant 43 times longer, if at the same density and temperature. The two particle gases would then come to equilibrium with each other with the time constant t_{eq}.

For our case of interest, the electrons would be produced in the trap by a burst of electrons from a field emission tip. These electrons will rapidly cool by emission of synchrotron radiation with time constant

$$t_s = 3mc^2/4e^2\omega_c^2 \approx 10^{-1} \text{ sec, at } B = 6T \qquad (21)$$

With sufficiently high electron density, all degrees of freedom will be collisionally coupled. The cold electrons can be axially coupled to a tuned circuit between the endcaps with frequency $\omega_z \approx 60$ MHz, and damping time constant T_d less than 1 second. The tuned circuit temperature will be 4 K.

When the antiprotons are transferred to the trap, the electrons will remain confined if the endcap potential is not reduced to zero. Although the equilibration time constant initially will be long due to the large temperature difference between antiprotons and electrons, it is calculated to be a few milliseconds using reasonable parameters for a proton temperature of 1 eV. Thus this method is expected to provide rapid cooling, once the antiproton energies have been reduced significantly by other means. The electrons will, of course, be heated while the antiprotons are cooled, but their temperature can be held to a relatively low value by the combination of synchrotron radiation cooling and coupling to the axial tuned circuit. Once cooling has been accomplished, the electrons can be selectively removed from the trap by resonant excitation. To provide an experimental input to these questions the collaborators at Rice University are preparing an experiment to inject low energy positrons into a Penning trap. The positrons will rapidly cool by synchrotron radiation until they reach an equilibrium temperature set by the experimental environment. Subsequently hot protons will be injected and the temperature and cooling rates will be monitored using standard bolometric techniques.[18]

Recently the collaborators from Genoa and Pisa have started to investigate the possibilities of stochastic cooling in ion traps.[2] Even though at first it appears that on such a small scale as in an ion trap the coupling between the kicker and the pick-up would be so strong as to

prohibit this approach, it might be a viable solution if the same set of electrodes are used for both actions by employing a fast switching network to define the status at each instant rather than using two separate electrode sets. Preliminary results are very encouraging but further detailed studies and experimental verifications are needed.

Thus far we have dealt with cooling the axial and the cyclotron motion. The third degree of freedom (the magnetron motion) is an entirely different problem. The energy stored in the magnetron motion is mostly potential energy, and reduction of this energy would cause the particles to slide down the potential hill created by the quadrupole potential in the radial direction. This would increase the trajectory radii of the particles until they would be lost from the active trapping volume. Fortunately, the damping time constant is very large, so that the magnetron motion is essentially stable. Still, to increase this time constant even further or to confine the particles to a small region in the center of the trap, which is necessary for precision experiments, the magnetron motion needs to be controlled externally. It is necessary to pump, not to dissipate, the energy in the magnetron motion. This can be done by exciting the particle's z-motion or cyclotron motion using the side band frequency $(\omega_z + \omega_m)$ or $(\omega_+ + \omega_m)$ respectively. This will increase the energy in the magnetron motion confining the orbits to the center of the trap. It is important to use the upper sideband, since the lower sideband excitation heats the ions, tending to increase the magnetron motion radius and to drive them from the trap. The net effect with the proper sideband choice is to reduce the magnetron radius, bringing the ions to the center of the trap. This is the desirable location for efficient ion transfer. At the same time this excitation will heat the axial or cyclotron motion unless this energy is dissipated by one of the above mentioned methods. The technique of side band heating (and cooling) has successfully been demonstrated for electrons, positrons, and protons.[19]

5. Experimental Sequence. In the actual experiment we intend to use a combination of different cooling mechanisms described above. After the particles have been captured in the first storage trap ($z_0 \sim 10$ cm) they will fill the entire potential well of 2.5 keV. Within about 5 time constants (approximately 3000 seconds for the current design) their mean energy will be reduced by resistive cooling to 20 eV. At this time the

physical size of the antiproton bunch will be reduced from its initial value of 30 cm at the output of the RFQ decelerator to about 2 cm and the entire bunch will be transferred to a second trap with $z_0 \sim 1.5$ cm. The proposed method is to weakly excite the stored, cooled, ions near axial resonance, with a potential difference varying with time between the endcaps, to establish coherent motion with a relatively well-defined phase. For weak damping, the axial oscillation amplitude will be given by

$$z(\omega) = \frac{\gamma q V(\omega) e^{i\omega t}}{2md(\omega_z^2 - \omega^2 - i\,\omega/\tau_c)} + z_i e^{i(\omega_z t + \phi_i)}, \qquad (22)$$

where the first term represents the coherent oscillation of the particle center of mass, and the second term the relatively undamped random motion of an individual ion before excitation began. For ω close to ω_z, the amplitude of the coherent oscillation can be made much larger than z_i. Because the frequency is relatively low ($\approx$ 1 MHz), the timing to suddenly lower the potential of the adjacent endcaps of the two traps can be well defined relative to the phase of the induced coherent motion. The detection of a pulse of charges by ejecting them in this manner into a detector has already been demonstrated. Because the phases are relatively well-defined, the length of the bunch transferred should be significantly less than either of the traps, making efficient transfer possible. We have already demonstrated the means of switching potentials in nanosecond times, much shorter than a period of the axial oscillation in either trap. Switching of the potential at the second trap with appropriate timing will allow us to capture the entire bunch without significant loss. After transfer a drastic further reduction of energy can be accomplished by adiabatic cooling. Lowering the potential from its initial value of 2.5 kV to 5 V the energy of the particles will be lowered to 1 eV with minimal boil off. In this trap (with z_o = 1.5 cm and V_o = 5 volt) the antiprotons will initially be confined in a longitudinal stretch of 1.5 cm. This second trap is the main storage and cooling trap and can serve a multitude of purposes depending on the specific experiment to be done with the antiprotons The antiprotons can be cooled further by resistive cooling (the time constant is reduced to ~ 30 seconds

due to the smaller z_0) or electron cooling can be employed here by injecting electrons from a field emission cathode. For the gravity experiment under discussion in this proposal it is necessary to cool the particles further to temperatures near 4 K (~ 3 x 10^{-4} eV energy) and at the same time to have only a few particles at a time (about 100) present at a time in the trap or drift tube respectively. To accomplish this, another transfer to the final measurement trap is necessary. This can be done using a technique similar to the standard ejection technique used in the time-of-flight (TOF) measurements developed at the University of Mainz.[20] On top of a linear reduction of the potential applied to the trap electrodes short triangular spikes are superimposed. Each of these spikes allows particles within a slice of the axial energy distribution between V and V + ΔV to escape from the trap. The percentage of the particles occupying this part of the distribution actually escaping can be controlled by the time length Δt of the spikes compared to the period of the axial oscillation. If the time is longer than the period for one oscillation, all the particles within the correct energy window will escape (half of them in the right direction); if the time is shorter than one period, only those moving towards the endcap and reaching their turnaround point during the time Δt will escape. The mean kinetic energy and the energy spread of the particles will be determined by the amplitude of the voltage spike and can be on the order of a few tens of milli-electron volts or less. Appropriate timing of the potential of the measurement trap again will enable us to capture the particles at low energy without significant losses.

Due to the small physical size of this trap, the coupling between the antiprotons and the external structure is drastically increased and therefore the time constant for resistive cooling is reduced to approximately 3 seconds. Thus the final cooling from about .1 eV to 3 x 10^{-4} eV (4 K) can be achieved in a time of less than 20 seconds. Rapid cooling becomes more and more mandatory at these low kinetic energies since the annihilation cross sections are increasing rapidly.

The described scheme relies entirely on established techniques of cooling. Should initial experiments with electron cooling or stochastic cooling prove successful these techniques can be implemented at the appropriate section (i.e. stochastic cooling in the first storage trap, electron cooling in the main cooling trap and/or the final launching trap).

F. The Drift Tube

The drift tube is the region where the extraneous forces on the antiproton are minimized so that the effect of gravity can be determined. All vertical forces must be reduced well below the expected gravitational force. Then the TOF of antiprotons in the drift tube can be measured. If the force is mg then the longest possible flight time through the tube for normal gravity is $t_{max} = \sqrt{2\ell/g}$. If a vertical electric field is superimposed, then the maximum time is obtained by substituting $g + \frac{e}{m} E$ for g in the original expression for t_{max}. To prevent horizontal forces from deflecting the antiproton path from the source to the detector, a magnetic field must be set up oriented vertically so that flux lines passing through the source also pass through the detector. Thus we arrive at the geometry of the drift tube; a long vertical tube surrounded by a coaxial solenoid. The magnetic field gradient needs to be small in order to minimize the interaction of the antiproton's intrinsic magnetic moment plus its orbital magnetic moment with the gradients which produce vertical forces. The smaller the diameter of the vertical tube, the smaller the dimensions of the magnet required.

We must also worry about the patch effect which is a variation of electric potential along the surface of the drift tube that is caused by differences in the work functions of the crystal surfaces that make up the inside of the drift tube. Statistical variations in the number of patches of different potential result in large scale potential variations on the order of 10^{-4} V a few centimeters away from the metal surface. The larger the drift tube diameter the smaller the potential variations along the center of the tube. Experiments on freely falling electrons done by Witteborn and Fairbank showed that the patch forces are shielded inside an electro-formed copper tube when that tube is cooled below about 5 K. Subsequent work by Lockhart showed that this shielding effect worked only if the drift tube temperature was below 7 K and the magnetic field was not too high. The limits on the magnetic field are not clearly defined because this field tended to quench the electron multiplier detector. In addition, recent advances in surface coating technology has allowed for the fabrication of conducting coatings with very small (atomic scale) grain sizes (see Section II-D). The effects of temperature and magnetic fields on

such surfaces will be studied by the collaboration in the drift tube development.

Drift tubes used in the electron free fall experiments were electroformed onto accurately machined aluminum mandrels. The aluminum was then dissolved away thus leaving an accurate bore inside the tube with surface smoothness comparable to the mechanically polished aluminum mandrel. Subsequent interaction with the atmosphere left a thin copper oxide coating. This approach was intended to leave an amorphous surface in order to minimize the patch effect yielding patches of the minimum size. The result at low temperature was so much better than anticipated that it was clear that some additional physical mechanism was at work. This mechanism is not fully understood. While it is not certain that this is the only surface that will give the desired shielding effects at 4 K, it is the only one that has been demonstrated. Experiments with microwave cavities* have shown unusual properties for such oxidized copper surfaces compared to other materials. Consequently we propose that the same method be used in manufacturing the drift tube for the antiproton experiment. In addition it would be highly desirable to precede the construction of the large drift tube with the production of several small tubes to determine what factors are most critical for successful fabrication. The surface coating techniques discussed earlier will also be studied using these short drift tubes.

G. Vacuum Requirements for the Ion Trap Drift Tube System

In addition to the vacuum requirement set by the induced dipole effect on antiprotons drifting up the drift tube (see Section II-D), a more important requirement is set by the annihilation rate of the particles with residual gas molecules. We can generally expect the annihilation cross section to increase with decreasing antiproton energy and to be larger than the geometric cross section due to induced dipole effects. The work reported in Ref. 15 estimates the annihilation cross section for $\bar{p}$ on hydrogen. For the ultra low energy cross sections required here, the adiabatic condition is satisfied ($v < \alpha c (M_e/M_p)^{1/2}$).

*Private communication, W. M. Fairbank.

From Ref. 15 we take the low energy (T < 1eV) cross section to be given by

$$\sigma = 3\pi a_o^2 \left(\frac{T_o}{T}\right)^{1/2} , \tag{23}$$

where $a_o = 0.529 \times 10^{-8}$ cm, $T_o = \alpha\, m_e c^2$, m_e is the electron rest mass, and T is the kinetic energy of the $\bar{p}$ in the center-of-mass (COM) system. We will assume, for simplicity, that the antiprotons and residual gas molecules are in thermal equilibrium which implies that the lab frame is the COM frame, aside from an averaging over the relative velocity direction. This assumption should be valid for the ultra-low energies of interest here. The mean free path for annihilation can be written as

$$\ell = \frac{1}{\rho\sigma} , \tag{24}$$

where σ is taken from Eq. 23 and ρ is the particle density in cm^{-3}. The annihilation rate will be given by

$$R_A = \frac{v}{\ell} , \tag{25}$$

where ℓ is given in Eq. 24 and v is the average velocity given by

$$\frac{1}{2} mv^2 = \frac{3}{2} kT . \tag{26}$$

The number density of particles can be related to pressure and temperature using the ideal gas law

$$\rho = \frac{P}{kT} \tag{27}$$

where P is the pressure, k is Boltzmann's constant, and T is the temperature. Assembling these results allows us to relate the annihilation rate to the antiproton temperature an residual gas pressure. This relationship is displayed in Fig. III-14 where contours of constant annihilation rate are plotted as a function of pressure and temperature. Evidently, 20 K antiprotons at a residual gas pressure of 10^{-15} Torr will have an annihilation rate of 10^{-6} sec^{-1}. This means that the 1/e time will be 10^6 sec or ~280 hrs. We plan to execute a TOF measurement on a time scale that is fast compared to this. Thus the low energy storage time is not a concern provided vacuums of the order of 10^{-14} to 10^{-15} Torr are achievable.

By normal vacuum standards, 10^{-15} Torr is an unusually high vacuum. However, the ultra-low energy end of our storage system and the drift tube will be operated at liquid helium temperatures. Under these cryogenic conditions diffusion through the walls becomes very low and much of the

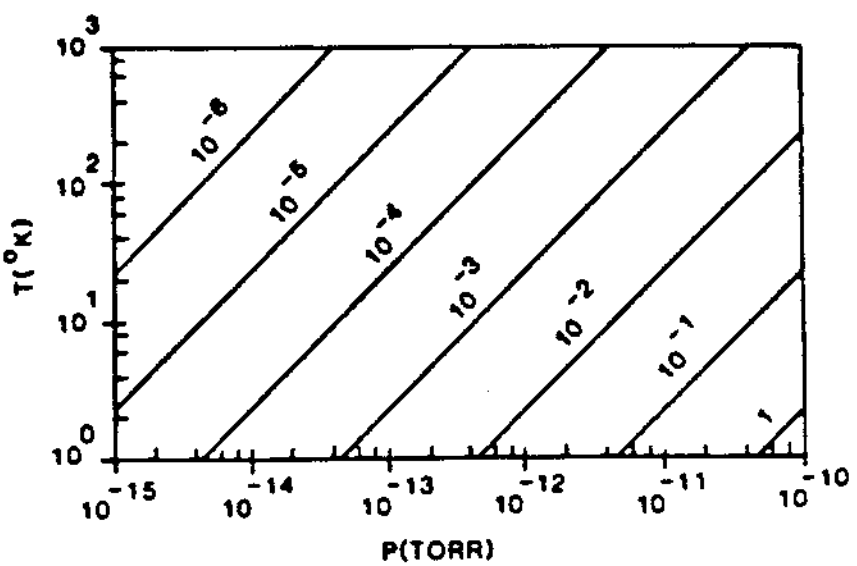

Fig. III-14. Contours of constant annihilation rate per particle (sec^{-1}) as a function of temperature and residual gas pressure. The cross sections are taken from Ref. 15.

residual gas is simply frozen out onto the walls of the vacuum vessel. The work of Thompson and Hanrahan[21] has shown that vacuums better than 10^{-14} are achievable at liquid helium temperatures provided that the system is closed. Thus vacuums of the order of that required by our experiment are achievable with a cryogenic sealed system.

H. Experimental Development

Development and testing of the antiproton deceleration system, the trapping apparatus, and gravity measurement techniques will be carried out before installation of the apparatus at LEAR. In this section we outline our development plans in the areas of bunching and RFQ deceleration, low energy beam transport and H^- calibration source, vacuum and cryogenic considerations, ion trapping, drift tube and particle detector, and data acquisition and analysis. We also discuss the collaboration expertise and funding for the experiment.

1. Bunching and RFQ Deceleration. The initial beam dynamics study resulted in the design of an RFQ decelerator system that includes two bunchers, an RFQ, and a final energy shifter cavity. The calculations show that this system will bunch 50% of the 5-MeV beam from LEAR and decelerate it to 100 keV. The RFQ length is about 3.2 meters and the rf frequency is nominally 200 MHz. The energy shifting cavity allows the final beam energy to be adjusted to a value within the range of 20 to 200 keV. For our experiment a final beam energy of 20 keV will be required.

Additional beam dynamics studies will be required to optimize the system, especially with regard to obtaining a smaller final energy spread than the present value of ± 4 keV. Lower energy spread will reduce the amount of debunching and longitudinal spreading of the final beam, thereby allowing an increased capture efficiency for the ion trap.

The RFQ structure, due to the 5×10^{-4} rf duty factor and 200 MHz frequency, will be similar to the RFQ1 at CERN; the vanes and the tank are of copper-plated mild steel with vanes cooled by heat transport to a water cooled tank. The difference here is the use of two pairs of shorting rings to stabilize the rf field of a much longer structure and a multi-driver loop setup needed by the rf generator arrangement for 600-kW peak power. The three buncher-type cavities in the transport line are also similar to the ones at CERN, although somewhat simpler because they are not housing any

focusing quadrupoles. During the operation, the transport line will be isolated from the LEAR ring by an orifice of sufficient impedance and differential pumping. The alignment of the decelerator elements is foreseen to be via optical targets and spirit levels.

The RFQ decelerator will require ~500 kW of pulsed rf power at a frequency of 200 MHz (see Section IV for average power requirements). There are several types of rf power systems available today that would be applicable. Four options have been studied at a preliminary level.

A klystron system of conventional design, while very well known, has several drawbacks, not the least of which is its high cost and nonportablility. The state-of-the-art in solid state rf power systems has reached a stage that makes it an attractive, although still expensive, candidate. A suitable system might incorporate 16 solid-state modules, at 31 kW each, into a single amplifier. Such a system would require some development by the vendor, while conventional components would be procured commercially. Los Alamos would assemble, integrate, and test the system. A prototype version of a planar triode ring amplifier has recently been built and demonstrated at Los Alamos. A variant of this design would be readily applicable to the requirements of the decelerator. A final option, and the most economical one, utilizes 11 cavity-tuned planar triode amplifiers and a solid-state driver to produce the required power. In these two final options, Los Alamos would design, fabricate, test, and integrate the entire system. Commercial vendors would provide the power supply and some specialized components.

Prior to delivery and installation at CERN, the RFQ decelerator system would be thoroughly tested and exercised at full power with beam. The decelerator would be considered a "turn-key" system. There are several critical stages of testing required to assure correct and reliable performance.

Prior to committing to the fabrication of the power version of the decelerator, a "cold" model will be built and studied at low power. These studies are considered an integral phase in the design and construction of any new linear accelerator and assure that the rf characteristics of the power model will be correct.

The rf power system will be connected to a dummy resonant load for final check out and final acceptance testing prior to driving the

decelerator itself. The decelerator and power system will then be integrated into a "turn-key" system and exercised thoroughly.

The final phase of testing would be performed using a low current proton or H^- beam at the Los Alamos Ion Beam Facility. This series of tests would serve to verify the decelerator design in the sense that it produces a beam having the expected properties. In addition, these properties would be fully characterized as a function of the operating parameters.

2. Low Energy Beam Line. We have constructed at the Los Alamos Ion Beam Facility a low energy beam test line that is nov operational. Figure III-15 displays the test line in an early phase of construction. In part (a) of the figure the beam enters from an existing accelerator line at the lower left and passes through a series of valves, cold traps, four-way slits, pumps, magnetic steerers, and electrostatic lenses. It is then turned to the vertical direction by the 90^o magnet mounted in the large vertical support stand at the center of the photograph. Above the magnet an ion pump and other ultra-high vacuum elements await the solenoid magnet, trap, and drift tube shown in Part (b).

In this development we used experience gained and some equipment from another experiment.[22] In particular, the hydrogen-ion source and accelerator we are using is larger than necessary for the final system, as it will attain a voltage of nearly 120 kV if desired. However it is an excellent source to use for the many tests we will carry out, and can be operated as low as 8 kV with good beam intensity. We can readily accelerate either protons (p) or negative hydrogen ions (H^-). Our ongoing tests of the low energy beam line and trap injection will allow us to study vacuum isolation procedures, bakeout procedures, ultimate vacua obtainable with the trap at room temperature, the ion trap pulsing to capture 20-keV p or H^- particles, the features needed in the final ion-trap design, and the characteristics we will need for a more portable p/H^- ion source to be a part of the apparatus when installed at LEAR. We expect to be able to purchase this calibration source from a commercial vendor.

Our first tests of directing a low-energy beam into the ion trap through the three-mm diameter apertures in the end caps was done with the solenoid magnet unenergized. In these tests we have achieved a 2.5-μA, 20 keV, H^- cw beam completely through both the lower and upper endcaps with excellent transmission. Because of the magnetic focusing effect mentioned

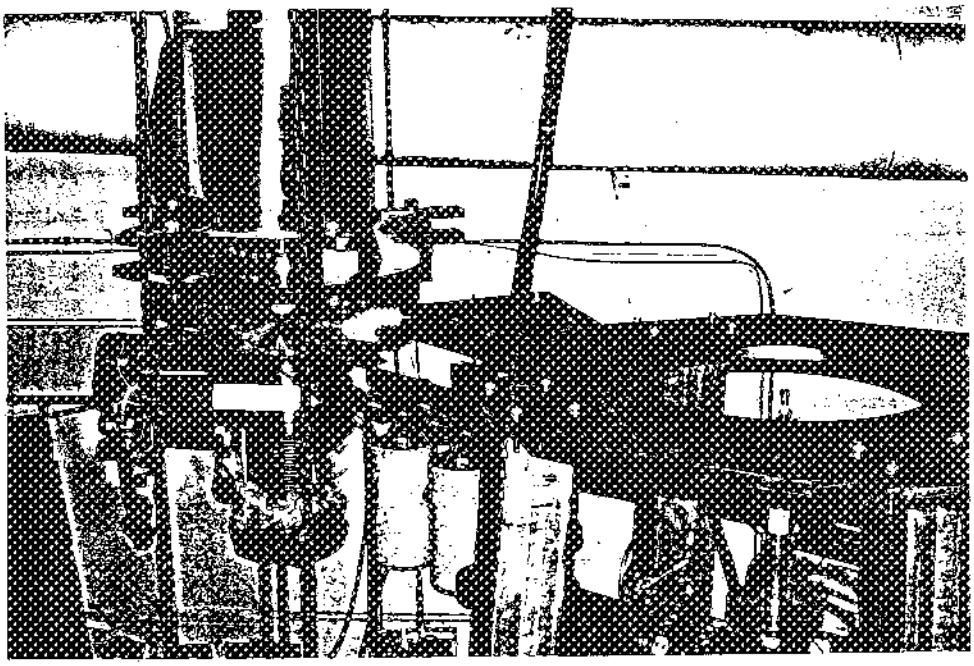

(b)

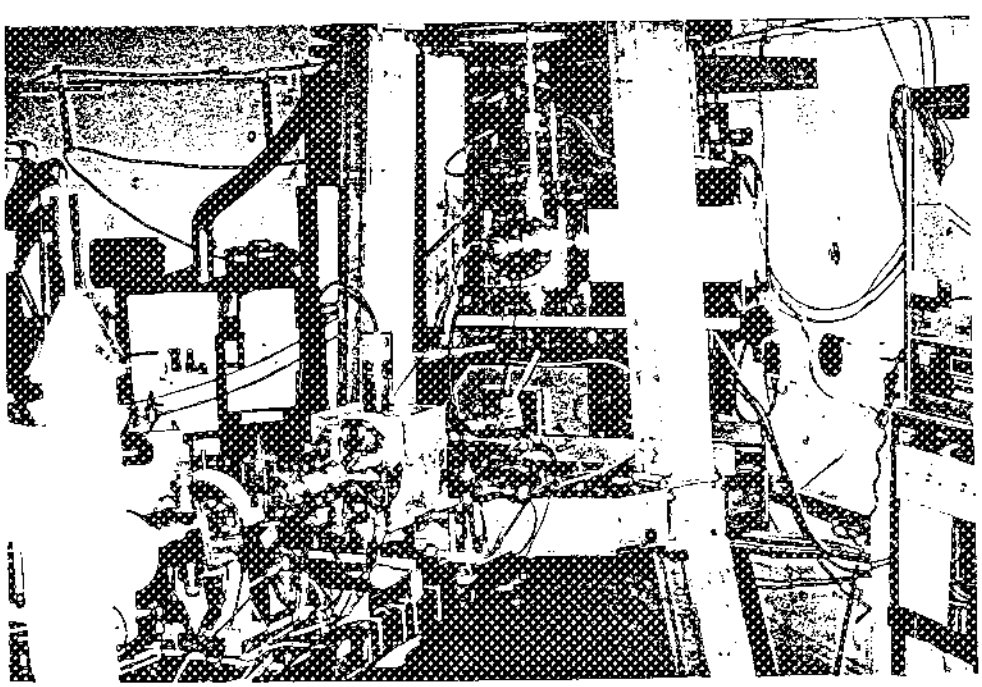

(a)

Fig. III-15. (a) Photograph of the now completed 20-keV beam transport system in an early construction stage. (b) The solenoid magnet, trap, and drift tube ready to be installed at the top of the support stand. Only the bottom one third of the outside of the cryogenic dewar arrangement is visible.

below, we expect to be able to achieve a higher beam current into the trap when the solenoid magnet is energized. The expected beam current would allow the capture of about 10^6 ions for a typical trapping procedure in our present trap. We anticipate that the pressure in the trap will be in the 10^{-9} range for these first tests.

In order to anticipate any problems that might arise in injecting particles into the trap through the fringing field of the 6-T superconducting solenoid magnet, we have used the computer code PSOL to study the trajectories of the incident particles. These trajectories are displayed in Fig. III-16. The calculation shows that the solenoidal field actually improves the transmission into the trap, provided that the particle trajectories are matched to the field lines of the fringe field and the magnetic axis is reasonably well aligned with the trap axis. This alignment is straightforward with the present test arrangement.

With the present system we are currently executing beam transmission tests with the solenoid energized. When these tests are complete we will energize the upper endcap of the ion trap at a potential greater than the beam energy and attempt to reflect the particles back out of the trap. Finally we will energize the lower endcap using the high voltage pulser we have developed when the beam-burst is in the trap, to capture the particles.

3. Vacuum System. Because the vacuum requirements for this experiment are rather stringent, they have to be addressed in some detail. To prevent the annihilation of antiprotons on residual gas particles from becoming appreciable on the 1 hour timescale needed for one complete TOF spectrum, the pressure in the final trap region has to be below 10^{-14} to 10^{-15} Torr. This is only possible using a rather closed system at cryogenic temperatures.[21] The fact that a low energy antiproton or H^- beam has to be injected prevents us from completely closing off the system. However, a series of cold baffles and apertures can be used to isolate the room temperature part from the final trap region, which will be held at liquid helium temperature. In addition to keeping the trap system as closed as possible and cooling the trap and the drift tube to 4 K, the surrounding vacuum shell will be held at 4 K as well. A graphite matrix applied to the inside of this vacuum shell will provide additional high speed cryogenic pumping. Finally this part of the vacuum system will be closed off from the beam line by an all metal valve after the antiprotons have been captured.

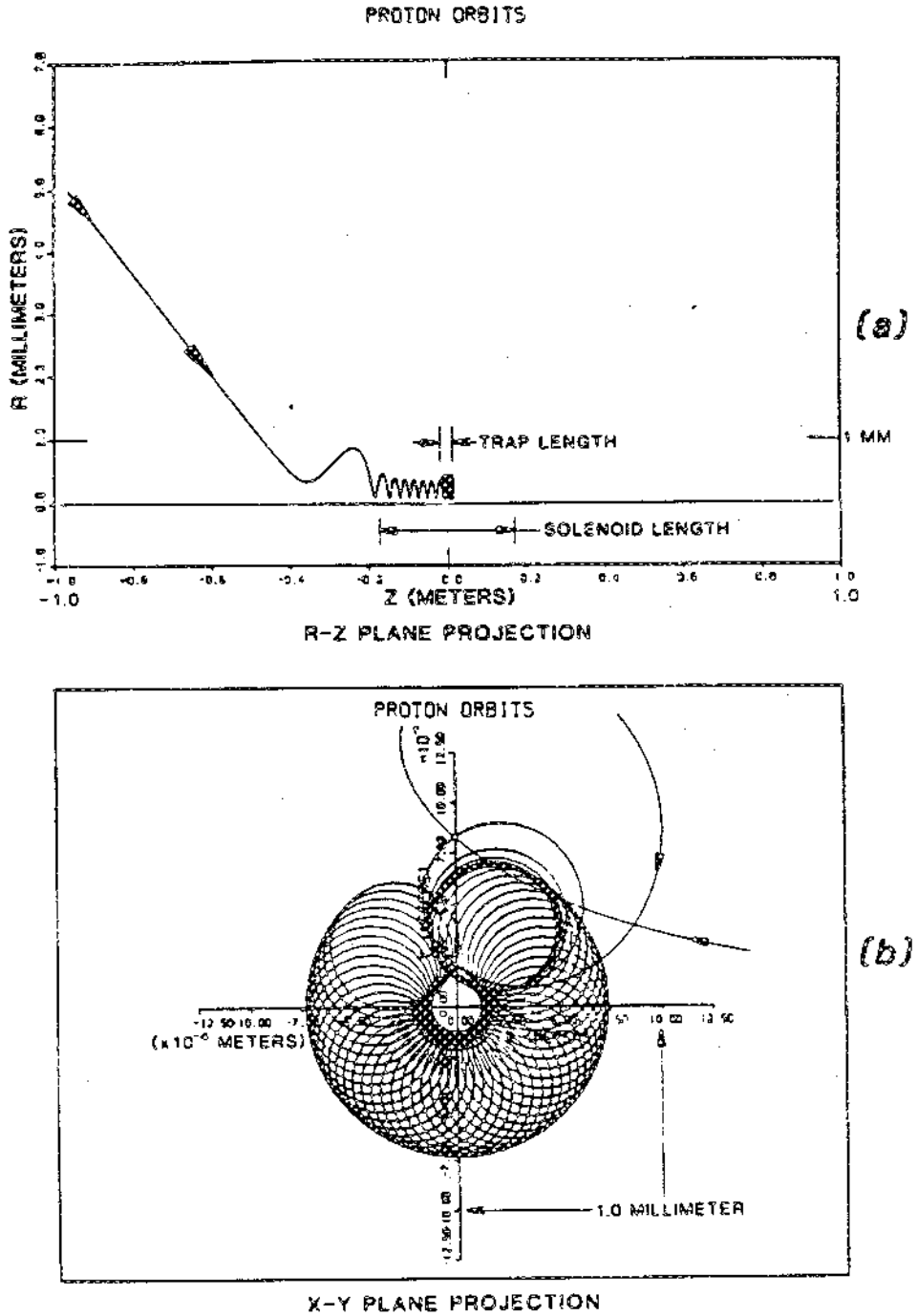

Fig. III-16. (a) Radial-axial orbit of a proton in the 6-T magnetic field. The entrance orbit is from the last (vertical) electrostatic lens. Note the greatly expanded abscissa. Calculations show that the ability to enter the trap is not very sensitive to a few mm displacement of the incoming beam axis. (b) End-on view of the orbit of Part (a). Note the appearance of the cyclotron motion (small orbits) superimposed on the larger circular magnetron motion. The ion trap in our present test system has a 3-mm diameter entrance aperture.

In addition, to avoid coating the trap and drift tube structure with residual gas molecules during initial cool down, the system will have to be pumped down to a pressure in the 10^{-12} Torr range first. The same pressure requirements are imposed on the remainder of the system in order not to interfere with the LEAR vacuum when accepting antiprotons. For the final arrangement to be used at LEAR all components will be manufactured to provide bakeability to at least 250°C and all seals will be made using oxygen free copper or gold gaskets. To avoid degrading the vacuum by deposition of organic molecules, only absolutely oil free pump systems will be used. Currently the pumping relies on a 600 ℓ/sec ion pump for the ion trap section and on cryogenic pumps for the remainder of the system and initial pump down. As roughing pumps we use only sorption pumps to avoid the entry of pumping oil into the system. In addition to these pumping stations, it is planned to introduce Non-Evaporable Getter pumps (NEG) into each section to provide additional high pumping speed at low pressure. These pumps have been very successfully implemented in the Electron-Cooling Device to be installed at LEAR[23] where a vacuum of 3×10^{-12} Torr was achieved. In addition, the outgassing from the internal surfaces of the vacuum chambers is reduced by carefully electropolishing all parts before installation. Using an entirely bakeable system, the complete pumping system described here will reach a final vacuum at the interface to the LEAR beam line (with a valved off H^- source) comparable to or better than the LEAR vacuum. As additional safety features, small diameter tubes will be used to separate the vacua of the different sections from each other and from the LEAR ring. A system of fast acting pneumatic all-metal valves will be used together with remote pressure sensing to prevent any possible interference with the LEAR vacuum. The valve to the H^-/p source will only be allowed to open when the main beam line is valved-off from the LEAR ring and opening of the valve between our system and LEAR will be subjected to the achievement of a minimum pressure requirement. We feel this system will present a satisfactory isolation between LEAR and the RFQ and should be sufficient to avoid the insertion of a vacuum window into the path of the antiproton beam which at the low energy to be used could lead to unwanted degradation of the beam emittance. Finally, the main valve between LEAR and the RFQ will only be opened for a short instant to accept the bunch to be

captured; otherwise our system will be completely separated from the LEAR vacuum during the experiment.

4. Ion Trap Development. As outlined in Section III-E a series of ion traps will be used, each suited best for its specific task. In our preliminary tests we are currently using a single trap which represents a compromise between the different requirements. This trap has a moderate axial dimension, $z_o \sim 1.5$ cm, which is large enough to capture a significant number of protons or H^- ions from our test beam. In addition it is built asymptotically symmetric ($\rho_o = \sqrt{2}\, z_o$) and reasonably harmonic so that it is useful for initial cooling tests and for the development of resonant excitation and detection schemes at room temperature. For the future development we are currently designing an elongated trap with $z_o = 5\rho_o = 10$ cm. To obtain a harmonic potential in a device like this we are presently constructing a system where we will place electrodes approximating the electric quadrupole potential at $z_o = 10$ cm and $\rho_o = 2$ cm and insert a series of guard rings in the gap between ring and the endcaps. All electrodes will

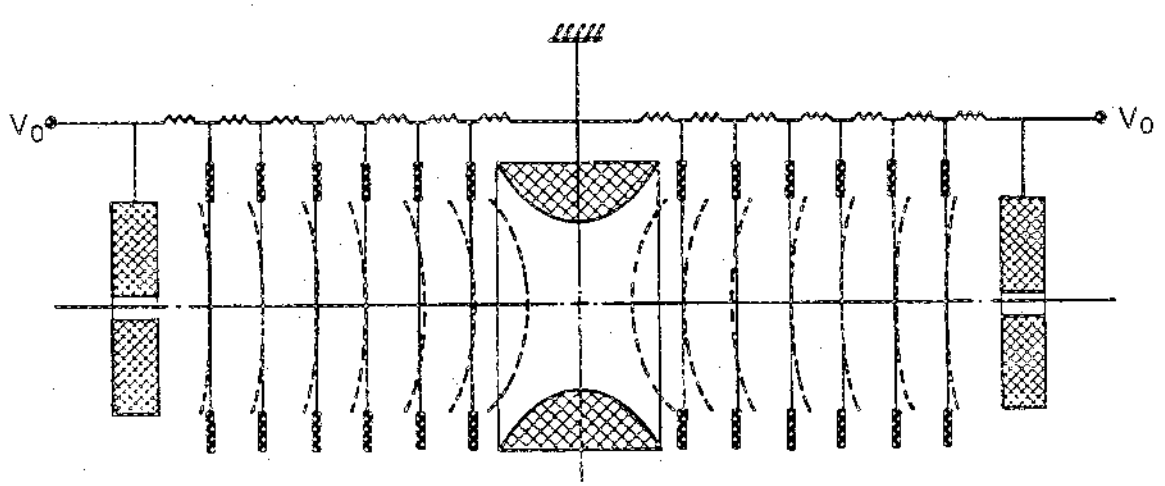

Fig. III-17. Cross sectional view of the proposed scheme to produce an elongated trapping structure, maintaining harmonicity of the trap potential for the near-axis orbits. Approximation of the quadrupole potential (dashed curves) is achieved by a set of individual electrodes.

then be fixed to the appropriate electric potential via a resistive divider network. This scheme is shown in Fig. III-17.

The second, or main storage trap will be built in analogy to the standard Penning traps used in many of the experiments conducted by us and others groups on stored ions. We will use an asymptotically symmetric trap ($\rho_o = \sqrt{2}\ z_o \sim 2$ cm) and introduce guard rings to correct for the anharmonicity caused by the truncation of the hyperboloids.

Finally, the compensated measurement trap for the ejection of antiprotons into the drift tube will be a smaller structure which can be made highly harmonic.

Depending on the outcome of initial vacuum tests with a room temperature trap currently under way at Los Alamos either the main storage trap and the compensated measurement trap or the entire trap section will be held at 4 K. This requires development of low heat conductance feed throughs and connections to the trap electrodes and of heat shields to isolate the room temperature part from the cryogenic section. Investigations along these lines, including the development of low temperature, low noise electronic circuitry to manipulate and detect the ions, are in progress at Texas A&M University.

The initial capturing tests using 10-15 keV H^- ions or protons will be done with the current single trap. In order to capture particles at an energy of 10-20 keV in a trap of this size, switching of the endcap potential between 0 and 20 kV on a time scale of a few nanoseconds is required. We have developed a first-generation switch capable of switching on a 20 kV potential from ground with a rise time of less than 5 nanoseconds. This first-generation pulser is in reality a slide switch in the form of a coaxial transmission line. Figure III-18 shows a simplified cut-away view of the pulser whereas Figure III-19 shows a picture of the operational wave form.

At t_o a large current pulse is fired through the drive coil propelling the slide contactor into the gap between part A and part B as shown in Fig. III-18. Just prior to physical contact at A a plasma forms between A and the slide contactor at t_1 (see Fig. III-19). Shortly thereafter the slide contactor makes physical contact at t_2.

The voltage rise time to the 17 kV step (t_1) is approximately 5 ns. The time delay between t_1 and t_2 is about 2 ms while the total delay from t_o

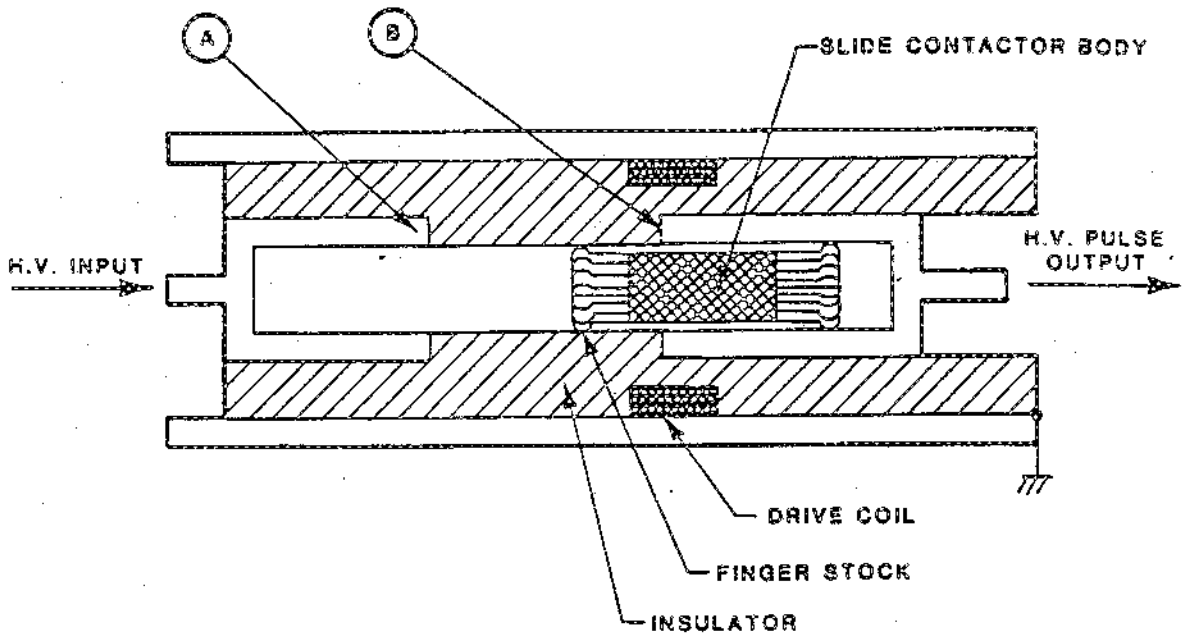

Fig. III-18. Cut-away view of the present high voltage pulser.

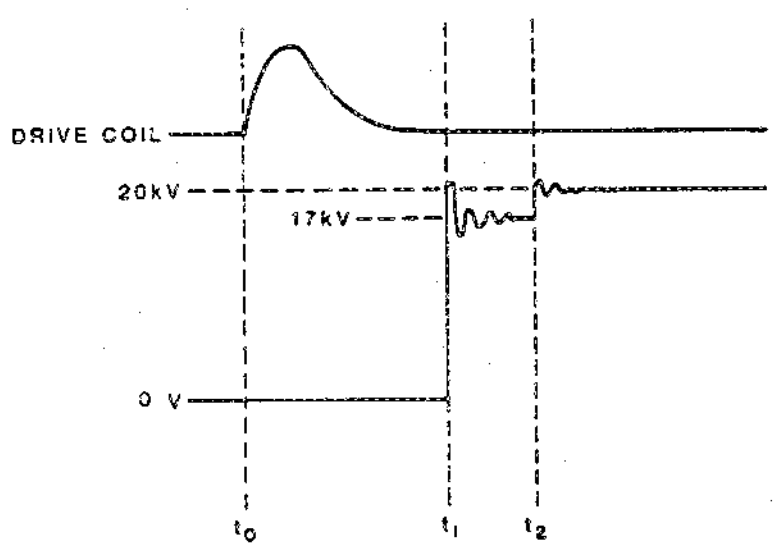

Fig. III-19. Operational voltage waveform of the first-generation pulser.

to t_1 is of the order of 18 ms. Because this device is partially based on a mechanical contact closure the repetition rate is very low and a second-generation pulser based on only electronic components is currently

under development. Nevertheless, our first-generation switch is well suited for the initial capturing tests.

The second-generation high voltage pulser for the antiproton trap is a much more complex device than the one shown in Figure III-18. Figure III-20 shows a block diagram of the second-generation device. This device will be capable of the complex wave shapes necessary for new trap structures. Rise and fall times will be at a maximum slew rate of 400 kV/ns. The maximum high voltage output will be 35 kV, and the maximum repetition rate will be greater than 120 Hz. The system uses two planar triodes connected in a totem pole. All controls are via fiber optic links

To verify the capture of particles, a microchannel plate is mounted at the end of a short drift tube at the 2 Tesla point of the solenoidal field. Initially, particles will be captured as described in Section III-E and, after a fraction of a second, released by suddenly lowering the potential at the upstream endcap.

After capture has been established, this system can be used to measure the axial and transverse energy of the charge cloud to study the cooling of the stored particles using the standard TOF technique developed by the Mainz group. At a later stage the initial trap will be replaced by the elongated

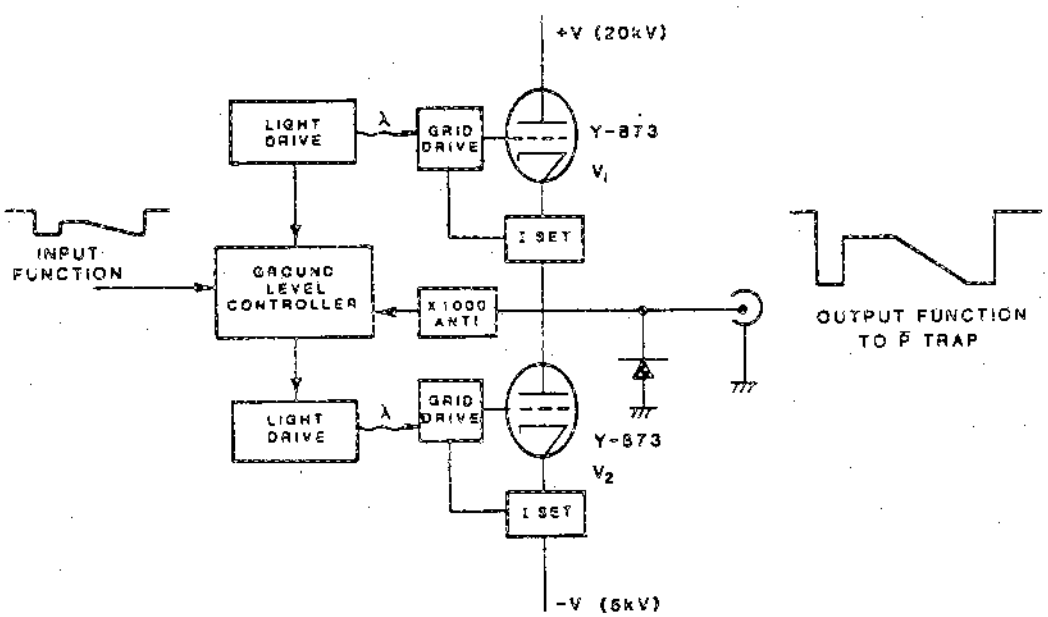

Fig. III-20. Block diagram of the high-voltage pulser currently under development.

version to investigate its catching and cooling properties. A second, similar, system will be built up with the main storage trap to study low energy ejection using internally created protons as a source of charge. Once these tests are completed the different ion traps will be mounted in series in the solenoidal field to study the transfer of the entire bunch, as well as partial transfer of a few particles from the filled storage trap to the compensated launch trap. All these tests can be done at room temperature at a moderate UHV (10^{-10}-10^{-11}Torr) in the first run. Only after these studies have been completed with satisfactory results will the cryogenic trap systems, which are being developed in parallel, be implemented.

As mentioned before we will initially rely on resistive cooling for this process in the different trap structures in use. In parallel, the collaborators at Genoa and Pisa are investigating the possibilities of stochastic cooling in ion traps. A highly harmonic trap operating with internally created protons and H_2^+ ions in a 5T field has been constructed and the coherent and incoherent motion of the stored particles has been detected. A system of detection circuits and amplifiers has been built to detect the noise fluctuations of a stored charge cloud and to apply it back to the trap structure with appropriate phase relation to produce negative feedback. Experimental results from this investigation are expected in the near future. At Rice University a trap experiment is being developed where low energy positrons can be injected into a Penning trap together with internally created protons. This will precisely test the situation of electron cooling of antiprotons, and should give the necessary experimental input to the questions about the feasibility of electron cooling in Penning traps.

5. Drift Tube Design and Fabrication. The design and construction of the drift tube into which the particles will be launched for the gravity measurement is a crucial step in the experimental plan. One member of this collaboration is a world recognized expert in this area, having designed and built the drift tubes used in the electron gravity experiment. We propose to develop several short drift tubes to isolate the fabrication difficulties associated with the amorphous surface coating on the drift tube interior. We will study the magnetic field dependence of the shielding effect observed by Lockhart. Once the fabrication technique has been established through

this program of testing, the drift tube for the actual experiment will be built and once again tested with H^- ions.

6. Particle Detection. Even though the antiprotons emerging from the drift tube could be easily detected using their annihilation radiation it is important to realize that our experiment is very strongly based on the comparison between antiprotons and H^- ions or protons. Therefore a universal detector which is well suited for all these different cases is mandatory. Our decision to use microchannel plates (MCP) as a detector system is largely based on the experience gained from the TOF spectroscopy of stored particles. In order to complement the existing literature on relative and absolute detection efficiency[24] we are currently setting up an independent vacuum chamber to study the properties of different MCP assemblies in detail.

7. Data Acquisition and Analysis. Data acquisition will be carried out via a computer-controlled system being developed at Rice University. We will use our own computer, dedicated to the experiment for data acquisition and both on-line and off-line analysis. To aid in the analysis and design we have developed a Monte-Carlo simulation code at Los Alamos that generates the time-of-flight distributions discussed in Section II-B. In addition we have written a fitting routine that has enabled us to estimate the measurement precision versus particle-number variation discussed in Section II-E. A great deal remains to be done to refine these Monte-Carlo simulator and fitting codes. In particular, we will include all electrostatic and magnetostatic effects for both H^- ions and antiprotons in the simulator. This simulator will be used to optimize the design of the drift tube ends where stray electric fields exist and to guide the design of the on-line and off-line analysis codes.

8. Personnel. The collaboration that has assembled to perform the gravity experiment proposed here represents a cross section of internationally recognized experts in accelerator, atomic, condensed matter, nuclear, and particle physics. In addition, the collaboration has parallel efforts addressing the theoretical and the experimental aspects of the experiment. Table III-3 lists the collaboration members according to specialty and area of interest. Note that some names are listed more than once.

Table III-3

Collaboration Expertise

EXPERIMENTAL		
RFQ development and Beam Lines	J. H. Billen K.R. Crandall T.P. Wangler M. Weiss W. Saylor	N. Jarmie R.E. Brown D. B. Holtkamp N.S.P. King J.E. Stovall
H^- Source	R.E. Brown	N. Jarmie
High Voltage Pulsers	M.V. Hynes	G. Krausse
Ion Traps	N. Beverini D.A. Church R.A. Kenefick G. Manuzio	B.E. Bonner M.H. Holzscheiter V. Lagomarsino G. Torelli
Drift Tube Development and Particle DetectionN.S.P. King	F.C. Witteborn M.H. Holzscheiter	M.V. Hynes
Ultra-high Vacuum systems and Cryogenics	R.E. Brown D.A. Church M.H. Holzscheiter	N. Jarmie R.A. Kenefick
Computer Controls and Code Development	B.E. Bonner S.D. Howe	M.V. Hynes
THEORETICAL		
Gravity Theory	T. Goldman M.M. Nieto	R.J. Hughes
Ion Traps	A. Picklesimer P.C. Tandy	R.M. Thaler
Atomic Physics	L. Bracci E.R. Siciliano	A.L. Ford
Condensed Matter Physics	L.J. Campbell	

In addition to the collaboration members listed, the experimental effort is supported by four highly experienced technicians at Los Alamos, five graduate students at different institutions, and two postdoctoral fellows (expected this Fall). Other personnel are available to us on a consulting basis and are not formal collaboration members as yet.

9. Funding. The funding for the gravity experiment we propose here draws from sources both internal and external to the Los Alamos National Laboratory (LANL). The Los Alamos National Laboratory is administrated by the University of California for the Department of Energy (DOE) of the United States Government. Table III-4 lists the level of funding required by the project according to fiscal year (our fiscal year starts on October 1). In addition the Table lists the funding at member institutions of the collaboration.

The levels of funding indicated are sufficient for us to proceed with the design and construction of major pieces of experimental hardware. However our funding sources require a commitment from CERN that the experiment we propose will proceed on a timely basis given the successful achievement of the technical milestones outlined earlier in this Section. Once conditional approval is granted, after discussion with the CERN management funding for the effort will become available.

Table III-4

Funding Summary M$

External Sources	FY85	FY86	FY87	FY88
DOE	---	0.45	0.55	0.55
Internal LANL Sources	1.00	2.85	1.17	0.70
Institutional Sources				
Universita di Pisa e Genova	0.04	0.04	0.04	0.04
Rice University	0.08	0.10	0.10	0.10
Texas A&M University	0.10	0.15	0.15	0.10
Kent State	0.05	0.05	0.05	0.05
Case Western	0.05	0.05	0.05	0.05
Totals	1.32	3.69	2.11	1.59

REFERENCES FOR SECTION III

1. P. Lefèvre and D. Möhl, private communication.
2. N. Beverini, L. Bracci, V. Lagomarsino, G. Manuzio, and G. Torelli, University of Pisa preprint, INFN PI AE 85/6 (1985).
3. W. Kells, G. Gabrielse, and K. Helmerson, FermiLab-Conf.-84/68-E.
4. M. Kapchinskii and V. A. Teplyakov, Prib. Tekh. Eksp. 2, 19(1970).
5. J. M. Potter, S. W. Williams, F. J. Humphry, and G. W. Rodenz, IEEE Trans. Nucl. Sci. NS-26, 3745(1979).
6. K. R. Crandall, R. H. Stokes, and T. P. Wangler, 1979 Linear Accelerator Conference, Montauk, New York.
7. R. H. Stokes, T. P. Wangler, and K. R. Crandall, 1981 Particle Accelerator Conference, Washington, D. C.
8. T. P. Wangler, K. R. Crandall, and R. H. Stokes, Symposium on Accelerator Aspects of Heavy-Ion Fusion, GSI, Darmstadt, (1982).
9. J. Byrne and P. S. Farago, Proc. Phys. Soc. (London) 86, 801(1965).
10. E. Fischer, Z. Physik 156, 1(1959).
11. D. A. Church and H. G. Dehmelt, J. Appl. Phys. 40, 3421(1969).
12. K. H. Kingdon, Phys. Rev. 21, 408(1923).
13. R. S. van Dyck, jr., D. J. Wineland, P. A. Ekstrom, and H. G. Dehmelt, Appl. Phys. Lett. 28, 446(1976).
14. G. Gräff and E. Klempt, Z. Naturforschung 22A, 1960(1967).
15. L. Bracci, G. Fiorentini, and O. Pitzurra, Phys. Lett. 85B, 280(1979).
16. L. S. Brown and G. Gabriels (in press).
17. L. Spitzer, jr., Physics of fully Ionized Gases, Interscience, New York(1965); T. H. Kho, Phys. Rev. A32, 666(1985).
18. H. G. Dehmelt, F. L. Walls, Phys. Rev. Lett. 21, 127(1968).
19. D. J. Wineland, W. M. Itano, and R. S. van Dyck, jr., Adv. At. Mol. Phys. 19, 135(1983).
20. G. Gräff, H. Kalinowsky, and J. Traut, Z. Phys. A297, 35(1980).

21. W. Thompson and S. Hanrahan, Jour. Vac. Sci. Tech. 14, 643(1977).

22. N. Jarmie, R. E. Brown, and R. A. Hardekopf, Phys. Rev. C29, 2031 (1984).

23. C. Rabfast, M. Girardini, L. Hutten, A. Poucer, H. Poth, B. Seligmann, and A. Wolf, Vakuum Technik 34, 195(1985).

24. R. S. Gao, P. S. Gibner, J. H. Newman, K. A. Smith, and R. F. Stebbings, Rev. Sci. Instr. 55, 1756(1984).

IV. FACILITY REQUIREMENTS AT CERN

The experiment we propose here is being designed to have minimum impact on the LEAR facility. However, due to the scale of the experimental equipment required for our measurement, we will need utilities, floor space, and general assistance at a commensurate level. In the following, "RFQ System" refers to the combination of buncher, RFQ, energy shifting cavity, and debuncher. The term "LEBL" refers to the low energy beam line that transports the beam from the energy shifting cavity to the 90° vertical bending magnet just below our ion trap system and drift tube.

A. Utilities

Our preliminary estimate for the utility requirement for our experiment is summarized in Table IV-1.

TABLE IV-1

UTILITY REQUIREMENTS

Service	Requiremnt
Electric Power (220 V, 50 Hz)	
--Detection Electronics, (clean separated ground)	2 kW
--LEBL and Ion-Trap-Drift-Tube Systems (including H^- source)	30 kW
--RFQ System RF	6 kW
Vacuum	7 kW
--On-Line Computer	10 kW
--Total	55 kW
Cooling Water (Demineralized)	
--LEBL and Ion-Trap-Drift-Tube	7 ℓ/min
--RFQ System	22 ℓ/min
Compressed Air	(as needed)
Cryogenic Fluids (maximum)	
--LN_2	15 ℓ/operating day
--LHe	25 ℓ/operating day
Helium Recovery Line	one connection

B. Electronic Equipment Pool

We plan to bring all the required electronic components (and spares) necessary for the experiment. However, we request 30 KSFr to cover emergencies.

C. CERN Computer Time

We will supply our own on-line computer that will be capable of preliminary off-line analysis. Most of the final analysis will be carried out using the computers at Los Alamos. We request 5 CPU hours per year at CERN for some analysis and networking.

D. Technical Support

We plan to bring our own technicians for the installation and operation of our experimental equipment. These technicians will require access to machine shop facilities and basic metal stock supplies for minor machining jobs. All major machining jobs will be executed by the collaboration members at their home sites.

Because the equipment installation involves a new beam line at LEAR, a close working relationship needs to be maintained between our technicians and the LEAR facility group. In view of this, we request the occassional assistance of two CERN technicians.

E. Beam Time Estimate

We estimate we will need one pulse per hour of 10^8 antiprotons (1/8 of the 10^9 $\bar{p}$'s in the ring) at 0.10 GeV/c in the fast-extraction mode. With the expected transmissions in the RFQ system (50%) and the LEBL (60%), the trapping and inter-trap transfer efficiency (40%), and the launch efficiency (50%), about 10^6 p^-'s are left. Because we need 10^7 $\bar{p}$'s for a one percent measurement, we will need one such pulse per hour for 10 hours. The rest of an operating day would be taken up with runs using our H^- source and other calibrations. Thus, we should not heavily interfere with other users of a fast extraction beam.

We estimate 25 running days in the above fashion, with intervals for analysis and repair. Should LEAR operate in the post-ACOL era with a more intense beam than 10^9 per fill, we could use a shorter fill time. In the interest of efficiency, we request some time in the initial set-up period using H^- ions to fine-tune the RFQ system and the RFQ-LEBL interface. See

also Section III-B and Table III-1 for the assumed characteristics of the LEAR beam.

F. Site Plan and Space Considerations

Our estimate of the required space for our experiment is listed in Table IV-2.

TABLE IV-2

FLOOR SPACE REQUIREMENTS

RFQ System and Beam Line	17 x 2 m	34 m^2
RFQ Supplies and Control Desk		10 m^2
LEBL Total Area	5 x 5 m	25 m^2
H^- Test Source		2 m^2
Total Floor Area		71 m^2

The vertical height of the experiment is significant (on the order of 8m) depending on the final ion-trap-drift-tube design. Therefore, we need to be served by the overhead crane for the PS rather than by the low crane serving the LEAR users. Once the gravity experiment is fully installed, the low crane must be blocked from hitting the vertical assembly of the experiment. Users of the building would then use a combination of both cranes for complete floor access. During extended periods when we are not running, the top part of our apparatus can be removed to allow the lower crane again to travel its full distance.

Figure IV-1 shows a suggested location for our experiment. Extra low energy beam-line ports could be placed at the H^- source injection magnet (see Fig. III-10) feeding, for example, the area of PS-189 and also placed at the end of the straight-through line near the 90° double focusing magnet for the use of other low-energy $\bar{p}$ experiments.

We do not expect a significant biological radiation hazard to exist from our experiment. We estimate at most 1 mR/hr at 1 m from our ion traps. It would be desirable to be able to work near the experiment during the runs. A small amount of shielding may be necessary around the RFQ for x-ray suppression.

We will need housing for our on-line computer and data acquisition electronics on the experimental floor. Some office space for experimenters both on and off the experimental floor will be needed also. We suggest two

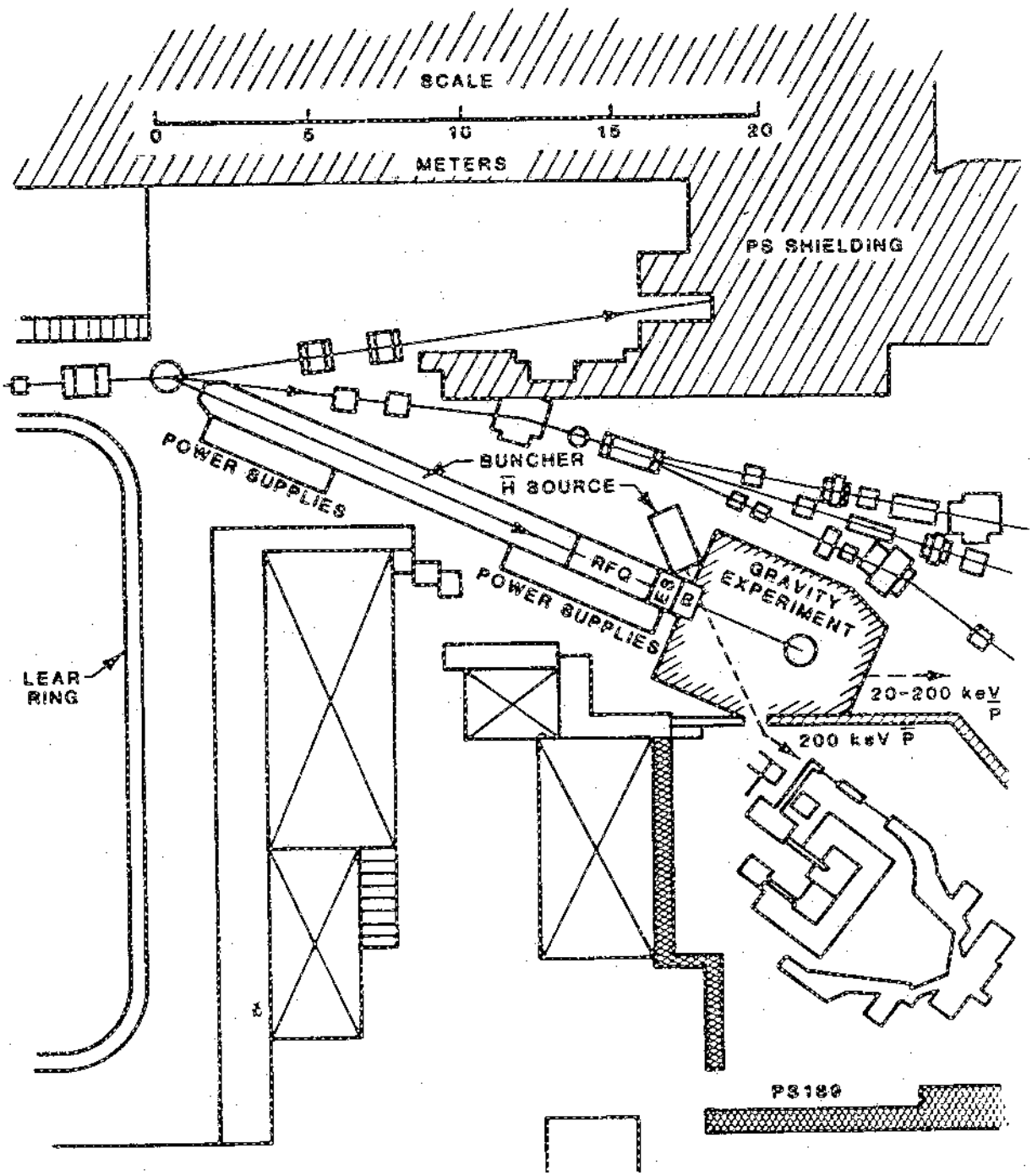

Fig. IV-1. A proposed layout for the placement of the buncher RFQ system and the gravity experiment at LEAR.

of the standard huts (15-20 m^2 each) on the floor, and some office space elsewhere, but near the LEAR facility.

V. FUTURE PROSPECTS

At the culmination of our experiment we will have constructed the last stage of the world's first source of antiprotons in the range below ~200 keV. This source will provide dramatic new research opportunities across a broad front of experimental physics. Some of the possibilities are sketched in the following subsections. However, the number and variety of alternatives seems to be limited only by imagination. It therefore seems likely that many of the more exciting possibilities remain to be identified. We intend to play an active role both in the further development of ideas and in research directed along some subset of the lines indicated below. Moreover, we are strongly committed to providing every possible assistance to other groups interested in taking advantage of this low energy antiproton source.

A. Spatial Anisotropy and Mach's Principle

The inertial properties of matter imply that at each point of space a set of reference frames exist in which Newton's laws hold. These are called "inertial" frames. If other frames are used instead, Newton's laws will only apply if fictitious (inertial) forces are introduced. Familiar examples are the centrifugal and Coriolis forces. One may then ask how the inertial frames are to be determined. Newton stated that they were determined by "absolute space", so that "inertia", in such a theory, is an intrinsic property of matter. However, "absolute space" is an abstraction which is not observable in any other way. This suggested to Berkeley[1] and to Mach[2] that it might be more satisfactory to correlate the inertial frames with observable properties of the Universe. They maintained that inertial frames are those which are unaccelerated with respect to the "fixed stars". This last statement is usually referred to as Mach's Principle. From this point of view, "motion" can be completely described in terms of "observables". Hence, a kinematical description of all the relative motions in the Universe constitutes a complete specification of the system. Therefore, kinematically equivalent motions must also be dynamically equivalent.

If Mach's Principle is accepted, it follows that inertia is not an intrinsic property of matter but arises from the interaction of matter with

the rest of the Universe. "Inertia", then, would have a dynamical origin.[3,4,5] This suggests that the non-uniform distribution of matter in our galaxy may produce a spatial anisotropy of inertia.[6] A search for such anisotropy was performed by Hughes[7] and by Drever,[8] with null results. (However, this does not necessarily provide evidence against Mach's Principle.[9]) These results have been reinterpreted as evidence for local Lorentz invariance,[10] and hence for the Einstein equivalence principle. This principle need not hold in non-metric theories of gravity, such as extended supergravities. Also, various local-Lorentz-invariance-violating interactions between matter and gravity have been proposed.[11,12] With such ideas in mind, the limits on spatial anisotropy set by the Hughes-Drever experiments have recently been improved[13] by a factor of 300. Moreover, it has been pointed out that combined measurements of the gyromagnetic ratio for the proton in horizontal and vertical magnetic fields would also yield information about spatial anisotropy.[14]

To date, all experiments to detect spatial anisotropy have been performed with ordinary matter. Given the huge preponderance of matter over antimatter in our part of the Universe, it would be of great interest to perform such an experiment with antiprotons. A determination of the orientation dependence of the antiproton gyromagnetic ratio could, perhaps, be performed in an ion trap. An experiment of this type is all the more interesting given that in extended supergravity theories the gravitational interaction is able to distinguish between matter and antimatter.

B. Broad-Range Physics Opportunities

In the last subsection an additional gravitational experiment was described that might be possible if (polarized) antiprotons were available in an ion trap. Furthermore, a vast array of new possibilities in atomic, nuclear, and condensed matter physics would be opened up by the availability of substantial quantities of cold antiprotons. These include, for example, line sources of kaons and pions (by tagging in two-body, stopped antiproton-nucleon annihilation) and atomic and nuclear physics studies of antiproton cascade and capture in antiprotonic atoms. The interest in antiprotonic atoms, centered around, but not limited to, experimental searches for baryonia, is apparent from many LEAR proposals. The advantages

of cold antiprotons and "thin" targets for these experiments have been discussed, for example, in the Aarhus Letter of Intent.[15] The antiprotonic atom can be studied in essential isolation, without complications from intermolecular collisions and associated Stark-mixing and external Auger effects.

A broad range of interdisciplinary physics can be conceived once an understanding of antiprotonic atoms in isolation is achieved. Because the properties of these atoms are sensitive functions of the details of the medium in which they are embedded, observed medium modifications of their properties contain unique new information about the characteristics of the medium itself. One can envision an extensive experimental program which employs antiprotons to investigate microscopic properties of a variety of gas, liquid, and solid state systems. Investigations of molecular collision rates and intermolecular potentials, atomic structure, molecular structure, chemical kinetics, and electromagnetic and electron fields in the vicinity of lattice sites and impurities are but a few examples of promising areas of application.

C. Dynamic Stability in Condensed Matter Systems

The intrinsic stability of the antiproton makes it ideal for the study of new stability mechanisms in condensed matter. Dynamic stability, wherein particles are held in a steady state (an excited state) for long times by virtue of compensating instabilities, is particularly interesting. The principle of dynamic stability is illustrated by the familiar alternating gradient synchrotron, but it is not limited to such macroscopic application. The existence of localized states of dynamic stability for antiprotons is currently an open question. Simple arguments based on electrostatics and variational principles that imply the absence of stable $\bar{p}$ ground states in condensed matter are not valid when excited states are involved. A possible example of nonlocalized dynamic stability is channeling, whereby a $\bar{p}$ in a certain energy range travels along a particular crystallographic axis without annihilation.

Unlike potential applications in the fields of atomic and nuclear physics, the perspectives in condensed matter physics are not at all clear. This is due to the novelty of conceivable applications; an extensive

previous literature from which to draw is not available. Nevertheless, four specific condensed matter environments can be identified as possessing unique features that might lead to significant payoffs.

1. Superfluid Helium. The superfluid state of liquid ^{4}He is remarkable in its display of a coherent quantum state over macroscopic distances. When disturbed by boundaries and impurities this quantum state recovers over a very short distance, approximately the size of the interatomic spacing. Much is known about the behavior of a variety of impurity ions in superfluid helium. Examination of the behavior of $\bar{p}$ impurities offers the possibility of new insights. Unlike free electrons, which create small bubbles in the liquid due to their zero-point motion and the Pauli exclusion principle, $\bar{p}$'s should act more like free protons and create high density clusters of ^{4}He atoms around themselves by electrostrictive attraction. The subsequent annihilation of the $\bar{p}$ should be preceeded by photon emission containing information about its immediate neighborhood. Superfluid helium is essentially transparent to a very wide spectrum of radiation and can be cooled to a temperature where its own excitations are effectively absent. In fact, approximately 13% of the superfluid helium atoms are in a Bose condensed state of zero momentum. These features ensure the greatest possible advantage in observing, with high precision, the $\bar{p}$ transition and decay products in condensed matter because of an extremely small energy spread in these products due to center of mass doppler broadening. It is also possible that the $\bar{p}$ would never see the condensed state of ^{4}He, especially if the electrostrictive cluster formation time is rapid in comparison to $\bar{p}$ annihilation time. In any case, the thermal center of mass motion would probably be the smallest achievable in any context.

It is tempting to speculate that the macroscopic quantum coherence of the superfluid state, including the delocalization of the fraction of the ^{4}He in the Bose condensed state, may give rise to truly dramatic effects in the behavior of the $\bar{p}$, such as coordinated annihilation, stable states, etc. Whether such effects exist is not known, but they seem unlikely in view of the large discrepancies in the size of the $\bar{p}$ impurity compared with the coherence length of the superfluid state and in view of the coulomb energy available in the $\bar{p}$-^{4}He atom compared to the energy associated with the loss

of superfluidity over a comparable volume. Nevertheless, surprises certainly have occured before in condensed matter physics.

The liquid surface of superfluid ^{4}He also offers a unique environment for $\bar{p}$ studies because it is microscopically smooth, in equilibrium with a vapor of effectively zero density (at low temperatures), and can be charged with ions either above or below the surface. In particular, electrons on the vapor side can be held against the helium surface by applying an electric field; they do not penetrate the surface because of the relatively high energy required to make the bubble state mentioned earlier. Because this electronic surface charge density can be substantial and can be excited in various plasma modes, the possibility exists of finding electron-$\bar{p}$ states that are bound to the surface but have negligible $\bar{p}$ density at the surface. In effect, the $\bar{p}$ would be trapped between the external electric field and the electronic surface charge, which in turn is repelled from the surface by the Pauli principle. As mentioned in the general remarks above, such trapping would have to occur in an excited state.

2. Superconductors. Many of the features of quantum coherence apply to both superconductors and superfluids: a superconductor is essentially a charged superfluid in a solid, neutralizing background. Electric and magnetic fields are shielded quite effectively in superconductors over distances comparable to the penetration depth: a length scale present only in charged superfluids and typically having a magnitude of many lattice spacings. Thus, one cannot expect known superconductors to shield and stabilize a $\bar{p}$ in any obvious way on an atomic scale, but what will happen is not clear either. The origin of the effective electron attraction, which gives rise to superconductivity, is a subtle and delicate interplay between electronic and lattice properties, both of which are disturbed by a $\bar{p}$. A best guess now is that the influence of a $\bar{p}$ impurity may be too localized to probe superconductivity, although it could give information on other electronic structure.

3. Semiconductors. A $\bar{p}$ is attracted to positive charge. In the presence of an effective source of positive charge, other than protons, one could expect $\bar{p}$ trapping. In many respects, especially involving dynamics and transport, the absence of electrons in a bulk medium is equivalent to positive charge. This "positive" charge can be either delocalized as holes

in a conduction band or localized as ionic lattice vacancies and certain crystal imperfections. Of course, such pseudo-positive charge cannot violate the laws of electrostatics, and the introductory remarks on the absence of ground state stability still hold. Nevertheless, the existence of localized excited states of the $\bar{p}$-hole system are possible in principle, and the model could serve as a fruitful paradigm.

4. Ionic Crystals. A charged particle at an interstitial position or a vacancy position in an ionic crystal can be localized at a point where the local electric fields cancel, i.e. at a position that is force free but nevertheless unstable. The possibility of stabilizing this position by imposing a time-varying external electric field which effectively creates an attractive local potential well, relative to the unstable directions, then exists. The strength and frequency of this field may be tunable to favor particular sites and to avoid combinations that would unduly disrupt the underlying crystal structure. A wide variety of crystal types and laser sources are available to explore this possibility.

Moreover, the possibility of forming localized, stable orbits which encompass one or more lattice sites should not be overlooked. This could be envisioned as a microscopic, quantum analog of a storage ring. Again, extensive knowledge from the science of crystal structure is available to aid in the search for the optimum environment.

D. CPT Invariance and Atomic Antihydrogen

The advantages presented by a low energy antiproton source in this particular atomic physics context are of special note due to the interest expressed in studies of CPT invariance in atomic antihydrogen. The experimental problem lies mainly in the formation time.[16] Even the slowest possible antiprotons in LEAR have a short transit time through the straight sections. These are the only locations where cold positron beams could be made to mix with the antiprotons to form antihydrogen beams. Even if operating conditions would allow the longitudinal energy spread of the proton beam to be minimized, the eV or higher temperature characterizing the transverse beam spread is extremely difficult to reduce. This, combined with the short transit time and small antiproton-positron capture cross

section at these (relative) energies, implies a very small antihydrogen yield for experimental purposes.

However, antiprotons from a trap, such as those proposed for our experiment, could be four orders of magnitude colder, in both transverse and longitudinal degrees of freedom. Positrons may be injected at very low energy to form antihydrogen at a very high rate. Stueckelberg and Morse[17] found an inverse energy dependence for the capture cross section of electrons on ions. Therefore, we can expect a minimum of four orders of magnitude improvement in the antihydrogen formation rate, assuming only the minimum of CPT invariance. But in fact, the improvement could be even much more: The cold antiproton and positron beams possible from traps have smaller emittances than those cooled in collectors and decelerators, thus the luminosity of the intersecting beams may be higher. Furthermore, laser-enhanced capture techniques designed to raise the formation rate will benefit from the reduced Doppler broadening, and more precisely defined beam velocity. The combined effect of all of these techniques may well raise the antihydrogen formation rate beyond 10^6 per second. Finally, one may well imagine that the experimental techniques for detection and utilization of the beam will benefit from the improved sharpness in the spatial and energy definition of the antihydrogen beam.

REFERENCES FOR SECTION V

1. G. Berkeley, The Principle of Human Understanding, (1710).

2. E. Mach, The Science of Mechanics, (1883).

3. D. W. Sciama, Mon. Not. Roy. Ast. Soc. 113, 34 (1953); Sci. Am. 196, 99 (February, 1957).

4. D. J. Raine, Rep. Prog. Phys. 44, 1151 (1981).

5. P. W. Bridgeman, Am. J. Phys. 29, 32 (1961).

6. G. Cocconi and E. E. Salpeter, Nuovo Cim. 10, 646 (1958).

7. V. W. Hughes, H. G. Robinson, and V. Beltrow-Lopez, Phys. Rev. Lett. 4, 342 (1960).

8. R. W. P. Drever, Phil. Mag. 6, 683 (1961).

9. R. H. Dicke, Phys. Rev. Lett. 7, 359 (1961).

10. C. M. Will, in General Relativity, eds. S. W. Hawking and W. Israel, Cambridge University Press, Cambridge, 1979.

11. J. Leitner and S. Okubo, Phys. Rev. 136, B1542(1964).

12. N. D. Hari Dass, Phys. Rev. Lett. 36, 393 (1976).

13. J. D. Prestage et al., Phys. Rev. Lett. 54, 2387 (1985).

14. J. C. Gallop and B. W. Petley, Nature 303, 53 (1983).

15. J. F. Bak, B. I. Deutch, A. S. Jensen, A. Miranda, S. P. Møller, G. C. Oades, A. H. Sørenson, E. Uggerhøj, W. Gruebler, P. A. Schmelzbach, V. Koenig, B. Bonner, R. E. Brown, M. V. Hynes, N. Jarmie, N. S. P. King, M. H. Holzscheiter, H. Pilkhuhn, J.-M. Richard, K. Elsener, Capture in Flight of Low-Energy $\bar{p}$'s in Polarized H^0 and D^0, submitted to CERN, September 9, 1985.

16. R. Neumann, H. Poth, A. Winnacker, and A. Wolf, Z. Phys. A 313, 253 (1983).

17. E. C. G. Stueckelberg and P. M. Morse, Phys. Rev. 36, 16 (1930).